January 2015

Direct and Indirect Searches for Anomalous Beta Decay

Jonathan Nistor
Purdue University

Graduate School Form 30
Updated 1/15/2015

PURDUE UNIVERSITY
GRADUATE SCHOOL
Thesis/Dissertation Acceptance

This is to certify that the thesis/dissertation prepared

By Jonathan Michael Nistor

Entitled

Direct and Indirect Searches for Anomalous Beta Decay

For the degree of Doctor of Philosophy

Is approved by the final examining committee:

Ephraim Fischbach
Chair

Ken Ritchie

Matthew Jones

Andrew S. Hirsch

To the best of my knowledge and as understood by the student in the Thesis/Dissertation Agreement, Publication Delay, and Certification Disclaimer (Graduate School Form 32), this thesis/dissertation adheres to the provisions of Purdue University's "Policy of Integrity in Research" and the use of copyright material.

Approved by Major Professor(s): Ephraim Fischbach

Approved by: Ken Ritchie 11/30/2015

Head of the Departmental Graduate Program Date

DIRECT AND INDIRECT SEARCHES FOR ANOMALOUS BETA DECAY

A Dissertation

Submitted to the Faculty

of

Purdue University

by

Jonathan M. Nistor

In Partial Fulfillment of the

Requirements for the Degree

of

Doctor of Philosophy

December 2015

Purdue University

West Lafayette, Indiana

For T

ACKNOWLEDGMENTS

My foremost gratitude belongs with my advisor, Ephraim Fischbach, for his counsel and support throughout the past decade. Along with Ephraim, I would like to thank Dr. Andrew Hirsch, Dr. Matthew Jones, and Dr. Ken Ritchie for both their participation on my committee as well as their contribution to many matters throughout my tenure at Purdue.

I owe my parents an impossible debt of gratitude. My father taught me the most valuable lesson: to be critical, to think critically, and to learn insatiably. I built this thesis much the way I would build a house, a skill set I owe to him alone. My mother has been a steadfast supporter of all of my endeavors. She has given me incredible insight into the value of people, connections, relationships, family, and compassion. From a house built on my father's lessons, a home I can make from my mother's. I love them both immeasurably.

A great deal of gratitude goes out to Jordan Heim and Tasneem Mohsinally—incredible friends and colleagues. Much of my growth, both personal and otherwise, is due to their profound influence in my life. Finally, I would like to extend my gratitude to the Physics Department for their financial support, through the invaluable opportunity to teach the beautiful field of Physics. The faculty and staff have become a family, from whom I truly do not want to leave.

PREFACE

While this document was being prepared, a very personal tragedy occurred to a dearest friend—someone who has become my closest family over the years. I cannot possibly quantify the depth to which he has influenced my life. Although it is currently a struggle, my deepest wish is that his recovery be swift and absent of long-term or permanent effects. For someone who has such a strong and curious mind, it is truly terrifying that he may struggle to regain those faculties. My intention here is not to excuse the quality of work presented in this document, but rather offer an explanation for the discontinuity in some of the treatment. At one point in time, I believed this document would be my utmost priority—however, I cannot conceive of any higher priority than the role I can serve in aiding his recovery. I hope to return to these topics soon, in collaboration with him, when his recovery is full.

JMN

TABLE OF CONTENTS

LIST OF TABLES

LIST OF FIGURES

SYMBOLS

MISC.

$\dot{x}$	first time-derivative of a function $x\,(t)$
$\langle x \rangle$	some type of average value of x
Υ	vernal equinox
$\underline{\frown}$	autumn equinox
$\earth$	referring to an attribute of the Earth
$\odot$	referring to an attribute of the Sun
$\sim$	equal within an order of magnitude
$\lesssim$	roughly less than or on the order of
δx	small change or variation in x

GREEK

α	alpha particle (^{4}He nucleus) or right ascension in equatorial coordinates or pileup parameter
α_{NGP}	right ascension of north galactic pole
α_ν	expansion coefficient for self-induced decay integral series
β	ecliptic latitude
$\beta^\pm$	beta particle emitted as a decay product or ecliptic latitude
δ	declination in equatorial coordinates
Δ	change in a quantity, usually amplitude of an oscillation
ε	Earth's axial tilt / obliquity or eccentricity of an orbit
$\varepsilon_\earth$	eccentricity of Earth's orbit
ϵ	relative fraction of unstable to unstable+stable nuclei
ϵ^*	saturation limit of activated nuclei
η	parameter in anthropogenic production involving self-induced

	decay process
γ	photon, typically one emitted during a nuclear de-excitation
$\gamma_{\sun}$	angle between Earth's orbital plane and galactic plane
Γ	transition rate for a particular process
Γ_0	transition probability in the absence of a perturbation
κ	parameter initializing a self-induced decay process or K–shell electron involved in electron-capture
λ	decay parameter for a radioactive sample
μ	number density of activated nuclei
ν_s	neutrino of species s
ϕ	particle flux or scalar particle / field
ϕ_n	thermal neutron flux
ϕ_ν	internally-generated neutrino flux
$\phi_{\nu,\odot}$	solar neutrino flux
ρ	mass density
σ_ν	total cross section for a novel neutrino-neutrino interaction
σ_n	thermal neutron-capture cross section
Σ	macroscopic cross section
τ	lifetime of an unstable particle or microscopic dead-time
ϑ	ecliptic / solar longitude
$\vartheta\,[t]$	ecliptic longitude of Earth as a function of time in days from the vernal equinox
ξ	initial fractional perturbation to self-induced decay rate

ENGLISH

$\mathcal{A}$	activity of radioactive sample
b	galactic latitude
c	speed of light
E	energy

f_P	pileup correction factor
$g\,(t)$	ratio function of SID and exponential decay rates
G_F	Fermi constant
I	count rate
I_0	event rate as seen by front-end of a detector
K	electron from the K-shell involved in EC
ℓ	galactic longitude
ℓ_C	longitude of celestial north pole in galactic coordinates
ℓ_i	distance between $\vec{r}_i$ and $\vec{r}_{i-1}$
m_A	atomic mass
$\mathcal{M}$	invariant amplitude
n	number density or decay rate
n_ν	neutrino number density
N	population of unstable particles
N_0	initial number of unstable particles in a system
N_A	Avogadro number
N_p	unstable population involving SID processes
p	differential probability of a self-induced decay
P	probability, usually referring to the survival probability
P_κ	survival probability for a particle undergoing SID
R	reaction rate for a particular process
$s\,(t)$	ratio of survival probabilities for SID and exponential processes
ss	summer solstice
S	arbitrary surface area
t	time
$t_{1/2}$	half-life of a given isotope
t_R	irradiation time
t_S	saturation time
$\vec{v}_{\overset{+}{\circlearrowleft}}$	velocity of Earth about the Sun

$v_c\,[R_\odot]$	rotational speed of the LSR
$\vec{V}_{\oplus}$	velocity of Earth through a larger structure
$\vec{V}_{\odot}$	velocity of the Sun through a larger structure
V	arbitrary volume
W_0	principal branch of Lambert W function
x	spatial location or time measured in units of mean lifetime λt

ABBREVIATIONS

CMB	cosmic microwave background
CνB	cosmic relic neutrino background
DM	dark matter
DT	macroscopic detector dead-time
EC	electron-capture
GCS	galactic coordinate system
GC	galactic center
HFIR	High Flux Isotope Reactor
LSR	local standard of rest
NEP	north ecliptic pole
NGP	north galactic pole
NIST	National Institute of Standards and Technology
ORNL	Oak Ridge National Laboratory
PDF	probability density function
ROI	region of interest
SID	self–induced decay
WIMP	weakly interacting massive particle

ABSTRACT

Nistor, Jonathan M. Ph.D., Purdue University, December 2015. Direct and Indirect Searches for Anomalous Beta Decay. Major Professor: Ephraim Fischbach.

We present a treatment of time-varying nuclear transition rates intended to guide future experimental searches, focusing primarily on the concept of "self–induce decay." This investigation stems from a series of recent reports that suggest that the decay rates of several isotopes may have been influenced by solar activity (perhaps by solar neutrinos). A mechanism in which (anti)neutrinos can influence the decay process suggests that a sample of decaying nuclei emitting neutrinos could affect its own rate of decay. Past experiments have searched for this "self-induced decay" (SID) effect by measuring deviations from the expected decay rate for highly active samples of varying geometries. Here, we further develop a SID formalism which takes into account the activation process. In the course of the treatment, the observation is made that the SID behavior closely resembles the behavior of rate-related losses due to dead-time, and hence that standard dead-time corrections can result in the removal of possible SID-related behavior.

Additionally, we discuss a long-running dark matter (DM) experiment which observes an annual signal predicted by standard DM models. Here, we consider the possibility that the annual signal seen by the DAMA collaboration, and interpreted by them as evidence for dark matter, may in fact be due to the radioactive contaminant ^{40}K, which is known to be present in their detector. We also consider the possibility that part of the DAMA signal may arise from relic big-bang neutrinos.

1. Introduction

In the century since Becquerel's discovery of radioactivity, many attempts have been made to alter the rate of decay of a radioactive source. Unstable isotopes have been subjected to extreme temperatures, pressures, accelerations and magnetic fields, and yet, have shown to be unaffected in their rate of decay. Much of the early work in Becquerel's newly discovered field was due to Rutherford, who contributed a wealth of important discoveries. Among these contributions is the conclusion that "the number of atoms that transform into new kinds of matter in a unit amount of time is a *fixed fraction* of the number of atoms remaining. The fraction depends on the radioactive substance, but is constant for that substance." This statement, which has been repeatedly tested and validated for more than a hundred years, can be expressed succinctly as the exponential decay law,[1]

$$-\frac{dN}{dt} = \lambda N, \tag{1.1}$$

where N represents the population of unstable atoms. Of course Rutherford's fixed fraction, λ, has come to be known as the decay *constant*, and after Rutherford and others exhausted their best efforts at altering λ, he concluded in 1930 that "the rate of transformation of an element has been found to be a constant[2] under all conditions" [1, p. 161].

With such a rich history of experimental verification, it may seem surprising that this statement is being revisited once again with the curious claim that λ may not be

[1]This applies to an arbitrary ensemble of unstable particles, elementary or otherwise—including those which do not decay via the weak interaction. The key ingredient is that a particle have no memory or knowledge of its age (e.g. a muon is identical to every other muon regardless of when it was created). A collection of memoryless particles will have an exponential distribution of lifetimes.

[2]There does exist the exception for decay modes involving atomic electrons, such as electron capture, which have been shown to be influenced by the chemical/physical environment. Nevertheless, the underlying physics of these exceptions is well–known, and intuitively understood to result from a perturbation to the overlap of nuclear and electron wave functions.

Table 1.1: Various experiments where time–dependent nuclear decay rates have been observed. For each entry the observed nuclides and their dominant decay modes are exhibited. Observed periodicities in the decay rates are noted.

Isotope	Decay Type	Detector Type	Radiation Measured	Effect/Periodicity Observed	Reference
^{3}H	β^-	Photodiodes	β^-	1 yr^{-1}	[2]
^{3}H	β^-	Liquid Scintillator	β^-	1 d^{-1}, 12.1 yr^{-1}, 1 yr^{-1}	[3]
^{3}H	β^-	Liquid Scintillator	β^-	$\sim$ 12.5 yr^{-1}	[4]
^{3}H	β^-	Solid State (Si)	β^-	$\sim$ 2 yr^{-1}	[5]
^{22}Na/^{44}Ti†	β^+, κ	Solid State (Ge)	γ	1 yr^{-1}	[6]
^{36}Cl	β^-	Proportional	β^-	1 yr^{-1}, 11.7 yr^{-1}, 2.1 yr^{-1}	[7–9]
^{36}Cl	β^-	Geiger–Müller	β^-	1 yr^{-1}	[10]
^{54}Mn	κ	Scintillation	γ	Solar flare‡	[11]
^{54}Mn	κ	Scintillation	γ	1 yr^{-1}	[12]
^{54}Mn	β^-	Scintillation	γ	1 yr^{-1}	[13]
^{60}Co	β^-	Geiger–Müller	β^-, γ	1 yr^{-1}	[14, 15]
^{60}Co	β^-	Scintillation	γ	1 d^{-1}, 12.1 yr^{-1}	[16]
^{85}Kr	β^-	Ion Chamber	γ	1 yr^{-1}	[17]
^{90}Sr/^{90}Y	β^-	Geiger–Müller	β^-	1 yr^{-1}, 11.7 yr^{-1}	[14, 15, 18]
^{108m}Ag	κ	Ion Chamber	γ	1 yr^{-1}	[17]
^{133}Ba	β^-	Ion Chamber	γ	1 yr^{-1}	[19]
^{137}Cs	β^-	Scintillation	γ	1 d^{-1}, 12.1 yr^{-1}	[16]
^{152}Eu	β^-, κ	Solid State (Ge)	γ♯	1 yr^{-1}	[20]
^{152}Eu	β^-, κ	Ion Chamber	γ	1 yr^{-1}	[17]
^{154}Eu	β^-, κ	Ion Chamber	γ	1 yr^{-1}	[17]
^{222}Rn§	α, β^-	Scintillation	γ	1 yr^{-1}, 11.7 yr^{-1}, 2.1 yr^{-1}	[21, 22]
^{226}Ra†	α, β^-	Ion Chamber	γ	1 yr^{-1}, 11.7 yr^{-1}, 2.1 yr^{-1}	[7, 9, 23]
^{239}Pu	β^-	Solid State	α	1 d^{-1}, 13.5 yr^{-1}, 1 yr^{-1}	[3]

†Only the count rate ratio data were available.

‡Decrease in count-rate was observed during Dec. 2006 solar flare.

♯Only the κ photon was measured.

§Decay chain includes several primarily β–decaying daughters which also emit photons.

constant under *all* conditions—namely, in the presence of an external neutrino field. Indeed, recently a number of groups have reported unexplained periodic variations in measured nuclear decay rates from experiments utilizing a variety of detector types and isotopes (see Table 1.1 and references therein for a non-exhaustive list). The common feature of the observed anomalies is that they appear to be associated with the Sun, as in the case of an annual signal presumed to arise from the annual variation of the Earth–Sun distance [24], a 10–15 yr^{-1} variation associated with the Sun's

rotation [23, 25], a Rieger periodicity [9], and a short-term statistically significant change in the ^{54}Mn decay rate coincident with a solar flare [11]. A possible mechanism to account for a solar influence would be a coupling of the decaying system to solar neutrinos ($\nu_\odot$) via some as-yet-unknown interaction. Although it is conceivable that other, *unkown* background fields could in a sense be moderated by the Sun and hence be the responsible party, neutrinos would seem to be the only known product of solar processes that could potentially significantly interact with decaying nuclei on Earth without conflicting with existing experiments.

Current theory, including a detailed quantum mechanical description of β–decay, would indeed find this alarming, since there is no place within its framework to accommodate this hypothetical dependence. Perhaps the more relevant question, however, is what would existing *experiments* have to say? Despite the many historical attempts to alter the decay rate of a radioactive source, some of which include the application of powerful external fields (e.g. magnetic fields, external gamma radiation), experimenters have traditionally been unable (and where able, lacked significant motivation) to subject a radioactive source to an external neutrino field, nor tune the field at will.[3] For this reason, and additionally since it is not possible to shield a sample from the *irreducible* ambient neutrino background, it is largely uncertain experimentally what effect neutrinos may have on a weakly decaying source.[4]Although such an exotic interaction is not supported by the Standard Model, the proposition that a novel neutrino interaction may be responsible for some observed anomalies in beta decays has been suggested previously—in particular as a way to explain the end-point anomaly of tritium (^{3}H) decay [26–29]. Furthermore, given the extreme weakness of Standard Model neutrino interactions and their elusive behavior in experiment, there most likely exists ample theoretical space to develop neutrino couplings (either to other

[3]Furthermore, prior to 1930 when Pauli first suspected its existence, the elusive neutrino had yet to make it into the average physicist's lexicon.

[4]Of course, we do not have in mind the neutrino-capture process (for which the cross section is $\sigma \sim 10^{-43}$ cm^2). Such a process as depicted in the following diagram cannot possibly account for the magnitude of observed fluctuations.

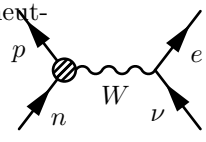

neutrinos or to unknown background fields) that lie outside the Standard Model and which do not conflict with existing experiments.

It is true that a level of caution should be considered when novel physics is proposed to explain the results of experiment. The claim that the observations in Table 1.1 indicate the existence of some heretofore unknown neutrino interaction does, indeed, deserve scrutiny—particularly with regard to the role that environment may have on detector response. Thus far, the observed variations have not been shown to arise from systematic or environmental origins. In fact, several experiments are currently underway which aim to reproduce the observed anomalies, while carefully scrutinizing detector behavior and closely monitoring environmental conditions. These experiments, some of which will require years of data collection to become conclusive, should be able to settle the role of environment in these decay rate variations. Additionally, a number of experiments have yielded results which appear to contradict the neutrino hypothesis [30–36]. However, while such caution is warranted, the possible resolution of various experimental puzzles by postulating a novel interaction is quite intriguing, and also deserving of some experimental and theoretical exploration.

2. Phenomenology of Neutrino Modified Decay

In this chapter we offer a sketch of how one might go about extending the theory of β–decay to accommodate a hypothetical (non)standard model neutrino coupling. We begin by presenting a rather concise and schematic toy theory in which neutrinos interact with each other through a scalar particle ϕ. Such a process would contribute to the self-energy of the neutrino emitted in a β–decay, given the presence of a background population of neutrinos[1]. As such, the overall transition rate will be modified. Most of this is not original work of the author but is provided nevertheless for completeness. The primary focus of this chapter, however, will be to outline a completely classical and phenomenological treatment of time–dependent decay parameters[2].

2.1 An Incomplete Theoretical Framework

In trying to construct a theoretical framework to accommodate a modified form of β–decay, a good starting point is considering the *simplified* process of free-neutron decay, the tree-level diagram of which is shown in Fig. 2.1. If a rigorous treatment is of particular interest, then one should incorporate various form factors, account for the Coulomb attraction between the final state proton and electron, include a non-zero vacuum neutrino mass, and account for quark mixing corrections to the quark-W vertex through the Cabbibo angle. However, given that the *fractional* variations of transition rates, $\delta\Gamma/\Gamma$, will presumably be insensitive to these corrections, they will not be included in what follows.

[1]This background population could be something as pervasive as the CνB or something more specific such as the $\nu_\odot$ flux or even the $\bar{\nu}$ flux produced from a sample undergoing β–decay.

[2]In order to avoid the awkward phrase "time–dependent decay constant," we will henceforth refer to λ as the "decay parameter."

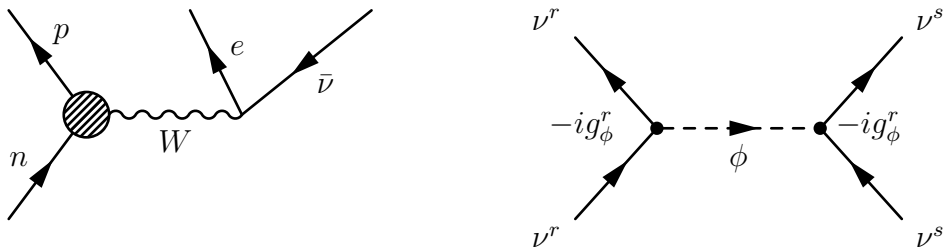

(a) Free-Neutron Decay (b) Neutrino-neutrino scattering

Figure 2.1.: In (a), a tree diagram for free neutron decay is presented. The hypothetical neutrino-neutrino scattering via a scalar particle ϕ in (b) would modify the overall $n \to p + e^- + \bar{\nu}$ transition rate.

As previously stated, it is possible to modify the free-neutron transition rate by introducing a novel neutrino-neutrino coupling—where perhaps the simplest approach is to suppose that neutrinos interact through the exchange of a scalar particle ϕ governed by the Lagrangian

$$\mathcal{L} = -g_\phi^r \bar{\psi}\psi\phi \,. \tag{2.1}$$

Here ψ denotes the neutrino field, and g_ϕ^r is the dimensionless coupling constant for a neutrino of species r. Neutrinos will then interact at a tree-level according to diagrams such as that presented in Fig. 2.1. The presence of these interactions will modify the neutrino self-energy due to corrections to the propagator, and consequently, also modify the decay rate.[3]

Returning to the free-neutron decay, the differential transition rate is given by the standard formula

$$d\Gamma = \frac{|\mathcal{M}|^2}{2m_n}\left(\frac{d^3p_{\bar{\nu}}}{(2\pi)^3 2E_{\bar{\nu}}}\right)\left(\frac{d^3p_p}{(2\pi)^3 2E_p}\right)\left(\frac{d^3p_e}{(2\pi)^3 2E_e}\right)(2\pi)^4\,\delta^4(p_n - p_{\bar{\nu}} - p_e - p_p). \tag{2.2}$$

Given the well-known result for the spin-summed invariant amplitude [37, p. 309],

$$|\mathcal{M}|^2 = 64 G_F^2\,(p_n \cdot p_{\bar{\nu}})\,(p_p \cdot p_e)\,, \tag{2.3}$$

[3]This is true since we can take the viewpoint that a background field of neutrinos essentially serves as a modified vacuum (so that background neutrinos do not appear as external lines in Feynman diagrams). Since there is no way to distinguish an emitted neutrino from a neutrino comprising the background, the neutrino propagator is modified in order to account for this ignorance, see [38].

we can write the differential transition rate (i.e. the distribution of electron energies) as

$$\frac{d\Gamma}{dE_e} = \left(\frac{2G_F^2}{\pi^3}\right) E_e\sqrt{E_e^2 - m_e^2}\,(E_0 - E_e)^2\,, \tag{2.4}$$

where G_F is the Fermi constant and $E_0 \equiv m_n - m_p$. To be explicit, since the Q–value[4] is significantly less than the proton mass, we can approximate $E_p = m_p$. Eq. (2.4) is obtained by making this approximation, as well as realizing that $E_0 \ll m_n$ and $m_e \ll m_n$. It is especially worth noting that the defined quantity E_0 for a more general β–decay, given by

$$E_0 = m_{\text{parent}} - m_{\text{daughter}}, \tag{2.5}$$

is essentially a measure of the phase-space energy available to the electron and antineutrino. Furthermore, we see that the transition rate is a function of this phase-space only, and not of the individual masses of the parent or daughter

$$\Gamma\left[E_0\right] = \frac{G_F^2}{30\pi^3}\left[p_0\left(2E_0^4 - 9E_0^2m_e^2 - 8m_e^4\right) + 15E_0m_e^4\ln\left(\frac{E_0 + p_0}{m_e}\right)\right], \tag{2.6}$$

where $p_0 \equiv \sqrt{E_0^2 - m_e^2}$, and the integration of Eq. (2.4) is over the electron's allowed energies, $E_e = m_e$ to $E_e = E_0$. As such, one would suspect that Eq. (2.6) largely accounts for the kinematic dependence of allowed β–decays other than the free-neutron (at least for nuclei with somewhat similar sizes and selection rules).

The next step would be to understand how Eq. (2.6) is affected given an external neutrino field (where g_ϕ^r is non-zero). A good deal of work was done in this regard by our colleague J. Mattes [38], whereby the main approach used was finite temperature field theory to compute the modification to the neutrino self-energy (and hence, the projection operator) in the presence of a thermal background. Perhaps the most relevant result of this exploration was the development of the *phase space prescription* as a phenomenological model of neutrino modified decay: under certain restrictive conditions, modifications to β–decay rates are due only to a change in the phase-space of the decay products. That is to say, there are no modifications to the matrix element $|\mathcal{M}|^2$ or the neutrino projection operator.

[4]The Q–value is the kinetic energy available to the decay products.

The relevance of this can be realized by considering Fermi's Golden Rule which expresses the transition rate Γ for a given process as

$$\Gamma = \frac{2\pi}{\hbar}|\mathcal{M}|^2\rho\,, \tag{2.7}$$

where again $|\mathcal{M}|^2$ is the *amplitude* or *matrix element* for the process, and ρ is the available phase space. Ultimately we see that the problem of altering Γ reduces to either a dynamical shift of $|\mathcal{M}|$ or a kinematic shift in the available phase space. One way in which a modification to the phase-space arises is with the presence of an external potential field, the simplest case being a spatially constant spin-independent medium. The interaction energy between an emitted neutrino and the external field, V, will alter the energy available to the decay products, such that

$$E_0 \to E_0 + V. \tag{2.8}$$

That is to say, the presence of a static background serves to shift the Q-value by an amount V. Therefore, we expect the overall transition rate in the presence of this background to shift according to

$$\Gamma\left[E_0\right] \to \Gamma\left[E_0 + V\right]. \tag{2.9}$$

The fractional change in decay rate (given a small interaction energy) can be estimated as

$$\frac{\delta\Gamma}{\Gamma} = \left(\frac{1}{\Gamma}\frac{d\Gamma}{dE_0}\right)\,\delta E_0 \tag{2.10}$$

$$= \frac{1}{\Gamma\left[E_0\right]}\left(\frac{d\Gamma\left[E_0\right]}{dE_0}\right)V. \tag{2.11}$$

There are several remarks that should be made regarding the decay rate modifications presented in this section. For one, the perturbed decay rates are strictly relative to the corresponding rates in the absence of a background field. Therefore, no variation in the measured rate will be observed unless there are *changes* in the background as experienced by the decaying system. Spatial and/or temporal modifications in V are likely expected if the Earth is moving through this particle background.[5] Further-

[5]Also possible, the density of neutrinos n_ν comprising the field can vary depending on changes in the generation rate from whatever sources the field. For example, neutrino production within the Sun may be sensitive to the solar climate (such as solar flares).

more, it is presumed that only coherent interactions take place between the emitted anti-neutrino and the ambient neutrino background. It would appear that coherence is required to ensure there is practically no alteration in the phase-space trajectory of the background particles, since V is simultaneously shared among a very large number of background particles. Presumably, if this were not the case, a neutrino comprising the background could lose an arbitrary amount of energy after a sufficient number of interactions, giving an implication which would conflict with existing experiments.

2.2 Time–Dependent Decay Parameters

In this section, we step away from first principles and investigate how one might model, macroscopically, the emergence of a time–dependent decay constant λ. On a phenomenological basis, a generic way to investigate the periodicities presented in Table 1.1, as well as a possible influence from neutrinos, is to model the behavior as a modification to the standard exponential decay law, Eq. 1.1, where the decay constant experiences a time–dependent perturbation.[6] That is to say,

$$\lambda = \lambda_0 + \lambda_1 [t] \ , \tag{2.12}$$

where, irrespective of the source of this perturbation, past experimental observations constrain λ_1 to be much less than λ_0, at least for conditions typically encountered in terrestrial experiments.[7] This constraint suggests that it is appropriate to simplify subsequent expressions to lowest order in λ_1/λ_0.

Now, if the perturbation is presumed to arise from a novel interaction with neutrinos, λ_1 will be proportional to (or more generally, a function of) the ambient neutrino flux, which in principle may have contributions from a variety of sources (e.g. Solar neutrinos, CνB relic neutrinos, geologic and atmospheric neutrinos, and reactor-generated neutrinos). Given that the perturbation in decay rates results from

[6]We note that a time–dependence in λ does not necessarily imply a departure from randomness, but rather suggests a deviation in the probability distribution which governs the decay.

[7]One could imagine locations where the ambient neutrino flux, for instance, is significantly larger than that encountered on Earth—such as near or within stellar bodies.

variations in the ambient neutrino field density n_ν, we can define an "effective" total cross-section by expressing λ_1 as

$$\lambda_1 [t] = \sigma_\nu \delta\phi_\nu \ , \tag{2.13}$$

where $\phi_\nu \sim n_\nu/c$ is the flux of ambient neutrinos (which are presumed to be moving at the speed of light). Therefore, this cross section σ_ν is related to the fractional change in the decay rate according to

$$\sigma_\nu = \left[\frac{\lambda_1}{\lambda_0}\right] \frac{\lambda_0}{\delta\phi_\nu} \ . \tag{2.14}$$

As an aside, we note there are perhaps two rather different interpretations in the meaning of Eq. (2.12). Since in practice we can never completely "shut off" the flux of neutrinos incident on a decaying system,[8] Eq. (2.12) could be thought by some to represent a radical shift from the long-held paradigm that radioactivity is a random process. That is to say, each and every decay is the result of an *external interaction* with a neutrino as opposed to an *internal transition* (spontaneous event). In this context, the constant piece of Eq. (2.12), λ_0, would emerge from the baseline flux of neutrinos, and $\lambda_1(t)$ would represent fluctuations about this baseline. The immediate implication being that if somehow the ambient neutrino flux could be turned off, an unstable sample of radioactive nuclei would never decay ($\Gamma \propto \phi_\nu$).

The more plausible interpretation (and in accord with the discussion presented in Sec. 2.1) is that Eq. (2.12) represents a generalization to (rather than a replacement of) the decay process which contains both spontaneous (random) decay, characterized by the λ_0 term, and stimulated decay, represented by the new term λ_1. With this view, an unstable sample will decay, although perhaps at a different rate, even in the absence of an external field. Consequently, λ_1 may also contain a time–independent contribution to the decay parameter arising from the baseline contribution of the ambient neutrino flux. For clarity, we may want to express λ_1 as:

$$\lambda_1 [t] = l_0 + l(t) \ , \tag{2.15}$$

[8]The baseline flux due to both solar neutrinos and the CνB represents an irreducible component to the terrestrial, ambient neutrino flux.

where l_0 emerges from the irreducible baseline neutrino flux, and $l(t)$ results from the fluctuation about the baseline. The time–independent portion of λ will thus be $\lambda_0 + l_0$, and $l(t)$ represents the strict time-dependence[9] of λ. The additional notation in Eq. (2.15) however is a bit cumbersome, and therefore we will refer to λ_0 as the time–independent portion of λ.

Returning to the more general discussion, we can use Eq. (2.12) to characterize the perturbed system by the differential equation:

$$\frac{dN}{dt} \equiv -\dot{N} = (\lambda_0 + \lambda_1 [t])\, N \,, \tag{2.16}$$

where explicitly, $N(t)$ represents the number of unstable particles surviving to a time t. To the extent that $\lambda_1 [t]$ is known, Eq. (2.16) has an exact solution given by

$$N(t) = N_0 e^{-[\lambda_0 t + \Lambda(t)]} \,, \tag{2.17}$$

where

$$\Lambda(t) \equiv \int_0^t \lambda_1 (t')\, dt' \,, \tag{2.18}$$

and N_0 is the number of activated nuclei in a given sample at $t = 0$. Of course, it is difficult to claim that Eq. (2.17) is exact since little may actually be known regarding the from of $\lambda_1 [t]$. However as we will discuss through various cases below, a lack of exact knowledge of λ_1 does not preclude us from developing experimentally testable predictions.

2.2.1 Periodic Fluctuations

Much attention has been given to the annual periodicity shared by many of the data sets outlined in Table 1.1. In addition, other frequencies have been observed which point toward solar processes, and moreover do not correlate with various environmental conditions. As such, it is useful to develop a model for periodic fluctuations in the decay parameter, which then can be matched to empirical data. To model

[9] Again, we note that the time–dependence need not be explicit but arise from spatial variations in the external field which couples to the decaying system.

a perturbation term λ_1 which has a generic periodic perturbation, it is sufficient to begin with a sinusoidal perturbation, and then to construct more general periodic functions as a Fourier expansion. To this end, we consider a decay parameter $\lambda[t]$ which has a form given by,

$$\lambda[t] = \lambda_0 (1 + \Delta \cos \omega [t - t_0]). \tag{2.19}$$

Explicitly, $\Delta \geq 0$ so that the phase of this perturbation (the time corresponding to when the perturbation is maximum) is set to $t = t_0$. Moreover, we have in mind the situation of small perturbations, and therefore the following condition is expected to be satisfied:

$$\begin{aligned} \frac{\lambda_1}{\lambda_0} &= \frac{\lambda[t] - \lambda_0}{\lambda_0} \\ &= \Delta \cos \omega t \ll 1 \\ \Rightarrow \Delta &\ll 1 \end{aligned} \tag{2.20}$$

In a similar fashion to the previous section, we define $N(t)$ to be the number of active nuclei at time t, which is related to the activated population by

$$-\dot{N} = \lambda_0 (1 + \Delta \cos \omega [t - t_0]) N. \tag{2.21}$$

The solution to this equation has a form given by Eq. (2.17), where $\Lambda(t)$ is

$$\Lambda(t) = -\frac{\lambda_0 \Delta}{\omega} [\sin \omega (t - t_0) + \sin \omega t_0]. \tag{2.22}$$

From this expression, an interesting observation can be made that the phase of $\lambda[t]$ and the measurable quantity, $-\dot{N}$,[10] are not the same. To see this we acknowledge that to first order in Δ, $N(t)$ takes the form

$$N(t) = N_0 e^{-\gamma_0 t} \left[1 + \Delta \left(\frac{\gamma_0}{\omega}\right) \sin \omega t\right], \tag{2.23}$$

where, for simplicity, we have set $t_0 = 0$. Therefore, to first order in Δ, $-\dot{N}$ is given by

$$-\dot{N} = \lambda_0 N_0 e^{-\lambda_0 t} \left[1 + \Delta \left(\cos \omega t + \frac{\lambda_0}{\omega} \sin \omega t\right)\right] \tag{2.24}$$

$$= \lambda_0 N_0 e^{-\lambda_0 t} [1 + \Delta a \cos(\omega t + \phi)], \tag{2.25}$$

[10]Here, we are neglecting the dependence on solid angle, detector efficiency, and other rate-related losses. That is, we assume here that the decay rate of a sample and the count rate measured by a detector are one and the same.

where,

$$a \equiv \sqrt{1 + \left(\frac{\lambda_0}{\omega}\right)^2}, \tag{2.26}$$

and

$$\phi = \arctan\left(\frac{\lambda_0}{\omega}\right). \tag{2.27}$$

Hence, we see that the phase ϕ of the observed count rate depends on the "half-life" of the sample, and therefore may serve as one explanation for differing phases attributed to different isotopes. Figure 2.2 depicts the decay rates, and phase-shifts, for various half-life values.

2.2.2 Case 1: Direct Searches, $N(t) \approx$ Constant

Clearly, the most direct way to search for anomalies in nuclear decay rates is by directly counting the decay products emitted from a radioactive sample. The situation can be simplified significantly if the radioactive sample being observed is sufficiently long-lived that the population of activated nuclei, N, remains practically constant. By *sufficiently long-lived*, we mean that each counting interval[11] and the total duration of experimental observation should be much less than the half-life of the sample being observed. If this condition is met (experimental duration $\ll T_{1/2}$) then the predicted decay rate according to Eq. (2.16) can be given simply as:

$$n(t) = n_0 \left[1 + \frac{\lambda_1[t]}{\lambda_0}\right], \tag{2.28}$$

where $n(t) \equiv -\dot{N}$, and $n_0 \equiv \lambda_0 N_0$ is a constant throughout the experiment, typically referred to as the *initial activity* of the sample.[12]

Many of the isotopes listed in Table 1.1 fall into this category (sufficiently long half-life), and estimates can be placed on λ_1/λ_0 from these experiments—at least for the particular isotopes observed. For the particular case of periodic fluctuations

[11] Of course, there may be a "balancing act" of sorts. This interval needs to be long enough in order to guarantee sufficient statistics, while also short enough resolve time fluctuations in $\lambda_1(t)$.

[12] Strictly speaking, if $\lambda_1[0]$ is non–zero, then $n_0\left(1 + \frac{\lambda_1[0]}{\lambda_0}\right)$ would be the initial activity.

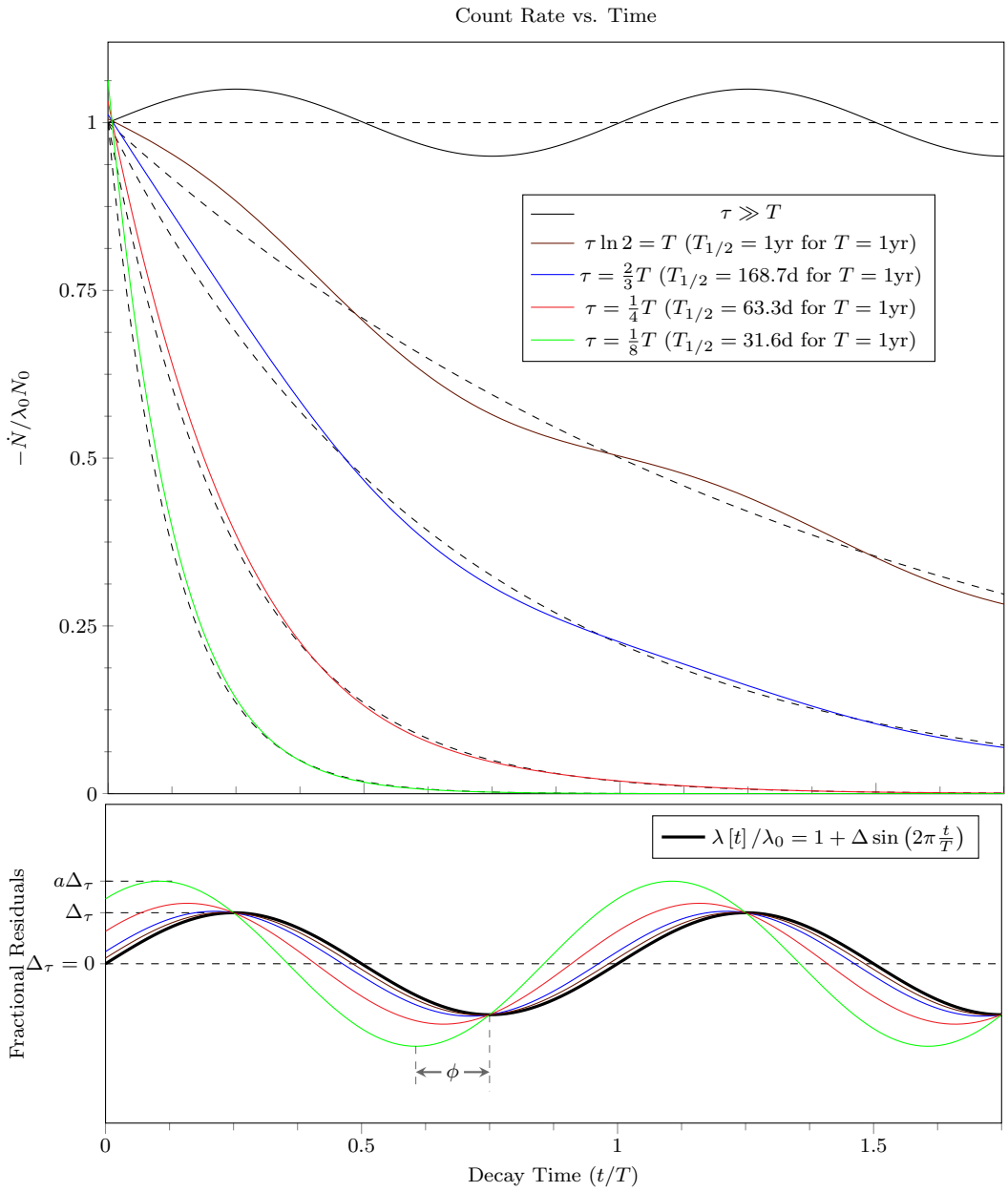

Figure 2.2.: Plot of the decay rate for samples subject to a time-varying decay parameter $\lambda[t] = \lambda_0(1 + \Delta \sin \omega t)$. The phase shift associated with various half-lives is demonstrated in the bottom plot of the fractional residuals.

in $\lambda_1[t]$, for example the apparent annual oscillation, we can express the fractional change in count rate as

$$\frac{\delta n}{\bar{n}} = \frac{\lambda_1}{\lambda_0} \sim \Delta, \tag{2.29}$$

where $\bar{n}$ is the average count rate over the period of oscillation. The typical fractional variations in decay rates (e.g. the amplitudes of annual oscillations) are on the order $\mathcal{O}(10^{-3})$. Therefore, we see that it is possible to determine the effective cross section defined in Eq. (2.14) by measuring the amplitude of oscillation in the count rate, given we have some measure of the variation in particle flux responsible for the oscillation:

$$\sigma_\nu = \Delta \left[\frac{\lambda_0}{\delta \phi_\nu} \right] . \tag{2.30}$$

2.2.3 Case 2: $\lambda_1 [t] \approx$ Constant

Since the prominent anomaly in decay rates appears to be annual (or other periodic) fluctuations, we can also consider the specific case for isotopes which are extremely short-lived when compared with a yearly period ($T_{1/2} \ll 1$ yr).[13] For such a case, the variation in $\lambda_1 [t]$ throughout the counting experiment is negligible, and thus we can approximate λ_1 as constant, i.e. $\lambda_1 [t] \approx \lambda_1 [t_s]$, where t_s indicates the starting point of the experiment. With this condition met, Eq. (2.16) reduces to the standard decay equation with a decay constant of $\lambda_{t_s} \equiv \lambda_0 + \lambda_1 [t_s]$. Consequently, the decaying system will be governed by a standard exponential decay rate given by:

$$n(t) = n_0 e^{-\lambda_{t_s} t} . \tag{2.31}$$

Specifically, in the case where $\lambda [t]$ takes the form in Eq. (2.19), we would expect the determined half-life for a short lived sample to take the form

$$T_{1/2} [t_s] = T_{1/2} [1 - \Delta \cos \omega (t_s - t_0)] , \tag{2.32}$$

where again, t_0 corresponds to when λ is a maximum.

There are several advantages to this situation. 1) The decay rate follows the familiar exponential decay law, despite the time–dependence of λ_1 which in general may produce a significant departure from the standard decay law. By retaining the

[13] More generally, we can think of conducting counting experiments on isotopes with half-lives significantly shorter than a day for instance, in order to address the other periodicities noted in Table 1.1.

form of exponential decay, the concept of *half-life* still has a well-defined meaning. Accurately determining the the decay constant λ or the half life $T_{1/2} = \ln 2/\lambda$ of a short-lived sample is readily accomplished. 2) The effects from "backgrounds" in the counting experiment are more manageable to deal with. By that we mean that even if environmental factors and background contributions vary throughout the year, presumably these effects are relatively constant for the much shorter experimental duration. Following a radioactive sample for many half-lives with successive counting is more tractable if these spurious effects are stationary—since it is not directly the count rate which is of interest, rather how the count rate decays in time.

There are two time scales of relevance to this particular case. The first is the time it takes for the activity of the sample to effectively decay away (the time scale here is on the order of the mean lifetime $\tau = 1/\lambda_{t_s}$ or half-life of the nuclide). The other relevant scale is the period of time in which $\lambda_1[t]$ is expected to vary significantly. From the periodicities noted in Table 1.1, we can take this length to be of the order of days or months, possibly up to a year. Therefore, the time at which the experiment is conducted (the value t_s we ascribe to λ) should be recorded with this latter scale in mind.

An experiment which is currently underway exploits the case discussed above. The experiment consists of irradiating several short-lived isotopes on a regular basis and subsequently tracking their decay in order to determine the half-lives repeatedly throughout the year. If an annual variation in λ exists, then one would expect a sufficient set of data points (of the form (t_s, λ_{t_s}) for example) to exhibit this annual signal. Additionally, another experiment [31] was performed which determined the half-life of ^{198}Au on seven distinct occasions and found agreement between half-life determinations within a relative precision of 10^{-4}.

2.2.4 Case 3: Indirect Searches, $\Lambda \gg 1$

An interesting observation can be made if we re-write Eq. (2.17) in a slightly different form

$$N(t) = N_0 e^{-\lambda_0 \left[t + \Lambda'(t)\right]} , \tag{2.33}$$

where

$$\Lambda'(t) = \frac{1}{\lambda_0} \int_0^t \lambda_1(t')\, dt' . \tag{2.34}$$

What Eq. (2.33) demonstrates is that we could effectively treat the perturbation to the decay rate as a *shift in time*[14]. That is to say, the population of activated nuclei can be expressed as

$$\tilde{N}(s) = N_0 e^{-\lambda_0 s}, \tag{2.35}$$

where $s \equiv t + \Lambda'$, and we stress that $\tilde{N}(s) \equiv N(t - \Lambda')$ is *not* the same function as $N(t)$. Now of course, this redefinition of the "starting time" continually migrates as the sample ages, since Λ' is a function of t. The conclusion would seemingly be that such an effect would be noticed if the migration were too rapid. However, in the context of astrophysics (and in particular, the aging of stars), this shift of t_0 may only be noticeable on cosmological time-scales.

In a simple model, one could determine the age of a star t_{star} by studying high-resolution measurements of emission spectra. The concentrations of various isotopes can be determined from the width of certain absorption lines. Presumably, one can estimate the initial concentrations of these elements, and the age of the star would be determined from the standard exponential decay law, Eq. (2.35). However for non-zero Λ, what is actually computed differs from the true age of the star according to

$$T = t_{\text{star}} + \Lambda'(t_{\text{star}}) , \tag{2.36}$$

where T denotes the computed age. The implication of this is that it may be possible to significantly overestimate (if $\Lambda > 0$) the age of the star. It is a curious observation

[14]Here, it is particularly explicit that the decaying particles are *not* memoryless, since all past information is stored within Λ.

that the ages of stars determined in this manner do in fact tend to give estimates which are on the high end—that is, as large or larger than the age of the Universe as determined through cosmological methods.

As this case is developed further, a key question is how discrepant can T be from the true age $t_{\rm star}$? In *case 1* we mentioned the periodic nature of λ_1. Clearly, if λ_1 is limited in form to periodic functions, then the integrated effect on Λ may in fact be negligible. Indeed, this is easily seen by rewriting Eq. (2.36) as

$$T = t_{\rm star}\left[1 + \frac{\bar{\lambda}_1}{\lambda_0}\right] \ , \tag{2.37}$$

where $\bar{\lambda}_1$ is the timed-averaged value of λ_1 over the life of the star. If we presume, however, that $\lambda_1 \propto \phi_\nu$, or more precisely that $|\lambda_1|$ and ϕ_ν are positively correlated, then it becomes plausible that regions with extreme neutrino densities (e.g. proximity to the neutrino production zones within a star) will have significantly larger values of λ_1. It therefore seems possible that significant error can be introduced into age determinations.

A final comment regarding this, which will be addressed further in later work, is that there may be a concern with the determination of the initial isotope concentrations mentioned above. In particular, one method to estimate the initial concentrations of various elements that form a star is by studying the initial generation of such elements in supernovae explosions. Since a supernova also produces an extreme concentration of neutrinos, it would stand to reason that the production of various radioactive isotopes may be altered at the outset, and therefore incorrect age determinations of stars could result from a misunderstanding of initial isotopic concentrations.

2.2.5 Case 4: Self–Induced Decay, $\lambda_1[t] \propto \dot{N}$

The final case of self–induced decay will be the focus of Ch. 3, however we will give a preliminary treatment here for completeness. In Sec. 2.1, we did not focus on a particular neutrino species. However, it is interesting to consider what effect

a background field of anti-neutrinos ($\bar{\nu}$) may have on a β–decaying source. If we suppose the effect from $\bar{\nu}$'s on a decaying system is similar[15] to the proposed effect from ν's, then it becomes plausible that a sample undergoing β–decay may in fact be able to affect its own rate of decay. Specifically, those atoms which have yet to decay will be bathed in a flux of $\bar{\nu}_e$'s which arise from the decaying atoms within the sample. This *self–induced decay* (SID) effect will likely only be manifest when a sufficiently large internal $\bar{\nu}$ flux is generated. Intuitively, we would expect the magnitude of this effect to be directly dependent on the activity of the sample ($\propto \dot{N}$) but also on the geometry of the sample[16], as well as on the parameters governing the fundamental interaction.

Before we continue, we note that a previous case (*Case 2*) is complicated somewhat by the possibility of a SID effect. Such an effect will preclude the assumption that λ_1 does not vary substantially throughout the lifetime of the sample. That is to say if $\lambda_1 \propto \dot{N}$, then obviously (for short-lived isotopes) there will never be the situation in which this perturbation is approximately constant throughout the duration of the experiment. Therefore, in performing an experiment suggested in *Case 2*, either the initial activity needs to be small enough that λ_1 is still dominated by the $\nu_{\odot}$ flux or the situation will need to be generalized to account for the potential SID perturbation.

2.3 Concluding Remarks

Ultimately, what remains to be done is an investigation for a suitable parametrization of this phenomenological model. Once the key ingredients have been sufficiently defined, only then, can experimental results be used effectively to narrow the "phase space" to an appropriate model. The various cases presented in Sec. 2.2 provide some structure to how this investigation could proceed. *Case 1* is by far the most direct method of observing variations in the decay parameter, and the initial set

[15]For example, g_{ϕ}^{ν} may be comparable to $g_{\phi}^{\bar{\nu}}$.

[16]The $\bar{\nu}_e$ flux at any particular location within a sample is dependent on the positions of the other decaying nuclei within the sample. For example, a "sheet" of activated nuclei will have a smaller internal $\bar{\nu}_e$ flux than a sample in the shape of a ball.

of experiments which led our group to investigate this phenomenon fall into this category. Of course, such experiments require years of data collection for a possible signature to emerge and become compelling. This protracted duration introduces concerns regarding long-term detector stability (e.g. possible environmental/seasonal bias in detector response). Perhaps related, the DAMA/LIBRA collaborations in their search for WIMP dark matter have been operating an enormous NaI detector for close to a decade. The periodic signal within the DAMA data is compelling, and has been given significant attention by a broad community. The possibility that DAMA is seeing modulation in the long-lived contaminant ^{40}K, not in a WIMP signal, has been studied by the author and is discussed in Ch. 4.

Case 2 is quite a simple idea which has traditionally not been studied before. The idea of tracking the half life of a short-lived isotope by repeatedly irradiating it and measuring its half-life would seem unnecessary unless one suspected a reason to do so. As it turns out, maintaining access to a reactor to readily activate samples is quite a challenge—at least for an extended period of time. The idea of *Case 3* is a nascent one at best, although perhaps it will be the most illuminating. Time will tell. Finally, *Case 4* has been the most recent area of research by the author and is discussed in more detail in Ch. 3.

3. Self-Induced Decay & Rate-Related Perturbations

The suggestion that a flux of solar neutrinos $\phi_{\nu,\odot}$ can modify the transition probability for an unstable isotope to decay motivates the possibility that a decaying sample, generating its own (anti)neutrino[1] flux, may in fact be able to affect its own rate of decay. Specifically, those atoms which have yet to decay will be bathed in a flux of neutrinos produced from the decaying atoms within the sample. Such an effect would be largest at the time of sample creation when the sample's activity, and hence neutrino generation, is largest. This modification to the decay rate should fall off as $t \to \infty$ since neutrino production is diminished. We will make these statements more quantitative beginning in Sec. 3.2

The initial proposal of this self–induced decay (SID) effect was published in [39]. As a result, a series of experiments were carried out at NIST to test the SID hypothesis [40,41] by comparing the decay rates of ^{198}Au in a thin gold foil, a gold wire, and a gold sphere having roughly the same mass (1 mg) and specific activity. The basis for this comparison was the observation that the proposed SID effect in the spherical sample could be measurably different from that of the foil or wire, in which more neutrinos would presumably leave the sample without significant influence on the decay process. The experimental results published in [40] were inconclusive, motivating a subsequent repetition using a wire in place of the foil [41].

The objective of the present chapter is to develop a formulation of the SID effect that is intended to provide clearer direction for future SID experiments—which in turn may shed light on a possible phenomenological model. In the course of this treatment, the observation is made that the SID behavior is similar in many ways to

[1]For this discussion we have in mind both β^- and electron-capture decay modes—which emit $\bar{\nu}_e$ and ν_e, respectively. For the sake of brevity, we will no longer distinguish between ν_e and $\bar{\nu}_e$, unless it is deemed relevant.

that of typical detector dead-time effects. This similarity, discussed in Sec. 3.5, is a consequence of the fact that detector dead time effects are non–linear in the activity of the sample (or more precisely the count rate),[2] and hence could be conflated with a similar non-linearity arising from the SID effect. In Sec. 3.6, we take as a case study the experiments conducted at NIST, and investigate whether the model adopted for dead-time correction can remove non–linearity which may arise from fundamentally physical, rather than instrumental, origins.

3.1 Detectability of the SID Perturbation

We begin more broadly with the question of viability, where one potentially serious concern is the prior lack of observation. Apparently, the activities achieved in routine metrology are insufficient for producing a measurable SID perturbation, as evidenced by this lack of detection. In one manner, lack of observation is an asset in that it constrains the size of potential SID perturbations, from which we can place an upper bound on proposed coupling strengths. Having said that, and although seemingly unlikely, we bear in mind that observation may have already occurred, but conflated with the systematics of rate-related detector bias.

The outline of this section is based primarily on answering two questions: what activities are required to produce an observable effect, and how feasible is it to achieve these levels of activation?

3.1.1 Criteria for Detectability?

To maximize the likelihood of detection, a sufficiently large internally-generated neutrino flux is necessary. The difficult task, of course, is to determine the criteria for "sufficiently large," without knowledge of an underlying mechanism. Given that the initial impetus for this endeavor was derived from possible interactions with solar

[2]To be explicit, "count rates" refer to the *detected* signal, wheres "event rates" or "transition rates" refer to the *actual* signal. Count rates will depend on a host of factors including detector efficiency, solid angle, Compton effects, pulse degradation, pulse pileup in the ADC, and so forth.

neutrinos, we might expect that a sample needs to generate a neutrino flux on par with the solar neutrino flux, $\phi_{\nu,\odot} = 6 \times 10^{10}$ cm$^{-2} \cdot$ s^{-1}. In other words, although the kinematics are likely different, we suppose here that the dynamics (across the various neutrino species) are essentially the same for the proposed influences of solar neutrinos and internally-generated neutrinos on a decaying sample. Then under this assumption, a generated flux similar in magnitude to $\phi_{\nu,\odot}$ could exhibit an experimentally detectable deviation in its decay rate. Furthermore, since observation cannot be done in isolation from the irreducible solar neutrino background, it is likely required that this generated flux be significantly greater than $\phi_{\nu,\odot}$— thereby ensuring the dominant perturbation is SID related.

It is perhaps surprising that an internal neutrino flux, ϕ_ν, higher than $\phi_{\nu,\odot}$ is even achievable for modest-sized samples. To demonstrate this, consider a sample containing a population of N unstable nuclei, with a volume V, and surface area S. We can define the average neutrino flux through the surface of the samples as

$$\phi_\nu = \frac{\lambda N}{S}, \tag{3.1}$$

where it is assumed that the activity of the sample, λN, is also the neutrino production rate. This can be expressed in terms of the relative fraction of the number of activated nuclei to activated+stable nuclei, ϵ, as

$$\phi_\nu = \epsilon\lambda \left[\frac{\rho N_A}{m_A}\right] \left[\frac{V}{S}\right], \tag{3.2}$$

where ρ is the mass density of the sample, m_A is the isotope's atomic (molar) mass, and N_A is Avogadro's number. It is instructive to parse Eq. (3.2) into three distinct blocks. The first quantity $\epsilon\lambda$ happens to be a direct measure of the production rate achievable in a given reactor—a fact which is developed in the subsequent section. The middle factor $\rho N_A/m_A$ is simply the atomic number density of the isotope, which for a homogeneous sample in a condensed state is typically on the order of 10^{22} cm^{-3}. The final geometric factor,[3] V/S, clearly represents the scale or size of the sample.

[3]It is more appropriate to take for this term the geometrically averaged V/S ratio for the sample. Nevertheless, this expression still takes into account "zeroth" order dependence on geometry—insofar as a "flatter" sample of the same volume admits a smaller flux.

As an example, a spherical sample of gold with a radius of $R = 0.1$ mm and relative fraction 1×10^{-4} of ^{198}Au to ^{197}Au will produce a neutrino flux through its surface of

$$\begin{aligned} \phi_{\nu,\mathrm{Au}}|_{r=R} &= \epsilon \lambda_{198\mathrm{Au}} \left[\frac{\rho_{\mathrm{Au}} N_A}{m_{\mathrm{Au}}} \right] \left[\frac{R}{3} \right] \\ &\approx \epsilon \times 10^4 \times \phi_{\nu,\odot} \\ &= \phi_{\nu,\odot}, \end{aligned} \tag{3.3}$$

where $\lambda_{198\mathrm{Au}} = 3 \times 10^{-6}$ s^{-1}, $\rho_{\mathrm{Au}} = 19.3$ g $\cdot$ cm^{-3}, and $m_{\mathrm{Au}} = 197$ g $\cdot$ mol^{-1}. For this sample, a relative fraction of $\epsilon = 1 \times 10^{-4}$ is necessary to achieve a flux as large as $\phi_{\nu,\odot}$. It is possible to achieve this level of activation (albeit marginally) in some neutron activation facilities such as the RT2 facility at the NIST Center for Neutron Research or the High Flux Isotope Reactor (HFIR) at Oak Ridge National Laboratory.

To illustrate how one could achieve the activities necessary for ϕ_ν to be greater than the solar flux, and to establish the framework necessary for generalization to account for the SID effect, we turn briefly to the anthropogenic production of radioactive isotopes by neutron activation.

3.1.2 Activity Production by Neutron Irradiation

Suppose we start off with a collection of N_0 target nuclei which we place in a reactor that generates a thermal neutron flux of ϕ_n. Furthermore, we assume that the N_1 nuclei that are formed by neutron capture are unstable and decay with a decay parameter λ to a daughter population of N_2 (refer to the illustration in Fig. 3.1). If the neutron capture cross section of the target nuclei is σ_n,[4] then the production rate of the radioactive products can be expressed as

$$R = N_0 \sigma_n \phi_n. \tag{3.4}$$

The population of unstable nuclei, N_1, increases as a result of this production but also decreases as a result of decay. Neglecting the small losses to the N_1 population

[4]For this cross section, it is most appropriate to take the differential cross section integrated over the reactor's energy profile, as often there is a sizable epithermal neutron fluence. Typically, a thermally-averaged cross section $\langle \sigma v \rangle / \bar{v}$ presuming a Maxwell-Boltzmann distribution is quite accurate.

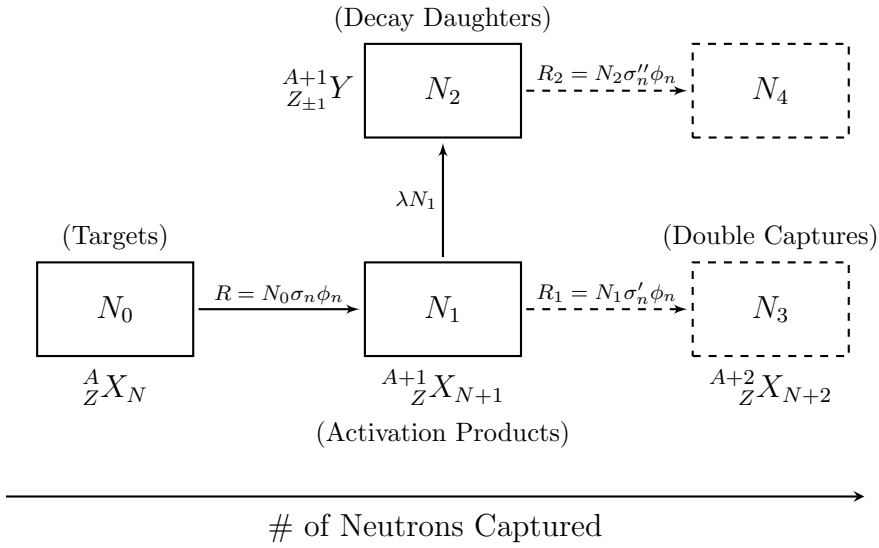

Figure 3.1.: Diagram for isotope production by neutron irradiation. The rate at which an N_i population changes is the sum of the "sources" (inward arrows) minus "sinks" (outward arrows). In particular, the N_1 population sees increases from R and decreases primarily from decay to it's daughter—with additional smaller losses due to the creation of double-capture products.

from double captures, we can express the change in the population of N_1 in a small time interval dt as

$$dN_1 = Rdt - \lambda N_1 dt, \tag{3.5}$$

where λN_1 is the activity of the radioactive sample. Strictly speaking, the production rate R decreases with time since the number of target nuclei, N_0, is depleted as targets are converted. Since the rate of change in number of target nuclei is simply $-R$, the target population decreases in time by a factor of $\exp\left[-\sigma_n\phi_n t\right]$, and thus the production rate as a function of time is

$$\begin{aligned} R(t) &= N_0\left[0\right]\sigma_n\phi_n e^{-\sigma_n\phi_n t} \\ &= R_0 e^{-\sigma_n\phi_n t}, \end{aligned} \tag{3.6}$$

where $N_0\left[0\right] \equiv N_0\left[t=0\right]$ denotes the number of target nuclei at the start of irradiation, and $R_0 \equiv N_0\left[0\right]\sigma_n\phi_n$ denotes the initial production rate when no targets have

been depleted. Using this expression for R in Eq. (3.5), the number of product nuclei N_1 is determined to be

$$\begin{aligned} N_1(t) &= \frac{R_0}{\lambda'}\left[e^{-\sigma_n\phi_n t} - e^{-\lambda t}\right] \\ &= \frac{R_0}{\lambda'}\left[1 - e^{-\lambda' t}\right] e^{-\sigma_n\phi_n t}, \end{aligned} \tag{3.7}$$

where $\lambda' \equiv \lambda - \sigma_n\phi_n$.

While Eq. (3.7) takes into account depletion of the target nuclei, it is still approximate since it neglects such effects as self-shielding and double-capture products.[5] In fact, it is usually reasonable to approximate the number of target nuclei as constant during the time of irradiation. In this case, the expression for N_1 simplifies to the typical form found scattered among the literature:

$$N_1(t) = \frac{N_0\,[0]\,\sigma_n\phi_n}{\lambda}\left[1 - e^{-\lambda t}\right]. \tag{3.8}$$

With this expression, it becomes explicit that the population of activated products eventually *saturates* (i.e. additional irradiation time does not yield a larger activated population). In regard to the previous discussion in Sec. 3.1.1, we find that the relative fraction of activated nuclei, $\epsilon = N_1/N_0\,[0]$, is constrained by

$$\epsilon \lesssim \frac{\sigma_n\phi_n}{\lambda}. \tag{3.9}$$

Furthermore, it is evident that the factor of $\epsilon\lambda$, in the expression for ϕ_ν, is a direct measure of a reactor's ability to activate the sample.

For perspective, the RT2 facility [42] at NIST produces a thermal neutron flux of $\phi_n = 3.1 \times 10^{13}$ cm$^{-2} \cdot$ s^{-1}, which is on the higher end of neutron fluence rates compared with typical facilities. Thus, for nuclei with neutron capture cross sections on the order of barns (10^{-24} cm^2), we can expect $\sigma_n\phi_n$ to be on the order of 10^{-11} s^{-1}. In the example of the ^{198}Au sphere, the RT2 facility could yield a relative fraction of at most $\epsilon = 1.0 \times 10^{-3}$, suggesting that a gold sphere with a radius larger than 0.1 mm would likely be necessary to achieve a neutrino flux larger than $\phi_{\nu,\odot}$.

[5] Accounting for double-capture products is rather straightforward. Since the production rate R_1 of double captures is proportional to N_1, replacing λ with $\lambda + \sigma_n'\phi_n$ in Eq. (3.7) fully accounts for losses from double capture. Clearly, this contribution is small if $N_1 \ll N_0$, but more importantly, double-capture losses are small relative to losses from decay as long as $\sigma_n'\phi_n \ll \lambda$.

3.1.3 Factors Suppressing Activity Production

There are several points which are worth underscoring. It should be stressed that the saturation limit of $\sigma_n\phi_n/\lambda$ overestimates the true limit owing primarily to several factors all conspiring in the same direction: (a) depletion of the target population, (b) production of double-capture products, and (c) diminished neutron fluence on the sample interior due to self-shielding.

(a) Taking into account the decreasing target population, we can calculate the largest size of the N_1 population directly from Eq. (3.7), or equivalently by setting Eq. (3.5) equal to zero. From this, the production limit for the population is determined to be

$$N_{1,\max} = N_0\,[0]\,e^{-\lambda t_S}, \tag{3.10}$$

where the "saturation time" is given by

$$t_S = [\lambda - \sigma_n\phi_n]^{-1} \ln\left[\frac{\lambda}{\sigma_n\phi_n}\right]. \tag{3.11}$$

Thus, we can replace the upper bound on $\epsilon = N_1/N_0\,[0]$ by the expression

$$\begin{aligned} \epsilon\,(t) &\leqslant e^{-\lambda t_S} \\ &= \left[\frac{\sigma_n\phi_n}{\lambda}\right]^{\lambda/\lambda'} \approx \epsilon^*\left[1 - \epsilon^* \ln\frac{1}{\epsilon^*}\right], \end{aligned} \tag{3.12}$$

where $\epsilon^* \equiv \sigma_n\phi_n/\lambda$, and the approximate expression on the right-hand side assumes the condition[6] $\epsilon^* \ll 1$.

(b) Additionally, we can account for double-capture losses by realizing that the rate of these losses is simply the negative of the production rate for double-captures. Thus, the equation governing the growth of the N_1 population becomes

$$dN_1 = Rdt - \lambda N_1 dt - R_1 dt, \tag{3.13}$$

[6]The condition $\sigma_n\phi_n \ll \lambda$ is more than reasonable, especially for the shorter-lived isotopes we will be interested in. Even on the higher end, a value of $\sigma_n\phi_n = 10^{-9}$ s^{-1} corresponds to a half-life of more than 20 years.

where $R_1 = N_1\sigma_n'\phi_n$ is the activation rate expected (for the N_1 population) and σ_n' denotes the neutron-capture cross section for this population. Hence, we see that new governing equation for the N_1 population takes the form

$$dN_1 = Rdt - (\lambda + \sigma_n'\phi_n)\, N_1 dt, \tag{3.14}$$

which is identical to Eq. (3.5) by sending $\lambda \to \lambda + \sigma_n'\phi_n$. Therefore, all subsequent relations derived from Eq. (3.5) can be modified to account for double-captures accordingly. For instance, the equation governing the N_1 population as a function of time, Eq. (3.7), becomes

$$N_1(t) = \frac{R_0}{\lambda''}\left[1 - e^{-\lambda'' t}\right] e^{-\sigma_n\phi_n t}, \tag{3.15}$$

where $\lambda'' \equiv \lambda + \sigma_n'\phi_n - \sigma_n\phi_n$. The modifications to the maximal saturation and saturation time are readily inferred.

(c) It is more cumbersome to address the issue of self-shielding. However, it is directly relevant for experiments designed to exploit geometric differences among samples, since after all, self-shielding effects are highly dependent on geometry. There are two major influences that a sample can have on ϕ_n, both within and around the sample. Materials that are high neutron absorbers (σ_n very large), will observe a decreasing neutron flux deeper into their interior. The other significant factor which decreases the observed neutron flux is scattering. We will return to this issue in Sec. 3.4 when discussing the effect that geometry has on possible SID perturbations.

3.1.4 Discussion

We set out to determine under what conditions a sample can be produced "hot" enough to admit an internally-generated neutrino flux as large as the solar flux. At the limit of saturation, we see that the maximum admitted flux is largely independent of the sample's half-life, and can be expressed as

$$\phi_{\nu,\max} = \sigma_n\phi_n \times [\text{atom density}] \times [\text{sample size}]\,, \tag{3.16}$$

where we have used the fact that $\epsilon^* \lambda$ equals $\sigma_n \phi_n$ in this limit.[7] Moreover, the only parameters that can essentially be "tuned" to increase this ceiling are the size of the sample and the "power" of the reactor used for irradiation:

$$\frac{\phi_{\nu,\max}}{\phi_{\nu,\odot}} \sim \left[\frac{\phi_n}{10^{12}\ \mathrm{cm}^{-2} \cdot \mathrm{s}^{-1}}\right] \times \left[\frac{\sigma_n}{1\ \mathrm{barn}}\right] \times \left[\frac{\text{sample size}}{1\ \mathrm{cm}}\right]. \tag{3.17}$$

Hence, we conclude that it is feasible to produce samples with ϕ_ν comparable to $\phi_{\nu,\odot}$, given the right combination of "strengths" outlined in the factors above.

Having said that, it is not usual for samples to be irradiated long enough for them to approximately saturate. In fact, irradiation times are generally on the order of minutes, whereas product half-lives (and thus saturation times) are usually days or longer. In these situations, we see that the relative fraction of activation products grows linearly in time:

$$\epsilon\,[t] \approx \sigma_n \phi_n t, \tag{3.18}$$

where the condition $t \ll t_S$ allows us to expand the exponential terms to first order. Extending this one step further, a reasonable estimate for ϕ_ν generated from samples irradiated for a duration t_R can be expressed as

$$\phi_\nu\,[t_R] \;\approx\; \sigma_n \phi_n \left[\frac{t_R}{\tau}\right] \left[\frac{\rho N_A}{m_A}\right] \left[\frac{V}{S}\right], \tag{3.19}$$

where $\tau = \lambda^{-1}$ denotes the sample's mean lifetime. For the original example of a 0.1 mm gold sphere, for which $\sigma_n \approx 100$ barns and $t_{1/2} = 64.7$ hrs, we see that it would be necessary to irradiate the gold sphere at the NIST RT2 facility for approximately 12 hours to produce an internal neutrino flux equal to $\phi_{\nu,\odot}$.[8]

This observation somewhat reduces the initial concern raised regarding the prior lack of detection. While it is definitely possible to produce a sample hot enough to generate a neutrino flux larger than the solar flux, it is not something accomplished incidentally. Furthermore, from this discussion it is evident that the levels of activity produced do not depend solely on the production rate, but also on the rate at

[7] It shouldn't be surprising that $\phi_{\nu,\max}$ is independent of the sample's half-life—since in this limit, saturation simply implies that the probability of activation is equal to the probability for decay. What does depend on the sample's half-life is the time necessary for saturation to occur.

[8] Interestingly enough, the maximum permissible irradiation time at NIST's rabbit facility is 6 hours.

which those products decay. It should be stressed that a potential SID perturbation will alter the activities achievable—in that, saturation will occur earlier and with relatively fewer nuclei activated. This alone may point toward an experimentally testable prediction. We will have to account for this by amending the decay term λN_1, for instance in Eq. 3.5, in which the current treatment presumes a constant value for λ.

Finally, it is worth noting that we are not solely interested in achieving a neutrino flux larger than $\phi_{\nu,\odot}$, but in addition we require this flux to change appreciably on short enough time scales to have a measurable effect. Take for example the extreme case of a sample of ^{40}K, which has a half-life of 1.25 billion years. Even if this sample were to generate a neutrino flux many times that of $\phi_{\nu,\odot}$, there would not exist a point of reference to determine if the decay rate were "elevated". There must exist a baseline for comparison. To observe a SID perturbation, it seems necessary to be able to observe a departure from the expected laws governing the size of the activated population. Therefore, we turn now to discuss SID phenomenology and to develop a description of SID-modified decay rates, in part, to address the issues raised here.

3.2 Qualitative Discussion of SID as a Stochastic Process

Our first objective is to model the number of activated nuclei $N(t)$ remaining after a time t, given that the population decays with a perturbation proportional to the density of neutrinos[9] emitted—which we will presume dominates over various contributions from external neutrino sources. Since the population's activity, and hence neutrino generation, decreases with time, the decay parameter takes the time-dependent form

$$\lambda\left[t\right] = \lambda_0 + \lambda_1\left[t\right], \tag{3.20}$$

where λ_0 is the conventional decay constant, and λ_1 is a term proportional to the density of emitted neutrinos. Additionally, the average density of emitted neutrinos

[9]It is not readily evident that the perturbation should be linear in neutrino density. This condition is reasonable if the "range of interaction" is sufficiently shorter than the average neutrino spacing $n_\nu^{-1/3}$. We will address the appropriateness of this when we present a more quantitative discussion.

within the sample is proportional to the decay rate, hence the perturbation in the decay parameter can be modeled by

$$\lambda_1 = -p\dot{N}, \tag{3.21}$$

where, at the moment, p simply represents a dimensionless proportionality constant. In general, Eq. (3.21) could contain additional perturbations arising from external neutrino sources. However, we have mind here the case where the sample's activity is sufficiently large as to overwhelm other possible perturbations. Moreover, shorter-lived isotopes are ideal candidates for two primary reasons. (1) As demonstrated in Sec. 3.1.4, it is more tractable to achieve larger activities for isotopes with shorter lifetimes. (2) In this case, the time–dependence in the decay parameter λ should arise primarily from $\dot{N}$—while other potential contributions (for instance, the yearly fluctuations in $\phi_{\nu,\odot}$) would remain approximately constant during the sample's short lifetime. Hence, with this model for $\lambda_1[t]$ we see that the decaying population of N unstable nuclei is governed by

$$\begin{aligned} -\dot{N} &= \left[\lambda_0 - p\dot{N}\right] N \\ &= \frac{\lambda_0 N}{1 - pN}\ , \end{aligned} \tag{3.22}$$

where it is evident that we recover the expected result ($-\dot{N} = \lambda_0 N$) when the perturbation strength p goes to zero.

Prior to solving for $N(t)$, the difference between exponential decay and Eq. (3.22) warrants a discussion regarding the issue of "randomness" and its role in decay processes. In particular, one concern that is raised by the suggested model pertains to the concept of *memory*, or *independence*. Therefore, we turn now to provide a concise construction of the statistics governing an ensemble of identical, unstable particles. Following from this, we then address self-induced decay processes and ask under what conditions a SID process remains stochastic. Moreover, this treatment will set the stage for analyzing counting effects and detector dead-time in Sec. 3.5, which rely on the distribution of time intervals between successive decay events.

3.2.1 Exponential Decay as a Stochastic Process

Exponential decay is the hallmark of unstable systems, observed broadly in all fields of science. In physics, decays are indeed ubiquitous, and here the exponential decay law has two distinct (albeit, often conflated) meanings. (1) The survival probability for a *single* unstable particle is expected to decay exponentially[10] in time. This should be understood as an exponential distribution of "times until decay" for a large ensemble of *single*-particle systems. (2) Alternatively, one could study a single system containing many identical, unstable particles. Here, the fraction of "survivors" remaining in this system at a time t admits an exponential decay law. The distinction between these two situations is often ignored, justifiably, given the fact of independence: the status (*not* decayed or decayed) of one particle has no bearing on the probability of another to decay. The very nature of "self-induced" decay challenges the notion of independence. As such, we will maintain this distinction proceeding henceforth.

We begin by first determining the probability for one unstable particle to survive through a time t. Given that Γ is the transition rate for the particle, then $\Gamma\delta t$ clearly denotes the probability that the particle will decay in the small time interval δt. Moreover, the quantity $1-\Gamma\delta t$ represents the probability that the particle survives during this short interval. In order for the particle to survive for the longer interval t, it must survive for each of the small intervals that subdivide t. Therefore, we can approximate the particle's survival probability for a length of time t as

$$P_\Gamma(t) \approx \prod_{\delta t_i \in t} (1-\Gamma\delta t_i) \ , \tag{3.23}$$

where the product is taken over all the sub-intervals whose union is t. The expression becomes exact in the limit that the measure of each δt_i sub-interval goes to zero. A trivial way to subdivide t is to partition it into m intervals of equal length $\delta t = t/m$,

[10]It has long been known that this law is not fully consistent with quantum mechanics—where departure from exponential decay is expected at very short as well as long times. One consequence of this is the prediction of the so-called quantum (anti)Zeno effect, in which the rate of decay is (increased)decreased by high-frequency successive "measurements."

so that all the terms in the product are identical. Now it becomes clear that $P_\Gamma(t)$ takes the form

$$P_\Gamma(t) = \lim_{m\to\infty}\left[1 - \frac{\Gamma t}{m}\right]^m = e^{-\Gamma t}. \tag{3.24}$$

Furthermore, it may be the case that the unstable particle has several independent modes by which it can decay. Given that the unstable particle has j distinct decay modes, with corresponding transition rates $\Gamma_1, \Gamma_2, ..., \Gamma_j$, the total survival probability becomes

$$\begin{aligned} P(t) = \prod_i P_{\Gamma_i}(t) &= e^{-(\Gamma_1+\Gamma_2+...+\Gamma_j)t} \\ &= e^{-\lambda t}, \end{aligned} \tag{3.25}$$

where the well-known decay constant is given by $\lambda \equiv \Gamma_1 + ... + \Gamma_j$. Incidentally, the quantity $f_{\Gamma_i} \equiv \Gamma_i/\lambda$ is referred to as the branching fraction for the i–th decay mode.

This expression for the survival probability allows us to determine the differential probability $P_e(t)\,dt$ for the particle to decay in the subsequent interval from t to $t+dt$, which is given by $P(t)\,\lambda dt$. Hence, the probability density function (PDF) governing the "time until decay" is given by

$$P_e(t)\,dt = \lambda e^{-\lambda t} dt. \tag{3.26}$$

Explicitly, for a large ensemble of single-particle systems, the distribution of survival times is given by $P_e(t)$. Consequently, from this distribution the *mean lifetime* of the particle can be determined from the expectation value of survival times: $\langle t\rangle \equiv \tau = 1/\lambda$. Moreover, $P_e(t)$ can be used to construct the statistics governing a collection of unstable particles. In particular, it is well known that a Poisson process can be defined as a stochastic counting process with an exponential distribution of time intervals between events (decays). We will utitlize this fact when discussing the issue of coincidence summing in counting experiments.

It should be explicit where the concept of independence arises thus far. For instance, in Eq. (3.25) we utilize the fact that the various modes of decay are *mutually exclusive*—in that a particle cannot decay one route if it has already decayed by another. That is to say, the Γ_i's represent independent avenues for transitioning. Hence,

the overall probability to survive decay is the product of the survival probabilities for each mode[11]. More relevant for this discussion is the role that independence has when considering an ensemble of many unstable particles. For a single system that initially contains N_0 unstable particles, the expected number of survivors at a later time t is given by

$$N(t) = \sum_{i=1}^{N_0} P_i(t), \tag{3.27}$$

where $P_i(t)$ represents the survival probability for the i–th particle. If all of the unstable particles are identical to one another, then it must be the case that they have the same probability to survive, $P(t)$. Thus, the fraction of particles surviving until a time t is given by

$$\frac{N(t)}{N_0} = P(t). \tag{3.28}$$

Having said that, the requirement that each particle is "identical" is not sufficient to equate $P(t)$ with the quantity $\exp[-\lambda t]$. It must also be true that the probability for a particle to decay is unaffected by the particle's "environment" (i.e. the presence of the other particles). Almost by definition, a self-induced decay process violates the latter requirement. A consequence of this, which we will return to later, is that the self-induced decay process can no longer be described by a Poisson process.

3.2.2 Generalization to SID Processes

To demonstrate the issue raised above, it is particularly instructive to express the perturbation term λ_1 as a function of N, as opposed to $\dot{N}$. From inspection of Eq. (3.22), it is rather straightforward to see that λ_1 can be written as

$$\lambda_1[N] = \lambda_0 \left[\frac{pN}{1-pN}\right]. \tag{3.29}$$

Thus, instead of regarding the perturbation as time-dependent, we can regard λ_1 as arising from the presence of additional particles. From this perspective, it follows

[11] Equivalently, the probability for a particle to decay in a short time interval, dt, is the sum of the transition probabilities for the individual modes available: $(\Gamma_1 + ... + \Gamma_j)\, dt$.

that the transition probability for a single (isolated) unstable particle remains λ_0. Whereas, in the presence of N other particles, the perturbation to that particle's transition probability becomes $\lambda_1[N]$. Of course, the same is true for any particle in the system. Consequently, the survival probability as defined in Eq. (3.28) will no longer be given by an exponential distribution.

Nevertheless, following the development of the preceding section, we can still regard λdt as the probability for an unstable particle to decay within a small dt time interval. As such, it is reasonable to interpret $\lambda_1 dt$ as the probability within this time for an unstable particle to decay via a self-induced process. In other words, the probability for an atom to decay is the sum of the two distinct mechanisms through which the decay can occur: a *spontaneous* decay ($\lambda_0 dt$), or an *induced* decay ($\lambda_1 dt$). In this context, the constant of proportionality p in Eq. (3.21) can be regarded as a differential probability (i.e. probability per emitted neutrino per unstable particle) for inducing a decay,[12] since $-\dot{N}dt$ is the approximate number of neutrinos emitted in time dt. Then, for a population of N activated atoms, pN represents the probability per neutrino to induce decay.

Given this interpretation for p, we very well could have constructed Eq. (3.22) simply by adding up all of the decays expected within a short time interval, dt, through the distinct ways a decay can occur. Since there are $\lambda_0 N dt$ decays expected to occur spontaneously, there will also be this many neutrinos available to stimulate additional events. With pN representing the probability to induce decay per neutrino, $\lambda_0 N dt\,[pN]$ is the expected number of stimulated decays. However, these induced decays, in turn, produce additional neutrinos—for which $\lambda_0 N dt\,[pN]^2$ decays are expected. The pattern continues since at each stage the additional decays in turn generate neutrinos. Therefore, we can express the total number of expected decays per unit time as

$$-\dot{N} = \lambda_0 N + p\lambda_0 N^2 + ... = \lambda_0 N \sum_{j=0}^{\infty} (pN)^j \,, \tag{3.30}$$

[12]It may be that p is negative, in which case, $-p$ is the differential probability of inhibiting a decay. We will assume a positive value for p, but the treatment for negative p can be readily inferred.

where the right-hand side is readily identified with Eq. (3.22), given that $pN < 1$.

3.2.3 Interpreting the Parameter p

From the treatment thus far, it is evident that the quantity p only appears coupled with N. Moreover, from the expression for $\lambda_1[N]$ in Eq. (3.29), it is evident that quantity pN represents the fractional change to the decay rate, as defined by λ_1/λ. Thus, at the outset of a counting experiment the quantity $\kappa \equiv pN_0$ represents the initial (and consequently, the largest) fractional change to the decay rate—suggesting that κ is a likely candidate to be experimentally measurable.

Although it may appear that something pathological occurs when $pN = 1$, it should be evident that this condition can never be realized. That is to say, any process implemented to increase N has to compete with SID processes which grow stronger as N increases. As an example, we can return to the discussion of producing activity by neutron irradiation. Since the activated nuclei in the sample subsequently decay, there is a saturation limit on the number of targets that can be activated. This limit is reached when the decay rate of the sample equals the activation rate of the reactor (refer to Fig. 3.2). If the sample being irradiated decays according to Eq. (3.22), we see that saturation will occur for a population of activated nuclei N that is strictly less than $1/p$. It would appear that "higher–order SID processes" may only have significant influence on the decay rate under extreme conditions which are not typically met by a conventional reactor. In this event, we can approximate the contribution from SID processes by retaining a finite number of terms in Eq. (3.30). For example, retaining only the first two terms, Eq. (3.22) has an approximate form given by

$$-\dot{N} = \lambda_0 N(t)\left[1 + pN(t)\right]. \tag{3.31}$$

This approximation, initially valid for $\kappa \ll 1$, becomes increasingly more accurate at later times, since all higher order corrections fall off more rapidly.

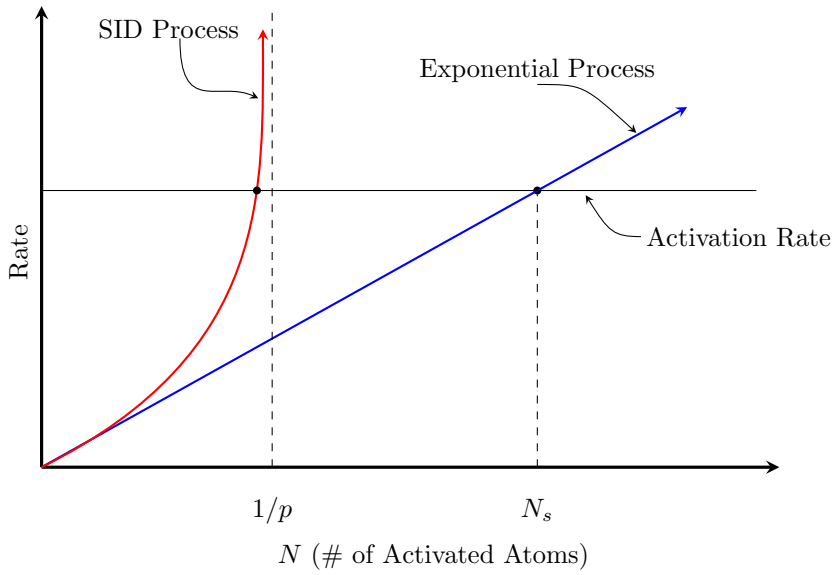

Figure 3.2.: Depiction of *secular equilibrium* for a sample exhibiting SID behavior (red) and a sample undergoing standard exponential decay (blue). For a given activation rate R, saturation occurs with *fewer* activated nuclei for the SID process.

As a final remark, the description of p as a differential probability indicates that p is related to a total *cross section*, of sorts. Thus, understanding the structure of p as it relates to more fundamental parameters would allow for calculations from a possible theory to be matched with the experimental quantity κ. To demonstrate the connection between p and a proposed interaction cross section σ_ν, we can relate the induced decay rate $\lambda_1 N$ to an interaction rate:

$$\begin{aligned} \lambda_1 N &= p\dot{N}N \\ &= N\sigma_\nu\phi_\nu. \end{aligned} \tag{3.32}$$

Explicitly, the quantity $N\sigma_\nu\phi_\nu$ represents the interaction rate for a neutrino flux ϕ_ν incident on N targets (which in this case is given by the number of unstable nuclei), with an interaction cross section σ_ν. Now, approximating the neutrino flux to be

given by the activity of the sample divided by the sample's surface area S, we can establish a relationship between p and σ_ν by

$$\begin{aligned} pN\dot{N} &= \sigma_\nu N\phi_\nu = \sigma_\nu N\left[\frac{\dot{N}}{S}\right] \\ &\Rightarrow \quad p = \frac{\sigma_\nu}{S}. \end{aligned} \tag{3.33}$$

This zeroth order approximation may or may not be sufficient, however, the geometric dependence of ϕ_ν is entirely lost by such a low resolution approach. As such, we turn now to present a more quantitative formalism of SID processes.

3.3 SID Phenomenology: A Quantitative Discussion

In order to make the discussion of Sec. 3.2 more quantitative, the first objective is to determine the number of active nuclei remaining at a time t, given that the population decays according to Eq. (3.22). This will provide us a functional form for the survival probability related to SID processes, which we will use to generalize the treatment and to ascertain possible experimental implications.

3.3.1 Exact Solution for $N(t)$

Supposing that their are N_0 active nuclei at $t = 0$, the separable differential equation, Eq. (3.22), admits an implicit relation for $N\,(t)$ of the form

$$N\,(t)\,e^{-pN(t)} = z_0 e^{-\lambda_0 t}, \tag{3.34}$$

where the condition that $N\,(0) = N_0$ requires that $z_0 = N_0 \exp\left[-pN_0\right]$. Now, with the assumption that pN is small, there are indeed many ways in which to approximate N. However, it is evident that we can express $N\,(t)$ exactly[13] by appropriately choosing a branch of the inverse relation determined from the complex function $f(z) = z\exp\left[z\right]$. On the real line there are two branches, W_0 and W_{-1}, defined from the equation

$$z = W\,(z)\,e^{W(z)}. \tag{3.35}$$

[13]By "exact", we mean an exact solution to the model presented—a model which may only approximate the true behavior.

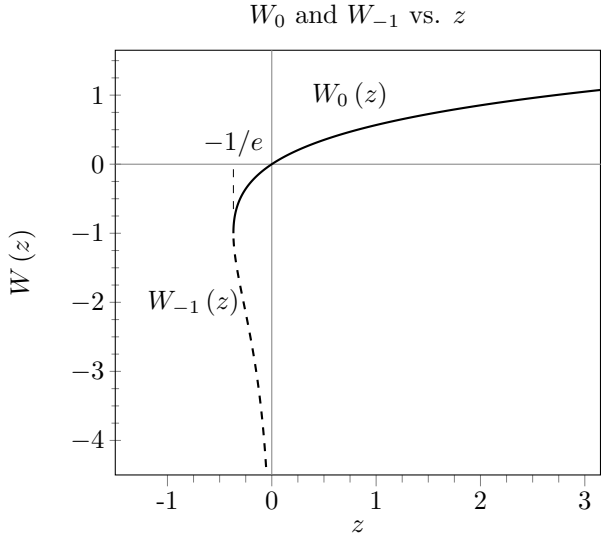

Figure 3.3.: The two real branches of W. The principal branch W_0 (solid curve) is defined on the domain $(-1/e, \infty)$. Whereas, the W_{-1} branch (dashed curved) tends to $-\infty$ as $z \to 0$, with a domain $z \in [-1/e, 0)$.

It follows from the properties of $f(z)$ that W has a branch cut occurring at $W = -1$, since for this value $f'(z)$ vanishes. The principal branch, W_0, is chosen to include $z = 0$ in its domain. For our system it is worth noting that the branch cut occurs for $pN = 1$, thus requiring all physical solutions to lie on the same branch.[14] The two branches are shown in Fig. 3.3.

From the comparison of Eq. (3.34) with Eq. (3.35), it is evident that we can make the following identifications

$$z(t) = -pN_0 e^{-pN_0} e^{-\lambda_0 t} \qquad W_0 = -pN(t), \tag{3.36}$$

where the principal branch W_0 is chosen so to satisfy the necessary condition that $N \to 0$ as $t \to \infty$. Thus, we arrive at an expression in terms of W_0 for the number of nuclei surviving until a time t, which is given by

$$N_p(t) = \frac{N_0}{\kappa} W_0\left(\kappa e^{\kappa} e^{-\lambda_0 t}\right), \tag{3.37}$$

[14]Incidentally, the Lambert W function, as it is known, describes a variety of physical systems, such as fluid and particle flows. In the case of the *Richards* Equation, both branches are physically meaningful: corresponding to capillary rise (W_0) and infiltration (W_{-1}).

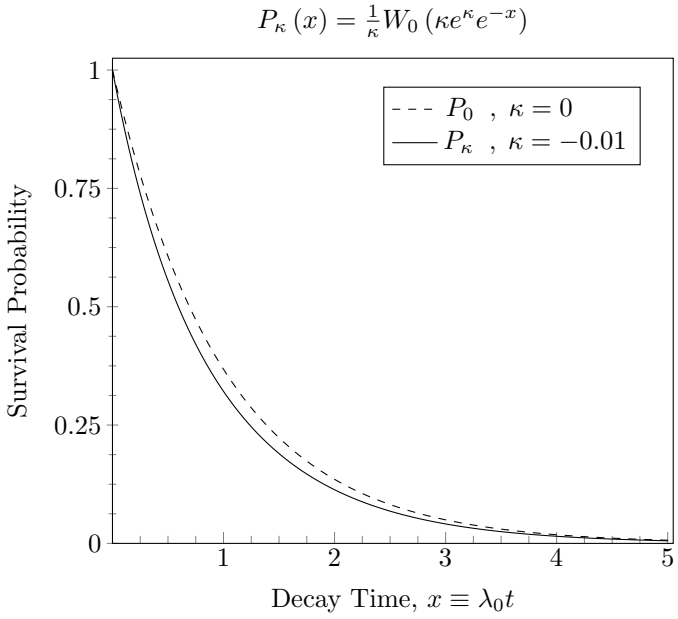

Figure 3.4.: The survival probabilities for a SID process (solid curve), with $\kappa = -0.01$, and an exponential (dashed curve) decay process.

where $\kappa \equiv -pN_0$. Moreover, retaining the definition for the survival probability defined in Sec. 3.2.1, we can express this probability for a SID process as

$$P_\kappa(t) \equiv \frac{N(t)}{N_0} = \frac{1}{\kappa} W_0\left(\kappa e^{\kappa} e^{-\lambda_0 t}\right). \tag{3.38}$$

With this expression, it is evident that the "memoryless" feature of the exponential distribution is no longer applicable to SID processes. That is to say, while exponential decay requires only one parameter (λ_0) to specify the distribution, SID processes require two parameters (λ_0 and κ) to describe the evolution of a system uniquely. Furthermore, since $\kappa = -pN_0$, one could argue that the system retains information about it's status at "$t = 0$" as it evolves to a later time t. As an illustration, a plot of P_κ (for $\kappa = -0.01$) is presented in Fig. 3.4 for several mean lifetimes. Additionally, in Fig. 3.5, the evolution of P_κ for early times is depicted for various values of κ.

For the sake of compactness, we have absorbed the negative sign into the definition of κ. Nevertheless, it should be stressed that a positive value for p corresponds to a negative argument for W_0. Moreover, for $p > 0$, the argument $z(t)$ ranges from the

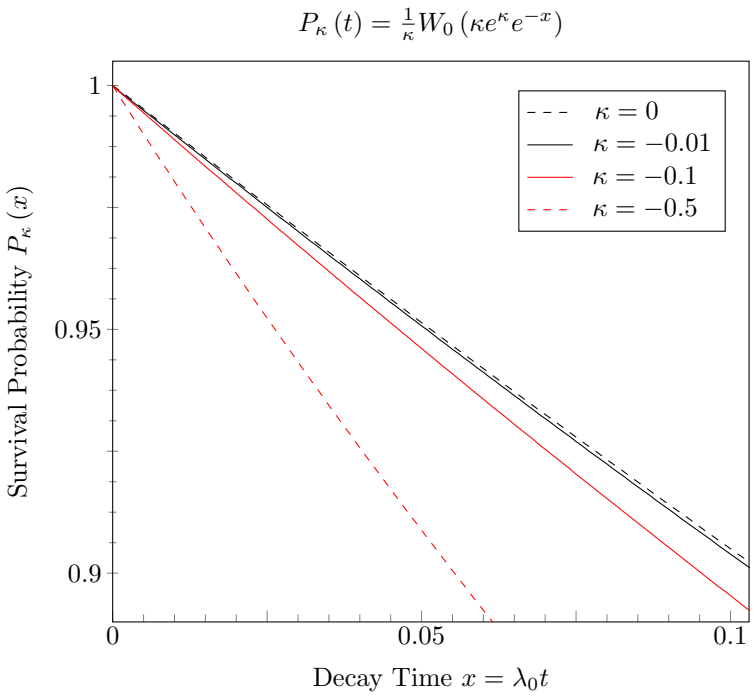

Figure 3.5.: Survival probabilities as a function of the particle's mean lifetime for various values of κ. Exponential decay (dashed black) corresponds to the value $\kappa = 0$.

value of $z = \kappa \exp[\kappa]$ for a time $t = 0$, to the value $z = 0$ as $t \to \infty$. The value of $pN_0 = 1$, which corresponds to $\kappa = -1$, is the limit point for the domain of W_0. In either the case of negative or positive value for p, the evolution of the system is towards $z = 0$. As such, an expansion about $z = 0$ is useful to demonstrate that the system approaches an exponential distribution for later times (large t), and also for smaller perturbations, p.

3.3.2 Small Perturbations or Later Times

We can expand W_0 about $z = 0$ by making use of the *Lagrange inversion theorem*,

$$\begin{aligned} W_0(z) &= z - z^2 + ... \\ &= \sum_{n=1}^{\infty} \frac{n^{n-1}}{n!} \left[\kappa e^\kappa e^{-\lambda_0 t}\right]^n, \end{aligned} \tag{3.39}$$

where, to be explicit, we use the expression in Eq. (3.36) for $z(t)$.

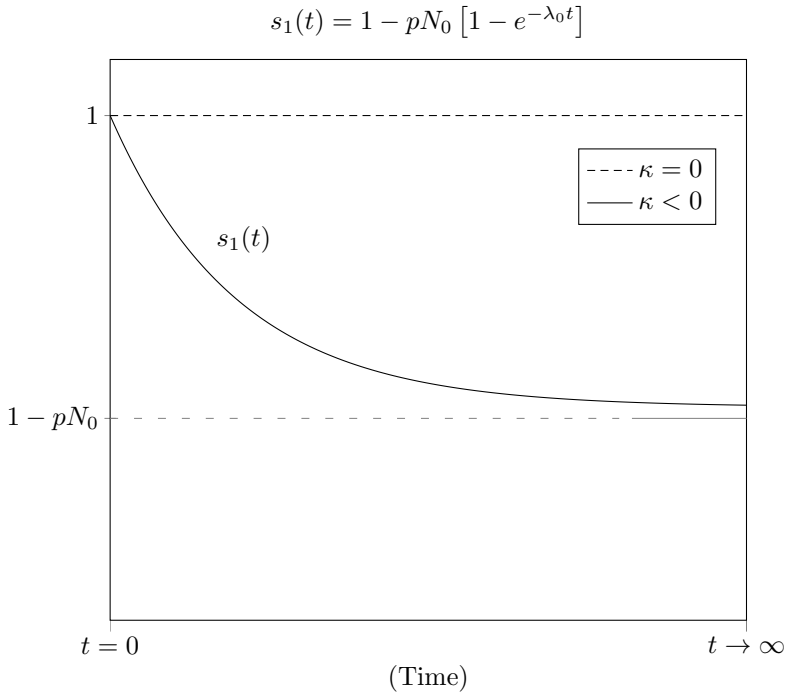

Figure 3.6.: The time evolution for the ratio of the survival probabilities, P_κ/P.

For our system, the condition that $|z|$ is significantly less than unity corresponds to either the case of a small perturbation κ, or large time t. That is to say, the condition which will allow us to retain the lower order terms in the exapnsion is given by

$$|\kappa| e^{\kappa} e^{-\lambda_0 t} \ll 1. \tag{3.40}$$

We expect this condition to be satisfied since we have in mind small perturbations to the decay parameter. As such, we can approximate the survival probability, and hence the number of surviving nuclei N, to be given by

$$\begin{aligned} N_p(t) &= N_0 e^{-\lambda_0 t}\left[1 - pN_0\left(1 - e^{-\lambda_0 t}\right)\right] \\ &= N_0 e^{-\lambda_0 t} s_1(t), \end{aligned} \tag{3.41}$$

where explicitly, we have retained terms up through first order in κ.

The quantity $s_1(t) \equiv 1 - pN_0\left[1 - e^{-\lambda_0 t}\right]$ is evidently the ratio between the SID and exponential survival probabilities, and as such can be regarded as a measure of the degree to which the two distributions deviate from each other. Figure 3.6 illustrates

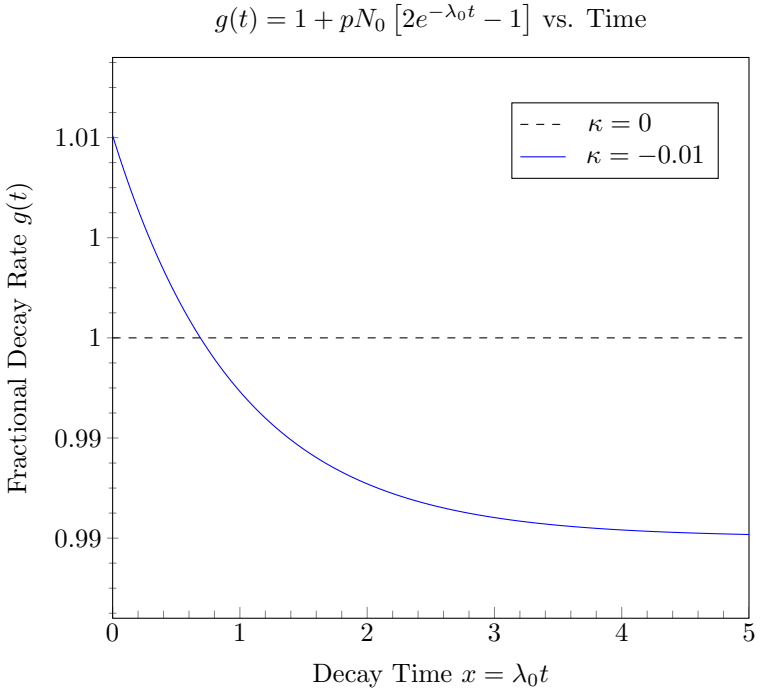

Figure 3.7.: The perturbed decay rate characterized by $g_1(t)$, with $\kappa = -0.01$. The dashed line, $g_1(t) = 1$, corresponds to a pure exponential decay process.

a plot of $s_1(t)$ for a generic value of $\kappa < 0$. It should be stressed that although $s_1(t)$ is approximate, the expression becomes more exact (for any value of p) as the system evolves. As such, it is evident that the system approaches the behavior of exponential decay at later times (hence, for small N), albeit decreased by a factor of $1 - pN_0$.

We can use the expression for N_p in Eq. (3.41) to arrive at an approximate expression for the self-induced decay rate, where differentiation with respect to t yields

$$-\frac{dN_p}{dt} \equiv -\dot{N}_p \approx \lambda_0 N_0 e^{-\lambda_0 t} g_1(t), \tag{3.42}$$

where,

$$g_1(t) \equiv \left[1 + pN_0\left(2e^{-\lambda_0 t} - 1\right)\right]. \tag{3.43}$$

Similar to the interpretation of $s_1(t)$, the function $g_1(t)$ is the factor by which a SID perturbed decay rate departs from a pure exponential decay. The behavior of $g_1(t)$ is depicted in Fig. 3.7. It is clear that the system initially decays more rapidly

than what would be expected for a system experiencing exponential decay. The feature that $g_1(t)$ crosses below the value of $g_1 = 1$ (i.e. the exponential behavior) can be explained by the fact that the initial accelerated decay depletes nuclei faster than an exponential process. Nevertheless, for $p > 0$ a self-induced decay rate will always be higher than an exponential decay rate for equal population sizes. As such, a system experiencing self-induced decay will reach the "finish line" earlier than a system experiencing exponential decay. This explains the behavior that at some time t, the SID system will appear decay "slower" than otherwise expected.

It should be stressed that, from Eq. (3.43), it would appear that this "cross-over" time, $t_\times$, always occurs at $t = t_{1/2}$, since $g_1(t) = 1$ at this time. Unfortunately, this condition is *never* true. In fact, for $p > 0$, this cross-over always occurs at time less than $t_{1/2}$. The reason that Eq. (3.43) is misleading is a consequence of the first order expansion in p, as opposed to a first order expansion in z. The latter expansion admits factors of the form $\exp[-pN_0]$. If these terms are retained, it then becomes evident that $t_\times < t_{1/2}[1 - pN_0]$ for positive values of p.

3.3.3 Self-Induced Decay Rates

Although the approximate expression, $g_1(t)$, is likely sufficient to describe the self-induced decay rate of most systems, an exact solution is clearly available. Given the expression for $N(t)$ in Eq. (3.37), we can obtain the decay rate directly from the initial model described in Eq. (3.22):

$$\begin{aligned} -\dot{N} &= \frac{\lambda_0 N}{1 - pN} \\ &= \lambda_0 N_0 \left[\frac{1}{\kappa} \cdot \frac{W_0\left(\kappa e^{\kappa} e^{-\lambda_0 t}\right)}{1 + W_0\left(\kappa e^{\kappa} e^{-\lambda_0 t}\right)} \right]. \end{aligned} \tag{3.44}$$

From this expression, it is evident that the decay rate for a SID process deviates from that of an exponential process initially by a factor of $[1 - pN_0]^{-1}$. Although this expression differs from $g_1(0)$, they clearly agree for $pN_0 \ll 1$. The exact expression for the decay rate (normalized by a factor of $\lambda_0 N_0$) is plotted in Fig. 3.8 for the value

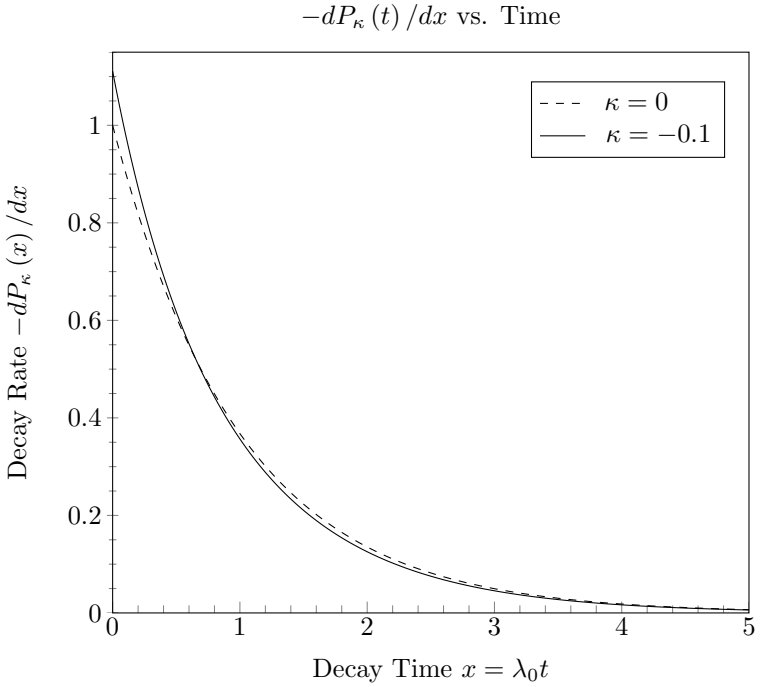

Figure 3.8.: Decay rate as a function of the particle's mean lifetime. The solid curve corresponds a self-induced decay rate with $\kappa = -0.1$. The exponential decay behavior in the absence of a SID pertubation (dashed black) corresponds to $\kappa = 0$.

of $\kappa = -0.1$. It is particularly useful to express the decay rate in terms of the survival probability P_κ. Supposing that time is measured in units of $x \equiv \lambda_0 t$, we can express the PDF, $P_{e,\kappa}(x)\,dx$, for a SID process as

$$P_{e,\kappa}(x) \equiv -\frac{dP_\kappa}{dx} = \frac{P_\kappa(x)}{1 + \kappa P_\kappa(x)} \tag{3.45}$$

Whereas from the discussion in Sec. 3.2.1, it is apparent that normalization by x implies

$$P_e(x) = P(x) = e^{-x}. \tag{3.46}$$

Thus, with this fact we can generalize our definition of $s_1(t)$ to be defined as the ratio of the survival probabilities for a SID and exponential process:

$$s(x) \equiv \frac{P_\kappa(x)}{P(x)} = P_\kappa(x)\,e^x. \tag{3.47}$$

In a similar manner, $g_1(t)$ can be generalized to

$$g(x) \equiv \frac{P_{e,\kappa}(x)}{P_e(x)} = \frac{s(x)}{1+\kappa s(x)\, e^{-x}}. \tag{3.48}$$

3.3.4 Anthropogenic Production with Self-Induced Decay

We take the opportunity here to revisit the discussion in Sec. 3.1.2 regarding the production of a population of unstable nuclei. As was noted there, it is clearly evident that the preparation of a sample via neutron irradiation will be affected if a sample decays according to Eq. (3.22). Specifically, at any given time the number N of activated nuclei will be overestimated, owing to the increased rate associated with the self-induced decays. Speaking more broadly, the notion that a sample retains a memory forces us to consider all stages of the sample's history—including the process through which it was created. As evidenced by our inability to disentangle N_0 from the particle's survival probability, it is expected that there will be identifiers of a sample's genesis which are manifest in the equations governing the activation process.

In order to quantify this, we must modify Eq. (3.5) to account for the $\lambda_1[t]$ perturbation. In a similar fashion to our previous analysis, we can express the change in the number of activated nuclei during a small time interval dt as

$$dN = Rdt - \frac{\lambda_0 N}{1-pN}dt, \tag{3.49}$$

where $R = M\sigma_n\phi_n$ is the activation rate. Here, we have changed the earlier notation for the number of targets to M in order to avoid conflating the various usages of N_0. In addition, recall that the production rate R decreases with time since the number of target nuclei decreases as targets are activated. Despite the modification in behavior of the N population, it should be clear on causal grounds that the time behavior of M, and thus R, is unaffected. Therefore, in accord with the previous treatment, the expression for the production rate as a function of time remains

$$\begin{aligned} R(t) &= M_0\sigma_n\phi_n e^{-\sigma_n\phi_n t} \\ &= R_0 e^{-\sigma_n\phi_n t}, \end{aligned} \tag{3.6}$$

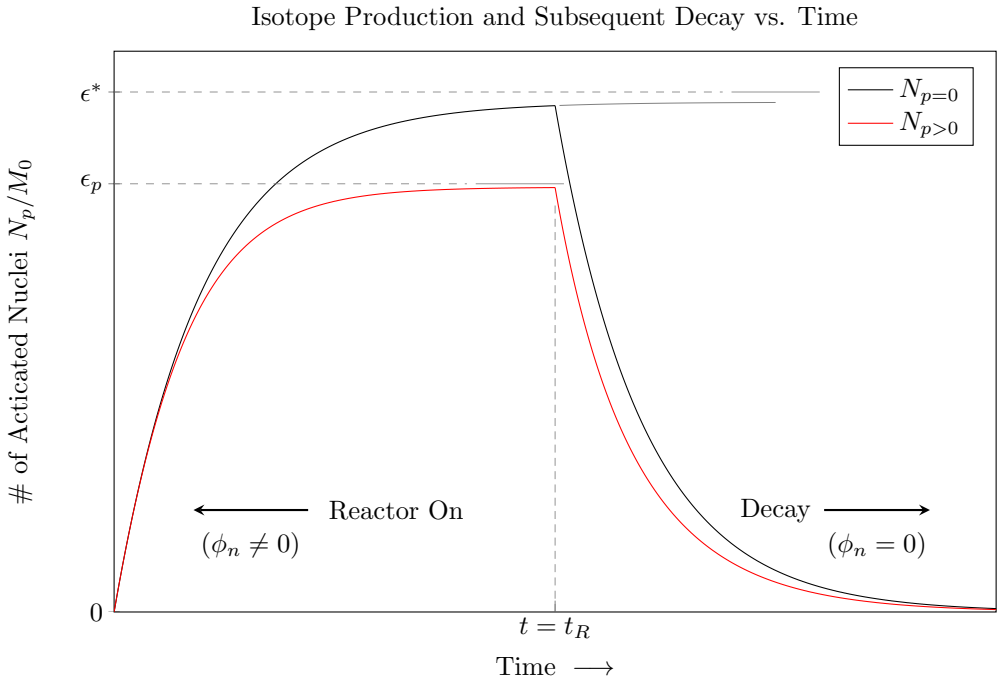

Figure 3.9.: Qualitative depiction of the activation (for $t < t_R$) and subsequent decay ($t > t_R$) of nuclei. For nuclei experiencing exponential decay (black), the production rate of the activated population is governed by Eq. (3.8). In contrast, a population governed by a self-induced decay law (red) behaves according to Eq. (3.51). For this case, saturation occurs earlier and results in a fewer number of activation products at the end of the irratdiation length t_R.

where $M_0 \equiv M\,[t = 0]$ denotes the number of target nuclei at the start of irradiation, and $R_0 \equiv M_0 \sigma_n \phi_n$ denotes the initial production rate when any targets have yet been depleted. The fact that the time dependence in M is not altered suggests that we are justified in approximating the number of target nuclei as constant during irradiation—that is to say, under the same conditions that permitted the use of Eq. (3.8). Then, under the approximation $R\,(t) \approx R_0$, we can write the differential equation governing N as

$$\frac{dN}{dt} = R_0 - \frac{\lambda_0 N}{1 - pN}. \tag{3.50}$$

Now, since the effect of $\lambda_1\,[t]$ on the evolution of a decaying system results in the

replacement of the exponential $\exp\left[-\lambda_0 t\right]$ with the Lambert W function, it would be reasonable to expect that the solution to Eq. (3.50) is similar in form to Eq. (3.8) with a comparable substitution. For convenience, we reproduce Eq. (3.8) here for inspection:

$$N_{p=0}\left(t\right) = \frac{R_0}{\lambda_0}\left[1 - e^{-\lambda_0 t}\right], \tag{3.8}$$

where explicitly, $N_{p=0}$ is the solution to Eq. (3.50) when $p = 0$. Indeed, after attempting a solution of the suspected form, it is trivial to show that Eq. (3.50) admits an exact solution for the general case of $p \neq 0$, given by

$$\begin{aligned} \epsilon_p\left(t\right) &\equiv \frac{N_p\left(t\right)}{M_0} \\ &= \frac{\epsilon^*}{1+\eta\epsilon^*}\left[1 - \frac{1}{\eta\epsilon^*} W_0\left(\eta\epsilon^* e^{\eta\epsilon^*} h\left(t\right)\right)\right], \end{aligned} \tag{3.51}$$

where $\eta \equiv pM_0$,

$$h\left(t\right) \equiv \exp\left[-\left(1+\eta\epsilon^*\right)^2 \lambda_0 t\right], \tag{3.52}$$

and $\epsilon^* \equiv \sigma_n \phi_n / \lambda_0$ is the so-called saturation limit as determined in Sec. 3.1. We can recover this saturation limit by studying the behavior of the above solutions at $t \to \infty$. For the $p = 0$ solution, indeed we see that N/M_0 approaches ϵ^* as the irradiation time t becomes very large. In the more general solution of Eq. (3.51), the saturation behavior takes the form

$$N_p\big|_{t\to\infty} = \frac{M_0\epsilon^*}{1+pM_0\epsilon^*} \tag{3.53}$$

where it should be clear that $h\left(t\right)$, and hence W_0, goes to zero as the irradiation time becomes very large. This expression for the saturation limit of N_p lends support to the qualitative discussion in Sec. 3.2.3. In contrast to exponential decay processes, there is an apparent upper bound on the number of activated nuclei that can be produced in SID processes—irrespective of reactor "power" ϕ_n. This behavior is depicted in Fig. 3.9.

3.4 Geometric Considerations on Activation and Decay

Thus far we have focused the discussion primarily on two principal aspects: (1) the process of creating an unstable sample through neutron activation, and (2) the subsequent evolution of the sample as it decays. The role that geometry plays in both regards is substantial. As briefly discussed in Sec. 3.1, the level of activation achieved differs from one location to another—due to the effect the sample has on the incident neutron flux. Consequently, the density of activated nuclei, μ, is not homogeneous, but rather a function of location within the sample. Whereas for the aspect of decay, the extent to which nuclei are *induced* to decay is dependent on the neutrino flux, and consequently the neutrino density n_ν within the sample. It is evident that these, too, are position dependent.

The latter situation has the advantage that it may serve as a means to test the SID hypothesis. However, an understanding of both aspects is essential to avoid misrepresenting potential experimental findings.

3.4.1 Self-Induced Decay Geometry

In order to better account for the influence that geometry has on a sample undergoing self-induced decay, and moreover to factor this geometric dependence into p, we must acknowledge that the decay parameter λ is a function of position, as well as time. This is due to the fact that the generated neutrino flux is different at different location within the sample. We can account for this by generalizing the model adopted thus far. To this end, consider a sample of arbitrary geometry and volume V. We suppose that $\Gamma(\vec{r}, t)$ represents the transition probability for the activated atoms within a small volume d^3r located at position $\vec{r}$ in the sample. Then, in a small time interval $\mathrm{d}t$, the number of decays expected, within the small d^3r volume, can be expressed as

$$\mathrm{d}\mathcal{A} \cdot \mathrm{d}t = \left[\Gamma(\vec{r}, t)\, \mu(\vec{r}, t)\, \mathrm{d}^3r\right] \cdot \mathrm{d}t, \tag{3.54}$$

where $\mathrm{d}\mathcal{A}$ is meant to denote the activity from this small volume.

In order to determine the activity from the entire sample, we must sum up all the small contributions throughout the volume V. In our case, this amounts to integrating over the entire volume,

$$-\frac{dN}{dt} = \int_V \mathrm{d}\mathcal{A} = \int_V \mathrm{d}^3 r \;\; \mu\left(\vec{r}, t\right) \Gamma\left(\vec{r}, t\right) \tag{3.55}$$

Now, in accord with our initial model, we suppose that the perturbation to the transition probability is linear in the neutrino density. Expressing the neutrino number density as function of position, $n_\nu\left(\vec{r}, t\right)$, we can write the position-dependent transition rate as

$$\Gamma\left(\vec{r}, t\right) = \Gamma_0 + \gamma n_\nu\left(\vec{r}, t\right), \tag{3.56}$$

where the parameter γ is the quantity we hope to relate to p. Using this expression for the transition probability, we evidently see that the total activity of the sample can be expressed as

$$-\frac{dN}{dt} = \int_V \mathrm{d}^3 r \;\; \mu\left(\vec{r}, t\right) \left[\Gamma_0 + \gamma n_\nu\left(\vec{r}, t\right)\right]. \tag{3.57}$$

At this stage, it is necessary to calculate the neutrino density for every position within the volume V. Presuming that the emitted neutrinos travel at the speed of light, it should be evident that we can relate $n_\nu\left(\vec{r}, t\right)$ to the neutrino flux $\phi_\nu\left(\vec{r}, t\right)$ by

$$n_\nu\left(\vec{r}, t\right) = \frac{1}{c}\phi_\nu\left(\vec{r}, t\right). \tag{3.58}$$

Again, it is apparent that an expression for $\phi_\nu\left(\vec{r}, t\right)$, at a location $\vec{r}$, will depend on the activity at all other locations within the sample. As such, we will consider another small volume $\mathrm{d}^3 r'$, centered on a position $\vec{r}\,'$. Then in this volume, the number of neutrinos produced every second is simply given by $\Gamma\left(\vec{r}\,', t\right) \mu\left(\vec{r}\,', t\right) \mathrm{d}^3 r'$. That is to say, we are presuming that each decaying particle emits a single neutrino. Moreover, given that the neutrinos from this small-volume source are emitted isotropically, we can calculate the flux of neutrinos at location $\vec{r}$ by

$$\mathrm{d}\phi_\nu\left(\vec{r}, t\right) = \frac{\Gamma\left(\vec{r}\,', t\right) \mu\left(\vec{r}\,', t\right) \mathrm{d}^3 r'}{4\pi \left|\vec{r} - \vec{r}\,'\right|^2} \quad . \tag{3.59}$$

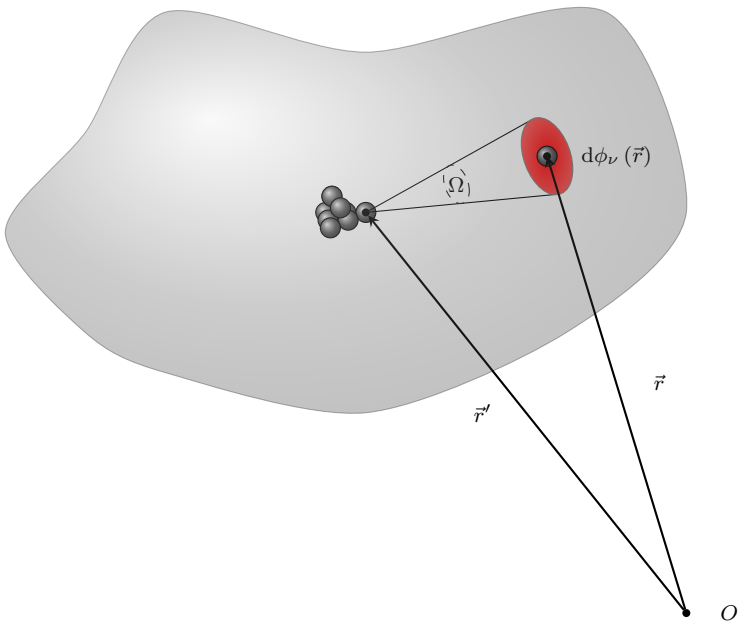

Figure 3.10.: A cartoon depicting the geometry discussed in the text. The activity within a small volume d^3r', produces a neutrino flux observed at $\vec{r}$ given by $\mathrm{d}\phi_\nu\,(\vec{r},t)$. The total neutrino flux at $\vec{r}$ is the sum from all small contributions.

The geometry for the current situation is depicted in Fig. 3.10. Given this expression, the neutrino flux at $\vec{r}$ from all contributions within the sample can be obtained, in a similar fashion as the total activity, by integrating over the sample's volume:

$$\phi_\nu\,(\vec{r},t) = \int_V \mathrm{d}\phi_\nu\,(\vec{r},t) = \int_V \mathrm{d}^3r'\ \frac{\mu\,(\vec{r}\,',t)\,\Gamma\,(\vec{r}\,',t)}{4\pi\,|\vec{r}-\vec{r}\,'|^2}. \tag{3.60}$$

Using this expression for the neutrino flux along with Eqs. (3.57) and (3.58), we can express the total decay rate of the sample as

$$\begin{aligned} -\frac{dN}{dt} &= \int_V \mathrm{d}^3r\ \mu\,(\vec{r},t)\left[\Gamma_0 + \gamma\int_V \mathrm{d}^3r'\ \frac{\mu\,(\vec{r}\,',t)\,\Gamma\,(\vec{r}\,',t)}{4\pi c\,|\vec{r}-\vec{r}\,'|^2}\right] \\ &= \Gamma_0 N + \frac{\gamma}{4\pi c}\int_V \mathrm{d}^3r\ \mu\,(\vec{r})\int_V \mathrm{d}^3r'\ \mu\,(\vec{r}\,')\cdot\frac{\Gamma\,(\vec{r}\,')}{|\vec{r}-\vec{r}\,'|^2}, \end{aligned} \tag{3.61}$$

where we have suppressed the time dependence, t, in the final line for compactness.

From this expression, the non-linearity in the system is quite explicit. To proceed from here in detail, specification of the geometry is necessary, and moreover some approximations are required. Having said that, we can partially alleviate the difficulty in requiring an explicit form for $\Gamma(\vec{r}\,', t)$ by constructing an integral series for the activity. To that end, we use the expression for Γ in Eq. (3.56), along with that for n_ν, to iterate Eq. (3.61). It should be evident that such a process yields an expansion for the sample's activity given by

$$-\frac{dN}{dt} = \Gamma_0 N + \alpha_\nu \Gamma_0 \int_V \int_V \mu \, \frac{\mu_1}{\ell_1^2} + \alpha_\nu^2 \Gamma_0 \int_V \int_V \int_V \mu \, \frac{\mu_1}{\ell_1^2} \cdot \frac{\mu_2}{\ell_2^2} + \cdots , \tag{3.62}$$

where $\mu_i \equiv \mu(\vec{r}_i, t)$,

$$\alpha_\nu \equiv \frac{\gamma}{4\pi c}, \tag{3.63}$$

and $\ell_i \equiv |\vec{r}_i - \vec{r}_{i-1}|$. Explicitly, the series can be written as

$$-\frac{1}{\Gamma_0}\frac{dN}{dt} = N + \sum_{n=1} a_n, \tag{3.64}$$

where the n–th term in the expansion is given by

$$a_n \equiv \alpha_\nu^n \int_V \int_V \cdots \int_V \mathrm{d}^3 r \, \mathrm{d}^3 r_1 \cdots \mathrm{d}^3 r_n \, \mu \frac{\mu_1}{\ell_1^2} \cdots \frac{\mu_n}{\ell_n^2}. \tag{3.65}$$

3.4.2 Geometry of a Sphere with $\mu(\vec{r}, t) =$ Constant

Given the specific case where the density of activated nuclei is uniform throughout a spherical sample, we can express a_n for a sphere of radius R as

$$a_n = \alpha_\nu^n \frac{3^{n+1}}{(n+3)} \left[\frac{N^{n+1}}{R^{2n}}\right] \prod_{i=0}^{n} \beta_i, \tag{3.66}$$

where

$$\beta_i = \int_0^1 \mathrm{d}u \, u^i \ln\left[\frac{1+u}{1-u}\right]. \tag{3.67}$$

Since it is presumed that $\alpha_\nu \ll 1$, it is most likely reasonable to truncate this series to lowest order in α_ν. In this case, we see that

$$-\frac{dN}{dt} = \Gamma_0 N + \alpha_\nu \Gamma_0 \frac{9}{4R^2} N^2 + \cdots . \tag{3.68}$$

From the previous discussion, we can relate this expression to an expansion in p, which demonstrates that for the geometry of a sphere, p is given by

$$p = \frac{9}{4R^2}\frac{\gamma}{4\pi c}. \tag{3.69}$$

Therefore, since it is apparent that $\sigma_\nu = \gamma/c$, we have

$$p = \frac{9}{4R^2}\frac{\sigma_\nu}{4\pi}. \tag{3.70}$$

3.4.3 Geometry in Neutron Activation

A more robust approximation for the density of activated atoms can be made by taking into account the geometric effects during the neutron activation process. As previously discussed, the neutron flux varies throughout the sample due to absorption and scattering. Accounting for these effects usually involves Monte Carlo modeling for arbitrary geometries. In specific cases, such as a slab or sphere, analytic expressions are available.

To account for absorption, it is useful to define the mean-free path of a neutron. For a sample with atomic number density n_T (number density of targets), and neutron-capture cross section σ_n, the probability that a neutron interacts with a target atom while traveling a distance dx in the sample is given by $\sigma_n n_T dx$. Thus, in a manner identical to Eq. (3.24), we can find the probability that a neutron avoids a collision while traversing a distance x to be

$$P_n(x) = e^{-\Sigma x}, \tag{3.71}$$

where $\Sigma \equiv \sigma_n n_T$ is referred to as the "macroscopic cross-section." Consequently, the mean-free path (i.e. the average path length for a collision to occur), is given by $1/\Sigma$. From this fact alone, we can construct an expression for density of activated atoms as a function of position within the sample, $\mu(\vec{r}, t)$.

3.5 SID and Dead Time

A somewhat unrelated experiment was conducted which provided the motivation for further investigation of the SID behavior (and which ultimately led to the observation of similarities to dead time behavior). In this experiment, several short-lived isotopes were irradiated on a regular basis and subsequently observed in order to determine the half-lives repeatedly throughout the year. The primary objective was to determine whether shorter lived isotopes also exhibit an annual time-dependence in their decay rates, similar to the isotopes presented in Table 1.1, which would be obscured by their short life-times (this experiment was motivated by *Case 2* in Sec. 2.2.3).

Of interest to this discussion are the data collected on ^{198}Au, which were in the form of thin foils, typically of mass 12-13 mg. The foils were placed in labeled polypropylene vials and heat-sealed. On a weekly basis, as possible, a sample was irradiated in Purdue's 1 kW research reactor (PUR1), at a flux of $\sim 1 \times 10^9$ n/cm^{2}s. Immediately after irradiation, the sample was moved to a 3-inch Bicron NaI(Tl) well detector, where consecutive 900–second live-time collection periods were recorded for 2 to 4 half-lives. Initial count rates were typically around 10 kBq, keeping dead time below 10%. Data were collected using an Ortec Digibase and the Maestro-32 MCA software package. A Region of Interest (ROI) was set around the 412 keV peak, and a peak-stabilization feature within Maestro was enabled.

The integral data from the dominant 412 keV peak were initially analyzed using Microsoft Excel and a weighted least-squares fit to an exponential decay law. Half-life determinations were near the expected values, but exhibited suspect variations within subsets of the data and for data sets with significantly higher count rates. Further analysis repeatedly showed an anomaly in the residuals of the de-trended count rates, as depicted in Fig. 3.11, which are expected to be distributed normally about unity. Similar anomalies were seen in data from other isotopes measured with different detection systems. While investigating the role of dead time in this behavior, it was

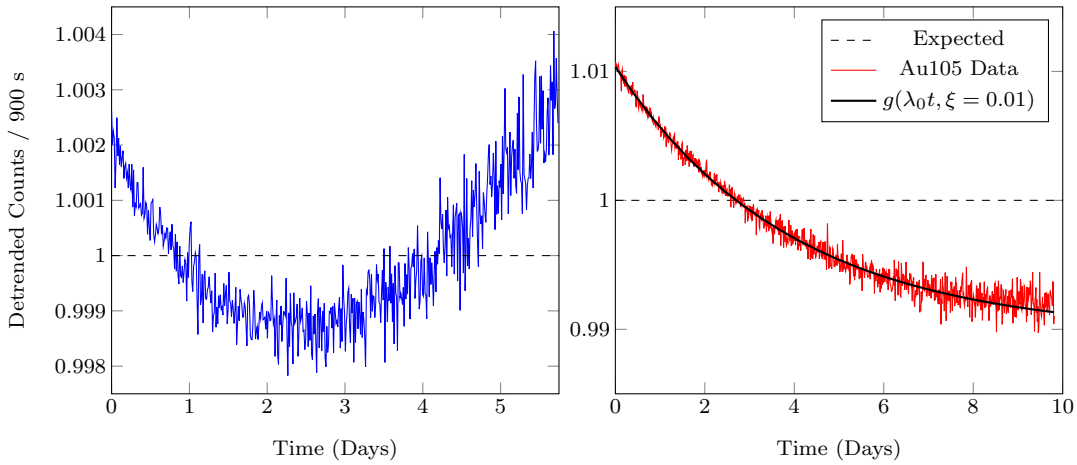

Figure 3.11.: (*Left*) Residuals of detrended and normalized ^{198}Au count rate. One expects the distribution to be normally distributed about unity. (*Right*) A representative example of the detrended ^{198}Au net counts (red, solid curve) using best-fit SID parameters. The expected behavior in the absence of SID or experimental bias (black, dashed line) is a random distribution of points about unity. The prediction from a SID perturbation is represented by the solid (black) curve.

discovered that a SID-corrected fit matches the data exceedingly well, and yields a more consistent result for half-life determinations for many of the data sets.

To evaluate the possible presence of a SID effect in our samples, the decay data were imported into Igor analysis software, and a weighted best-fit to the first-order SID function was performed. The relevant fit parameters were then used to de-trend the decay data, and the results (illustrated in Fig. 3.11) match the SID prediction very closely. A SID presence would initially cause depopulation of the sample more quickly than predicted by purely exponential behavior, which causes the subsequent decay rate to be smaller than expected under exponential behavior, with a crossover occurring at $T_{1/2}$.

Calculated values for χ^2 per degree of freedom, presented in Table 3.1, show improvement for the SID prescription compared to an exponential fit. Of particular note is run 'Au502', whose initial activity was roughly double that of the next most

Table 3.1: Exponential and SID fits to net counts for various ^{198}Au data sets. The NIST published value for ^{198}Au is $T_{1/2} = 64.684 \pm 0.005$ hr.

Run	$T_{1/2\,\mathrm{exp}}$ (hr)	χ^2_{exp}	$T_{1/2\,\mathrm{SID}}$ (hr)	χ^2_{SID}
Au105	64.365 ± 0.007	1.44	64.642 ± 0.008	0.98
Au301	64.062 ± 0.017	1.52	64.629 ± 0.019	1.04
Au401	64.394 ± 0.005	1.56	64.610 ± 0.006	1.12
Au501	64.484 ± 0.007	1.10	64.574 ± 0.008	1.05
Au502	64.078 ± 0.004	6.32	64.672 ± 0.005	1.05

active ^{198}Au sample observed. A higher specific activity should lead to a stronger SID effect, and while the SID model continues to fit the data very well, the purely exponential fit is poor, yielding $\chi^2_{\mathrm{DOF}} \approx 6$. It is also true that a larger initial activity corresponds to a higher count rate, and hence, increased dead time in our experiment. While the Gedcke-Hale livetime clock utilized in this experiment corrects for rate-related losses such as dead time and pileup, there exists an uncertainty in each time-correction. A systematic over or under-correction could resemble the SID behavior.

Additional analyses of the residuals of the net counts for both the exponential and the SID fit highlight the differences between the two models, as shown in Fig. 3.12. The histogram of residuals for the SID fit demonstrates an approximate Gaussian distribution, whereas the distribution for the exponential fit is skewed. Plots of the residuals as a function of time demonstrate a temporal bias for an exponential model which is absent for the SID model. Analysis of data for other elements also shows improvements in fit under SID analysis. Table 3.2 displays the averages of the determined half-life for each isotope, weighted by the associated error for each datum in the determination. The average χ^2 per degree of freedom for the exponential and SID fits is also presented, including the range. In all cases, the SID model described the data better than a pure exponential model.

The similarity of the proposed SID phenomenon to known dead time effects requires careful consideration. The experiment discussed here was not designed to test

Table 3.2: Weighted averages of the half-lives of various isotopes using exponential and SID fits to net counts. The associated mean χ^2 per dof and range are presented.

Isotope	$T_{1/2\,\mathrm{exp}}$ (days)	χ^2_{exp},(min, max)	$T_{1/2\,\mathrm{SID}}$ (days)	χ^2_{SID}, (min, max)
^{198}Au	$2.684 \pm 3.9\times10^{-5}$	2.39 (1.10, 6.32)	$2.693 \pm 1.4\times10^{-4}$	1.05 (0.98, 1.12)
^{76}As	$1.092 \pm 8.7\times10^{-5}$	1.17 (1.03, 1.29)	$1.091 \pm 3.6\times10^{-4}$	1.14 (1.00, 1.24)
^{122}Sb	$2.677 \pm 9.5\times10^{-5}$	5.30 (1.72, 12.3)	$2.653 \pm 3.5\times10^{-4}$	2.06 (1.14, 3.33)
^{56}Mn	$0.107 \pm 5.9\times10^{-5}$	8.38 (1.14, 24.5)	$0.1076 \pm 1.3\times10^{-5}$	1.19 (0.78, 2.01)
^{116m}In	$0.038 \pm 9.3\times10^{-6}$	1.83 (0.97, 2.17)	$0.0376 \pm 1.8\times10^{-5}$	1.25 (0.95, 2.14)

for SID. In fact, the choice of an approximate initial activity was based on balancing higher statistics with lower dead time. In what follows, we will discuss several *idealized* dead time models to demonstrate the similarities to the SID behavior. A thorough understanding of the intricacies of the two effects is necessary for devising an experiment to distinguish between them.

3.5.1 Dead-time behavior

In this section, we will want to compare the rate-related effects from dead time to self-induced decay rates. From previous discussions, it should be evident that we can re-write the SID rate in terms of a purely exponential rate. In fact, the *event rate* from a SID process, $m_\xi(t)$, as seen by the front end of a detector can be written as

$$m_\xi(t) = m_0(t)\Big[1 + \beta m_0(t)\Big] \,, \tag{3.72}$$

where $\beta \equiv 2\xi/m_0(0)$, $\xi \equiv pN_0$, and $m_0(t)$ represents an exponential decay rate with decay constant λ_0. It is apparent from Eq. (3.72) that the fractional change in the count rate $(m_\xi - m_0)/m_0$ shares the same time–dependence as $m_0(t)$. It is *also* true that rate-related perturbations associated with dead time losses are proportional to the count rate. Therefore, we turn now to investigate the effects of dead time on a SID perturbed rate and compare these effects to standard exponential decay rates.

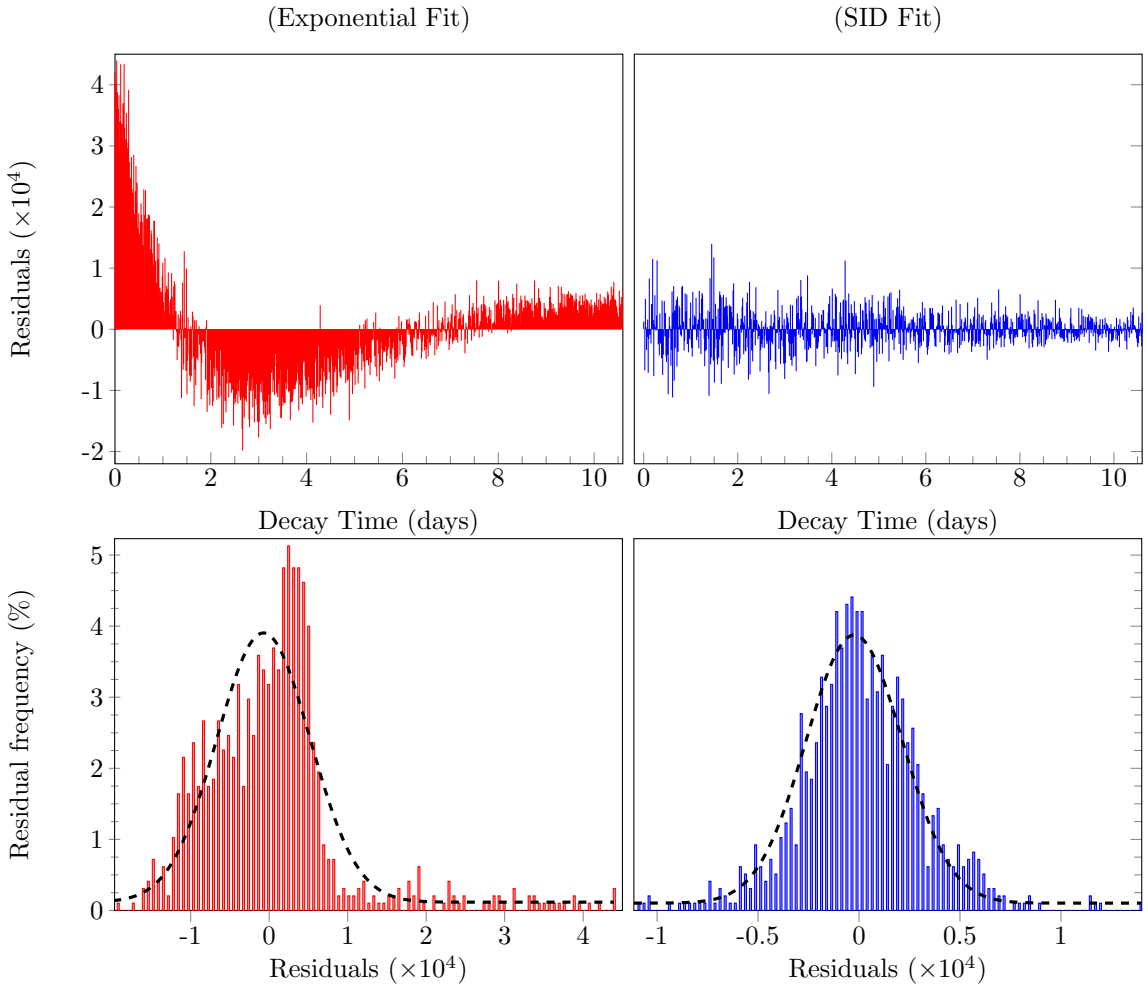

Figure 3.12.: Residuals for run Au105 are presented for both exponential (*left*) and SID (*right*) models. The residuals for the exponential model demonstrate a significant temporal bias which is absent for the SID fit. The histograms for each set of residuals are displayed in the bottom set of graphs.

There are many opportunities for bias to affect the accuracy of measurements in gamma-ray spectrometry. These include self-absorption of gamma-rays within the sample, efficiency calibration, bias in peak integration, and counting losses due to finite response time (dead time) of the spectrometer system, to name a few. The last of these is the subject of this section. Rate-related losses due to dead time may arise

from any part of the counting system, and the magnitude of these losses is directly proportional to the counting rate itself.

A host of correction procedures have been devised to account for rate-related losses. Typically these procedures are validated under conditions far more severe than those found in routine metrology, and thus are considered well-motivated. The subject of this section is to study these dead time models in an effort to elucidate their effects on time-dependent event rates which may be inherently non-exponential in time. To this end, we consider the somewhat idealized behaviors of *extending* dead time and *non-extending* dead time.

Extending dead time

Pileup in the amplifier (also called random summing) is a classic case of *extending* dead time. When counting rates are not low, the random spacing of radiation pulses may result in interfering effects between pulses. *Peak pileup* occurs if two pulses are sufficiently coincident in time that they are treated as a single pulse in the counting system. The effect of peak pileup of two events is to essentially remove both from their proper position in the energy spectrum. *Tail pileup*, which can occur significantly even at relatively low count rates, involves the superposition of two slightly overlapping pulses. The main effect of tail pileup on the measurement is to worsen and distort the spectra resolution.

The counting losses which result from pileup can be modeled as the those events which occur within a time spacing less than a time α following a previous event. If $I_0(t)$ is the instantaneous event rate of the decay within the detector, then the measured event rate out of the amplifier, $I(t)$, can be characterized by

$$I(t) = I_0(t)e^{-\alpha I_0(t)}, \tag{3.73}$$

where α is the extending dead time (pileup) parameter, which is on the order of $(1 - 10)$ μs for Ge gamma spectrometry systems. The general form of Eq. (3.73) is arrived at by considering the probability of two incoming events (governed by a

Poisson process) occurring within an interval shorter than the pulse shaping time. Now, pileup correction factors, f_P, by which each datum is adjusted, take the form

$$f_P \equiv \frac{I_0}{I} = e^{\alpha I_0}. \tag{3.74}$$

Another representation of these correction factors is obtained by using the macroscopic dead time (DT) to approximate the counting rate, yielding

$$\frac{I_0}{I} = e^{P \cdot DT/LT}\ , \tag{3.75}$$

where LT denotes the detector live time for the counting period. The unknown pileup constant P and I_0 are determined from a least squares fit of $\ln I = \ln I_0 - PDT/LT$. Even if pileup rejection circuitry is implemented (which is very effective at discarding events subject to tail pileup), corrections will still be necessary for losses occurring from peak pileups.

It is a curious observation that a SID–related deviation from an exponentially decaying event rate resembles the effect of pileup in the amplifier. In fact, expanding Eq. (3.73) in orders of α, we have

$$I(t) = I_0(t)\Big[1 - \alpha I_0\,(t)\Big] + \mathcal{O}(\alpha^2), \tag{3.76}$$

which bears the same form as Eq. (3.72) when the typical assignment of $m_0(t)$ is chosen for I_0. Although α is strictly positive to represent losses from pileup, ξ can be positive or negative depending on the particulars of the mechanism – appearing as "rate-related gains" ($\xi > 0$) or rate-related losses ($\xi < 0$).

In light of this observation, one immediate question is raised: What would the effect of pileup be on a SID–perturbed count rate, $m_\xi(t)$? The general form of Eq. (3.73) is valid for arbitrary homogeneous Poisson processes. Strictly speaking, radioactive decay is a non-homogeneous Poisson process, however if the counting interval T is sufficiently small when compared with the half-life of an isotope $T_{1/2}$ (so that decay during the counting period is negligible), Eq. (3.73) remains valid. We presume that this requirement is satisfied when $m_\xi(t)$ is considered in place of m_0, although it

should be noted that the Poisson distribution does not necessarily apply to a SID rate. The exact distribution which governs the spacing of SID events within a large ensemble is currently being investigated by the author. For now, we overlook this issue and use Eq. (3.73). In this case, the effect of pileup on the SID rate, Eq. (3.72), is

$$I(t) = m_0(t)e^{-\alpha' m_0(t)} \ , \tag{3.77}$$

where $\alpha' \equiv \alpha - \beta = \alpha - 2\xi/m_0(0)$ can be considered the "effective" pileup parameter, and $\mathcal{O}(\alpha \cdot \xi)$ terms are considered to be of second order.

Since m_0 represents a pure exponential decay rate, the result obtained in Eq. (3.77) shows that a SID–modified signal can be mistaken for an exponential decay (with the same decay constant λ_0) after subject to pileup corrections. Stated another way, it is plausible that procedures (manual or software implemented) which correct each datum for pulse pileup will remove the SID behavior almost entirely. In particular, the correction factors which are obtained from inferring the true input rate through the macroscopic dead–time and measured rate, or by a priori assuming an exponential decay, may have this effect.

A typical hardware solution to pileup is accomplished through the use of a pulser to estimate the correction factor as the ratio of pulser frequency with and without a source. This procedure is perhaps immune from the removal of a SID behavior – although a minor source of error is introduced since a periodic pulser is free from having its pulses pile up with each other. Corrections for this perturbation which rely on the counting rate may reintroduce a bias.

Non-extending dead time

Non-extending dead time is perhaps the simplest model for a detector's response to an input signal I_0. For this model, the counting system is "busy" (i.e. unable to receive any additional pulses) for a fixed time τ after each registered event. As a

result, the measured counting rate, I, will be an underestimate of the true event rate according to:

$$I = \frac{I_0}{1 + \tau I_0}. \tag{3.78}$$

The total amount of time for which the detector is "dead" during a counting interval, called the macroscopic dead time DT, is given simply as the total accumulation of these small intervals τ for the total number of registered events. That is to say, if M is the total number of registered counts in a time CT, then the detector is unable to register events for a time given by $DT = M\tau$. The effective counting interval, therefore, is the time $LT = CT - DT$.

When the true event rate into a detector is small (that is when the time between events $\sim 1/I_0$ is significant in comparison to the detector response time τ), the non-extending dead time behavior given by Eq. (3.78) will agree with the *extending* dead time model in Eq. (3.73)—simply because the probability of two events piling up is negligible. We can see this from expanding Eq. (3.78) in τI_0:

$$I = \frac{I_0}{1 + \tau I_0} = I_0 \left[1 + \tau I_0 - \mathcal{O}\left((\tau I_0)^2\right)\right] \ . \tag{3.79}$$

Although the two models agree for low event rates, the behaviors diverge significantly for high rates, and for the non-paralyzable model, the observed count rate will asymptote to a value of $1/\tau$ for large, true event rates.

It is common practice in nuclear spectrometry to perform successive counting measurements by fixing the livetime clock, since the dead time DT is expected to change from measurement to measurement when the decaying source has a lifetime comparable to the total time through which the experiment is conducted. If, on the other hand, the clock time CT is fixed, the true counting intervals will differ for different measurements. This issue can be addressed either by manual correction of the livetime or by automatically fixing the livetime clock in the multi-channel analyzer (MCA). There are various "livetime clocks" built into the systems widely used in research and industry. The Gedcke-Hale livetime clock is an example of one of the more well-proven, reliable livetime clocks.

Bias can be introduced in counting measurement by inaccuracy in the livetime clock. The degree of this bias appears small in general, and over-correction by the MCA livetime clock appears most common in practice. One test of the livetime clock performance would be to insert a pulser into the counting system and compare the measured rate with the rate measured directly with a precision frequency counter. As a simple model, the effect of overcorrection (or bias) in the livetime clock can be thought of as an error $\delta\tau$ in Eq. (3.79) associated with each registered pulse. Then, the perturbation from this deadtime overcorrection is given by:

$$\delta I_0 = \left(\frac{\partial I_0}{\partial \tau}\right)\delta\tau \tag{3.80}$$

$$= \left(\frac{I}{1-\tau I}\right)^2 \delta\tau = I_0^2\delta\tau \ . \tag{3.81}$$

We thus see that the effect of this bias is to overestimate the true counting rate in a manner once again similar to the SID perturbation:

$$I_0 + \delta I_0 = I_0\left(1 + \delta\tau I_0\right) \ . \tag{3.82}$$

In fact, systematic over or under-correction in the livetime clock will lead to an observable behavior similar in form to the SID behavior. Furthermore, a legitimate SID perturbation may resemble the effect a bias in the livetime clock.

A model for pileup, dead time, and decay

The model adopted by Lindstrom *et al.*to correct each datum for dead time losses is given schematically in Fig. 3.13. Given an instantaneous event rate $I_0(t) = I_0(0)\exp(-\lambda t)$ into the detector which is subject to an extending dead time α in the detector-amplifier combination, the instantaneous event rate out of the amplifier, I, is given by Eq. 3.73. Accounting for a non-extending dead time τ in the ADC, the instantaneous event rate I' out of the ADC is given by Eq. 3.78 where now the input

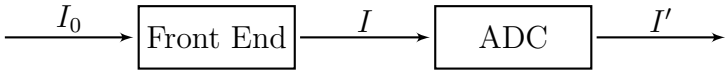

Figure 3.13.: The model adopted by Lindstrom *et al.* to correct for extending (front-end) and non-extending (ADC) dead times in series. Figure reproduced from Ref. [43].

rate is I rather than I_0. With this prescription, the number of counts M recorded in clock time CT beginning at t_0 is

$$M = \int_{t_0}^{t_0+CT} I'(t)dt, \tag{3.83}$$

where, explicitly, $I'(t)$ is given by

$$I'(t) = \frac{I_0(0)e^{-\lambda t}e^{-\alpha I_0(0)\exp(-\lambda t)}}{1+\tau I_0(0)e^{-\lambda t}e^{-\alpha I_0(0)\exp(-\lambda t)}}. \tag{3.84}$$

In the absence of dead time and pileup, the true counts M_{true} measured in a live time LT beginning at the same time t_i would be given by

$$M_{\text{true}} = \int_{t_0}^{t_0+LT} I_0(t)dt = \frac{I_0(0)}{\lambda}e^{-\lambda t_0}\left[1-e^{-\lambda LT}\right]. \tag{3.85}$$

The effect of the model described above is an underestimation of the measured counts according to:

$$M_{\text{true}} = f_P \cdot f_{DT} \cdot M\ . \tag{3.86}$$

The factor f_P is the a correction for pileup given by Eq. (3.74), and f_{DT} is a correction for the bias associated with dead time on a decaying source. The latter factor, which has the explicit form

$$f_{DT} = \frac{e^{\lambda DT}-1}{\lambda DT} > 1, \tag{3.87}$$

is significant for rapidly decaying sources where the counting interval becomes a sizeable fraction of the half life. As discussed above, the correction for pileup can serve to effectively remove any SID perturbations.

3.6 Discussion

The central observation of the present chapter is that the modifications to nuclear decay rates arising from a SID effect are mathematically identical to lowest order with those arising from standard dead-time effects, as we show explicitly in Eqs. (3.72) and (3.76). Both of these effects produce perturbations from the exponential decay law which have a similar functional dependence on count rates. It then follows that by implementing dead-time corrections, one could be suppressing or eliminating evidence for the non-exponential behavior expected from the SID effect.

For the experiment conducted in Ref. [40], a model similar to that discussed was adopted to correct for counting losses due to pileup. In particular, the decay data were fitted to Eq. (3.73) with $I(t) = I(0)\exp(-\lambda_0 t)$. A χ^2 minimization then yielded best-fit determinations of the decay parameter λ_0, the initial activity $I(0)$, and the pileup parameter α. We note that if there were a SID effect present in the decay data of Ref. [40], it would be manifest via a ξ-dependence in the pileup parameter α, given explicitly by

$$\alpha = \alpha_0 - \frac{2\xi}{I(0)} \,, \tag{3.88}$$

where α_0 is meant to denote the true effect from pileup in the absence of SID. What is interesting is that a pulser was also inserted into the system used in Ref. [40], which allows for an alternate method to estimate pileup losses. It is evident that the pulser data should allow for a determination of the pileup parameter which lacks the ξ-dependence potentially present in Eq. (3.88). It follows that a discrepancy between the two methods for obtaining α may serve as an indication of SID ($\xi \neq 0$).

The pulser and decay data for the gold sphere in Ref. [40] are plotted in a linearized form of correction factors, similar to Eq. (3.74), in Fig. 3.14. The slopes of the best-fit regressions yield the pileup parameter α, and as can be seen in Fig. 3.14, the pulser and decay data fit the expected linear models closely. However, Fig. 3.14 also suggests that the pileup parameter as determined from the pulser data disagrees with α as determined from the decay data, where the discrepancy is approximately 3σ.

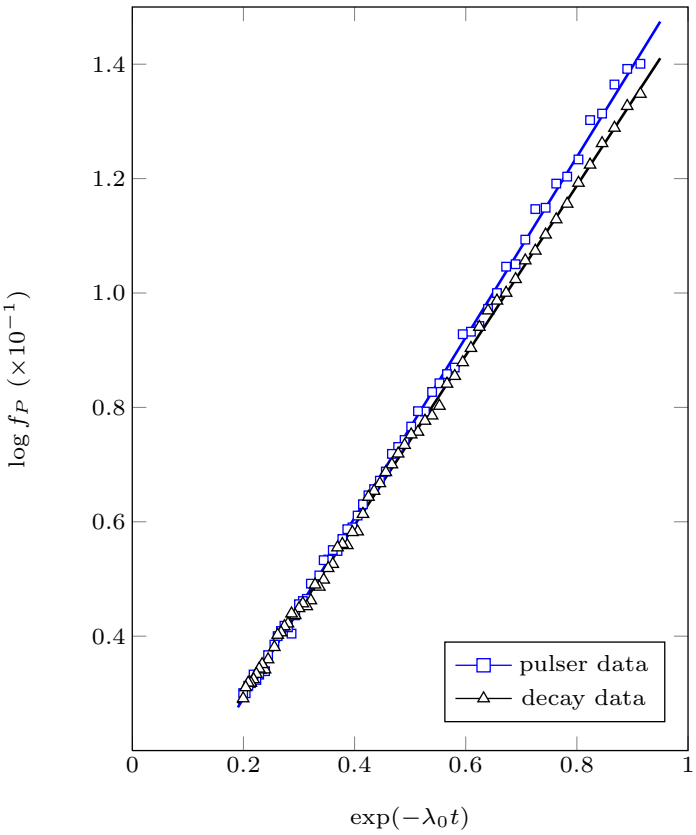

Figure 3.14.: Correction factors for pileup obtained from the data according to the model discussed in the text and obtained from the pulser data. The prediction from a potential SID effect is to decrease the pileup parameter (the slope) for the black curve. We note that the pulser data and decay data disagree most significantly at $t = 0$ when the count rate is large, and converge to each other as $t \to \infty$ when the count rate tends to zero.

Although this observation is suggestive of the presence of SID, it is unclear what other sources may be contributing to this discrepancy. The experiment conducted with the PUR1 reactor raises a similar issue. Although there may be an indication of SID within the data presented, it is also possible that over-correction in the livetime clock is responsible for the anomalous behavior.

Nevertheless, if we consider the possibility that the discrepancy between the pulser and decay data, as demonstrated in Fig. 3.14, is in fact due primarily to a self-induced

decay process, then we can estimate the interaction cross section σ_ν. For the first experiment conducted by Lindstrom *et al.*, a 1 mg gold sphere was irradiated to an activity of 1.1 GBq. Using the density of gold $\rho_{Au} = 19.3$ g/cm^3, we can estimate the radius of the sphere by:

$$\frac{4}{3}\pi R^3 = \frac{10^{-3}\text{ g}}{19.3\text{ g}\cdot\text{cm}^{-3}}\ , \tag{3.89}$$

which yields a radius of $R = 2.3 \times 10^{-4}$ m. Given that the determination of ξ from the discrepant slopes in Fig. 3.14 is

$$\xi = 0.005 \pm 0.002\ , \tag{3.90}$$

we can determine p to be given by,

$$p = \frac{\xi}{N_0}. \tag{3.91}$$

Since the initial activity of the sample was estimated to be 1.1 GBq, the initial number of activated atoms, N_0 is approximately

$$N_0 = \frac{1.1 \times 10^9\text{ s}^{-1}}{\lambda_0} = \frac{1.1 \times 10^9\text{ s}^{-1}}{2.97 \times 10^{-6}\text{ s}^{-1}} = 3.7 \times 10^{14}\ . \tag{3.92}$$

Therefore, $p = 1.36 \times 10^{-17}$. Finally, we have that the effective cross section, σ_ν, is

$$\sigma_\nu = 4\pi p\frac{4R^2}{9} = 4.05 \times 10^{-25}\text{ m}^2. \tag{3.93}$$

While this cross section is significantly larger that what can be explained by the Standard Model, it agrees with the cross-section inferred from the ^{54}Mn flare data in [11]. Having said that, there is little justification in presuming the discrepancy between the pulser and decay data arises from an inherent SID effect without further experimentation.

In principle, the effects of SID can be experimentally distinguished from those of dead-time in a number of ways. One possible way to resolve this issue is an experiment in which a sample is irradiated to varying degrees of activation and is placed at varying distances from a detector so as to maintain a fixed initial count rate within the detector. In such a configuration the SID effect (which is internal to the sample) should vary, while dead-time and pileup should remain constant.

Alternate methods to search for SID exist which eliminate the ambiguity introduced by dead-time effects. As an example, we note from Fig. 3.2 (and related discussion), that the level of activation achievable in irradiation experiments is affected by the presence of SID. In particular, it is not possible to achieve as high a degree of activation (for $p > 0$) for a sample experiencing SID as opposed to one which does not. An experiment could potentially be designed to test for the presence of SID based on this observation.

4. The DAMA/LIBRA Experiment

We now shift our focus slightly (albeit it may appear to be a dramatic shift) to the topic of particle dark matter (DM). Our focus thus far has been related to anomalous beta decay—where in part, the evidence has been apparent annual modulations observed in counting experiments. Direct detection searches for DM rely on large detectors designed to count the number of nuclear recoils that occur as a result of collisions with particle DM. These detectors, incidentally, function well at measuring the decay products of radioactive backgrounds. Consequently, many techniques have been deployed to distinguish genuine DM events from those events arising from the background. One approach is to identify unique signatures that DM signals possess which would preclude the interpretation as signals originating from backgrounds. In particular, the annual modulation signature, which arises from the yearly-periodic motion of the Earth through the local dark matter halo, has been suggested as evidence for DM detection by the DAMA/LIBRA experiment where an annually varying event rate has been observed. This is the connection to our current effort.

4.1 Introduction

Among the many ongoing dark matter (DM) searches, the most compelling evidence to date for DM comes from an annually varying signal reported by the DAMA collaboration which is compatible with expectations from standard[1] DM scenarios [44, 45]. Although there is a degree of support for the DAMA/LIBRA results from the CoGeNT collaboration [46, 47], the claims of both DAMA/LIBRA and CoGeNT are not supported by other DM detection experiments—such as CDMS [48], CDMS-

[1]Throughout this chapter, and in the context of dark matter direct detection, the term "standard" refers to both 1) traditional WIMP-nucleon elastic scattering by a momentum-independent contact interaction, and 2) a canonical dark matter halo model.

II [49, 50], XENON10 [51], XENON100 [52], and EDELWEISS [53]. Attempts have been advanced to reconcile the various DM results within the framework of alternative DM models (e.g [54–63]), but these are viewed as somewhat speculative.

Given the apparent conflict between the DAMA/LIBRA (hereafter DAMA) results and other DM searches, the suggestion has been put forward that the DAMA signal may not be due to DM, but could arise instead from backgrounds (e.g. muons [64, 65], neutrons [66])—including radioactive contaminants in the DAMA system [67–71]. This suggestion is attracting increased attention, including from the DAMA collaboration itself [72, 73], in the wake of recent reports of an annual variation in the decay rates of a number of different isotopes (see Table 1.1 and references therein). In the case of DAMA, the most obvious contaminant in their experiment is the long-lived isotope ^{40}K ($T_{1/2} = 1.25 \times 10^9$ yr)—which is known to be present in their system [74]. Potassium-40 is unusual in that it decays via both β^- and β^+ emission as well as by electron capture (EC). The 3.2 keV photon emitted following the EC decay could in principle simulate a DM signal, provided that ^{40}K decays exhibit an annual modulation similar to what is observed for other decays (see Table 1.1). Due to the long ^{40}K half life, its decays have not yet been studied by techniques that would allow for the determination of the amplitude and phase of a possible ^{40}K annual modulation. The objective of this chapter is to answer the question of whether the DAMA signal could in fact be due to ^{40}K contamination.

4.2 Potassium-40 Decay Scheme and Products

Radioactive contaminants, in general, play a significant role in the background spectrum for DM detection experiments (see discussion throughout Sec. 4.3). Serious efforts are devoted to minimizing contamination—usually involving careful selection and chemical/physical purification of detector materials. Even then, the handling and transportation of these components are a concern due to the possibility of inadvertent contamination or cosmogenic activation. Potassium-40 is a common source

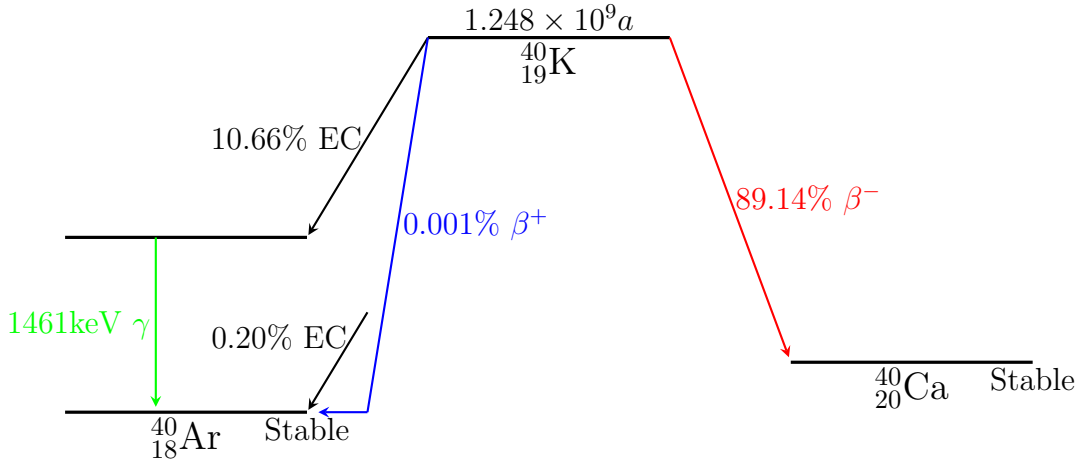

Figure 4.1.: The decay scheme of ^{40}K. The decay of ^{40}K to ^{40}Ar via EC occurs with a branching ratio of 10.86%, and is subsequently followed by the emission of X-rays/Auger electrons with energies within the energy range that DAMA reports a signal.

of background events in DM detection experiments due to its relatively high natural abundance and long half life. As it pertains to DAMA, this is particularly evident given the chemical affinity of potassium for sodium (the DAMA detector is an array of sodium iodide crystals).

Potassium-40 is a naturally occurring isotope with a half life of 1.248×10^9 yr. The abundance of ^{40}K in natural potassium is close to 0.0117%. As stated in Sec. 4.1, ^{40}K decays by both β^- and β^+ as well as by electron capture (see Fig. 4.1 for the ^{40}K decay scheme). The principal decay mode β^- occurs with a branching ratio of 89.14% directly to the ground state of ^{40}Ca. Transition to other levels of ^{40}Ca is kinematically prohibited. The EC decay occurs to both kinematically available levels of ^{40}Ar, either to the ground state ($J^\pi = 0^+$) with branching fraction $f_{EC(gs)} = 0.20\%$, or the first excited level ($J^\pi = 2^+$) with $f_{EC(1461)} = 10.66\%$. Decay by positron emission occurs rarely (but has been observed experimentally, see [75]) with a branching ratio of $\sim 0.001\%$.

Of particular interest as it concerns DAMA is the K–capture decay of ^{40}K, since this represents the most prominent background in the energy region in which DAMA claims a signal. K–capture occurs most often with a probability of $P_K = 76\%$. A capture involving shell L occurs with $P_L = 21\%$, and in the remaining $P_{M^+} = 3\%$ of the cases, electrons from upper shells are involved.[2] The captured electron creates a vacancy in the K-shell of ^{40}Ar leaving it in an excited electronic state. This results in transitions of outer shell electrons to fill the inner shell vacancies—accompanied by the emission of X-rays/Auger electrons (the ejection of an outer shell electron resulting from this transition). The X-rays/Auger electron emissions will give rise to a ~ 3.2 keV peak—the binding energy of shell K for ^{40}Ar—in the energy spectrum of DM detectors (binding energy for an L shell electron is $E_L = 0.3$ keV). Furthermore, when the EC transition is to the excited 1461 keV level of ^{40}Ar, there will be a nuclear de-excitation to the ground state by the emission of a 1460.8 keV γ photon.

We note in passing that the EC branching fraction for the decay of ^{40}K directly to the ground state of ^{40}Ar is obtained more or less from theoretical grounds since no direct experimental measurement of this *unique third–forbidden* transition appears to have been obtained. As pointed out in [71], no other EC decay of this kind is known to exist and its empirical verification would provide a resounding closure to the theory of unique forbidden decays.

4.3 DM Direct Detection

The nature of direct detection of DM has necessitated the construction of ultra low-background, low-energy detector systems, forcing these setups deep underground. Unfortunately, common to all these low-noise experiments is the presence of naturally occurring radioactive contaminants, or cosmogenically activated detector materials. As a result, the principal energy regions where detectable DM event rates reside are

[2]These fractional capture probabilities correspond to the unique 1st forbidden transition of ^{40}K to the excited state of ^{40}Ar. For the transition to the ground state of ^{40}Ar we have $P_K = 0.88$, $P_L = 0.086$, and $P_{M^+} = 0.013$.

inundated with X-rays and other decay products which may mimic or conceal actual DM events. A thorough investigation of background processes is thus of utmost priority in order to distinguish noise from positive events.

A likely candidate for particle dark matter is the WIMP (Weakly Interacting Massive Particle). A DM halo primarily composed of WIMPs would yield a potentially large enough WIMP flux crossing the Earth ($\sim 10^5$ cm^{-2}s^{-1}) to detect the small fraction of WIMPs which elastically recoil off target nuclei. Direct detection efforts aim to detect WIMPs via the measurement of the rate R and energies E_R of these nuclear recoils. The difficulty in direct detection is two-fold. 1) Despite the sufficiently large WIMP flux, WIMP-nucleon interaction cross-sections are expected to be prohibitively small, and hence obtaining a sizeable event rate R poses an extreme challenge. This difficulty necessitates rather large target volumes and very low backgrounds; this represents a difficult task since contamination also scales with detector size. 2) Under standard assumptions, the differential energy spectrum of WIMP-induced nuclear recoils is relatively featureless with a quasi-exponentially decreasing tail towards higher recoil energies ($dR/dE_R \sim e^{-E_R}$). This constrains DM searches to low-energy regions where lowering detector thresholds and limiting low-energy backgrounds become serious challenges.

4.3.1 Annual Modulation Signature

Due to these challenges, time-dependent features (or signatures) of the energy spectrum are valuable in that they can be exploited to help distinguish DM induced events from terrestrial events. The *annual modulation signature* [76] is one such feature which results from the Earth's changing velocity through the DM halo. The flux of DM particles incident on the Earth results from the Earth's motion through the Galaxy. This motion has contributions from both the Earth's motion around the Sun and the Sun's rotation about the Galactic center (see Appendix A). As a consequence of the Earth's annual revolution, it will be crossed by the largest DM particle flux

when its rotational motion is most directly aligned with that of the Sun's ($\sim$ June 2$^{\text{nd}}$) and by the smallest flux when the motions are mostly subtracted ($\sim$December 2$^{\text{nd}}$). The direct implication of this effect on the event rate (averaged over an energy interval k), R_k, is given by:

$$R_k(t) = \bar{R}_k(1 + A_k \cos\omega(t - t_{dm})), \tag{4.1}$$

where A_k is the amplitude of modulation in the kth energy interval, $\omega = 2\pi/T$, $T = 1$ year, and t_{dm} corresponds to the day (from Jan 1$^{\text{st}}$) of maximal signal. Although the functional form of Eq. (4.1) is a model-independent result attributable to the Earth's motion about the Sun, both the phase[3] and amplitude are dependent on the form of the DM halo, and more directly on the local DM distribution in our solar neighborhood. For the standard halo model, the phase is $t_{dm} \sim 152.5$ days (June 2$^{\text{nd}}$), and the amplitude of modulation, A_k, can be as large as $\sim 7\%$—depending on the portion of the recoil spectrum measured.[4]

4.3.2 The DAMA/LIBRA Direct Detection Experiment

The DAMA collaboration has sought to detect WIMP-induced nuclear recoils by searching for an annual modulation in the recoil spectrum compatible with predictions from the annual modulation signature. The target choice, radiopure thallium-doped sodium iodide (NaI(Tl)) scintillators, has afforded them by far the largest and longest exposure to date when compared to the other direct detection experiments—a cumulative exposure greater than 1.17 ton $\times$ yr corresponding to 13 annual cycles (DAMA/LIBRA and it's predecessor DAMA/NaI). The detector apparatus consists of a modular array of 25 NaI(Tl) crystals (5×5) with 9.70 kg mass each. One crystal is not operational, resulting in a total target mass of $M_{target} = 232.8$ kg. Each crystal is monitored by 2 phototubes (working in coincidence) through suprasil-B lightguides, with impressive light collection abilities (5.5–7.5 photoelectrons/keV).

[3]The phase may depend on non–thermalized halo substructure such as streams.

[4]For inelastic dark matter models [54], the modulation amplitude can be $\gtrsim 30\%$ resulting from the greater dependency on the Galactic escape velocity.

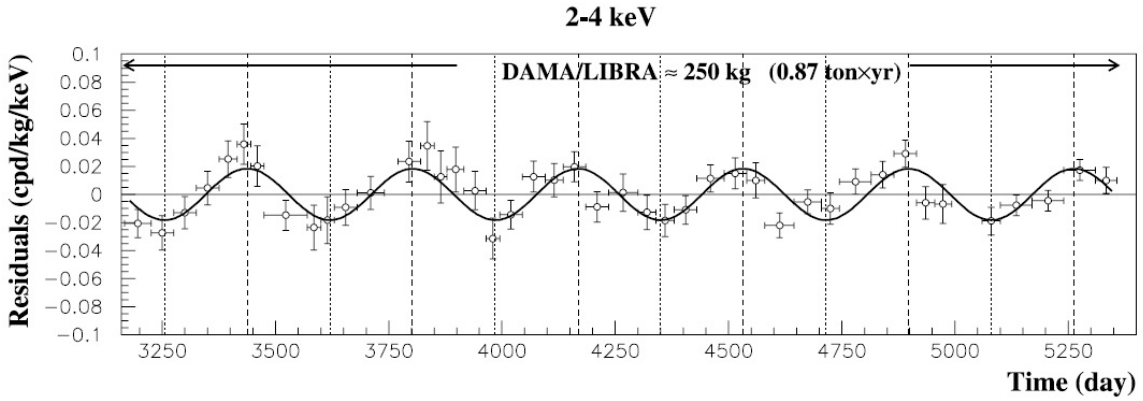

Figure 4.2.: The residual differential rate of the scintillation events in DAMA/LIBRA for the first 6 annual cycles in the 2 – 4 keV energy interval as a function of time. Figure obtained from [44].

This design allows DAMA to acquire both *single–hit events* (where one crystal fires) and *multiple–hit events* (where more than one crystal fires simultaneously). However, only the subset of single-hit scintillation events is considered for analysis, since DM particle multiple interaction probability is considered negligible. DAMA's analysis of the data over this large exposure has shown a clear modulation in the single-hit event rate in the low-energy ranges: 2 – 4 keV, 2 – 5 keV, and 2 – 6 keV (see Fig. 4.2), consistent with the annual modulation signature with a confidence level now exceeding 8.9σ [44]. Above 6 keV no modulation is evident which is also compatible with a WIMP-induced signal. Additional analyses published by DAMA (see Fig. 9 of [45]) suggest that the greatest contribution to the modulation comes from events with recoil energies ~ 3 keV. Thus particular attention should be given to the energy range of 2 – 4 keV (which is the common subset to all three intervals considered). The baseline differential count rate averaged over the first four annual cycles of DAMA/LIBRA for this interval, determined from [45], is $\bar{S} = 1.15\,\mathrm{cpd/kg/keV}$, see Fig. 4.3(a). The total count rate in the 2 – 4 keV region is given by:

$$\bar{R} = \bar{S} M_{target} \Delta E \approx 530\,\mathrm{cpd}, \tag{4.2}$$

where cpd $\equiv$ counts per day. Fitting the residuals from this baseline to $A\cos\omega(t-t_0)$, DAMA reports a modulation amplitude $A = 0.0213 \pm 0.0032$ cpd/kg/keV and phase $t_0 = 139 \pm 10$ days for these four annual cycles [45]. For comparison to Eq (4.1), these results may be written as:

$$R(t) \approx 530(1 + 0.018\cos\omega(t - 139))\,\text{cpd} \qquad (2 - 4\,\text{keV}), \tag{4.3}$$

where $T = 2\pi/\omega = 0.997 \pm 0.002$ yr is in good agreement with an annual signal. In other words, the observed modulation of 1.8% results from an excess/deficit of at most $\sim$ 10 cpd over/under the 530 cpd measured on average. Tempting as it is to juxtapose Eq. (4.1) and Eq. (4.3) for comparison, it must be noted that Eq. (4.3) has contributions from both background sources and possible signals. Irrespective of the source of modulation, the amplitude of modulation cannot be ascertained without knowledge of the background contributions to the 530 cpd baseline. To account for background contributions to the 2 – 4 keV energy region, it is perhaps more appropriate to write the DAMA event rate as:

$$R(t) = B_0 + S_0 + S_m \cos\omega\,(t - t_0)\,, \tag{4.4}$$

where B_0 are the contributions from unmodulated backgrounds, S_0 is the constant (in time) contribution from the modulated signal, and S_m is the amplitude of the modulated signal (in cpd). From this representation we have that $B_0 + S_0 = 530$ cpd and:

$$1.8\% = \frac{S_m}{B_0 + S_0}\,. \tag{4.5}$$

In order to obtain the signal modulation (S_m/S_0) one must accurately account for the remainder of events B_0. This, in part, is the impetus for the current investigation of ^{40}K , due to the substantial contribution it has to the DAMA signal energy region. A more complete understanding of the ^{40}K decay products will either indicate that ^{40}K is responsible for the modulation S_m, or alternatively, allow for a narrower determination of the DAMA modulation amplitude, thereby guiding those models which attempt to remain consistent with the DM interpretation of DAMA.

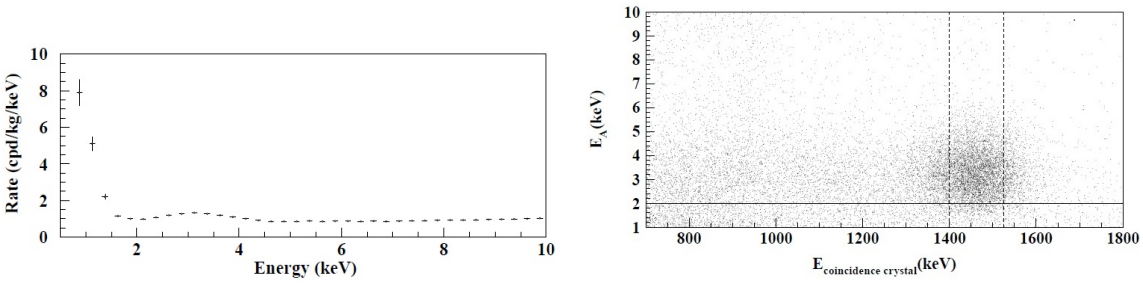

(a) (b)

Figure 4.3.: (a) Cumulative low-energy distribution of single-hit events measured by DAMA/LIBRA during the first 4 annual cycles. The peak evident in the spectrum near 3 keV is presumably due to ^{40}K. Figure from [45]. (b) Scatter plot of double-hit events. The low-energy events in one crystal are plotted as a function of the energy deposited in another crystal. The higher density region is attributable to the 3.2 keV X-rays and 1461 keV γ associated with ^{40}K EC decay. Figure from [74].

4.3.3 The ^{40}K Background in DAMA/LIBRA

Despite the results detailed in Sec. 4.3.2, the claim for the DAMA signal originating from WIMP-induced nuclear recoils is at variance with exclusionary limits set on the WIMP cross-section and mass by other experiments. Furthermore, legitimate concerns have been raised regarding the influence of the background spectrum in the DAMA detector. A particular concern is the lack of nuclear recoil discrimination. WIMPs are expected to interact with the nuclei (as opposed to the electrons) inside a target material and therefore give rise to nuclear recoils. Electron recoils arise from interactions with particles such as photons, electrons, or alpha particles—which are primarily the result of radioactive decays. The two types of recoils are distinguishable by measuring the density of the energy deposited within the detector. Detectors which have the ability to measure both the energy and some additional parameter (e.g. cryogenic detectors can make simultaneous measurements of ionization and thermal energies) can discriminate among recoils.

Since DAMA cannot determine which of their events result from nuclear recoils, they do not distinguish between WIMP signal and background on a per event basis. Instead, they posit that a WIMP signal distinguishes itself from background events by exhibiting an annual periodicity with characteristics that no "known" background process can imitate (a claim which deserves scrutiny in light of the annual periodicities observed in the decay rates of many isotopes, see Table 1.1). It has also been argued by DAMA that consideration of only single-hit events excludes a majority of backgrounds since these processes are usually associated with multiple, highly-correlated events (an argument which does not pertain to certain decay modes of ^{40}K (see Sec. 4.2), and depends on the collection efficiency of the DAMA/LIBRA detector).

The concentrations of radioactive contaminants (such as $^{\text{nat}}$K, ^{238}U, and ^{129}I) within the DAMA apparatus have been investigated by the DAMA collaboration [74]—and simulations performed using these estimates suggest that much of the DAMA cumulative event rate is attributable to radioactive contamination [67]. Of primary importance is the presence of ^{40}K since part of its decay scheme (Fig. 4.1) has decay products with energies that fall within the range in which DAMA claims a signal. Indeed, the decay of ^{40}K to ^{40}Ar via EC is followed by the emission of 3.2 keV X-rays which will give rise to a peak within the energy range of the putative signal (2 – 4 keV). DAMA has verified the occurrence of this process by investigating over a large exposure the presence of double coincidences associated with the decay of ^{40}K to the excited nuclear state of ^{40}Ar. Although the low-energy X-rays will be contained within the crystal (in which they were produced) with an efficiency $\sim$1, an escaping 1461 keV γ can hit another detector and cause a double coincidence. Their analysis revealed a large clustering of such events to support the emission of 3.2 keV X-rays/1461 keV photon pairs, see Fig. 4.3(b). From this analysis, DAMA claims the $^{\text{nat}}$K content in the crystals at $\sim$ 20 ppb [74]. Hence the total particle concentration of ^{40}K can be estimated according to:

$$N_{^{40}\text{K}} = 20 \text{ ppb} \cdot 0.0117\% \cdot M_{target} \cdot (N_A/M_{^{40}\text{K}}) = 8.2 \times 10^{15}, \tag{4.6}$$

where $N_A = 6.022\times10^{23}$ mol^{-1} is Avogadro's number, and $M_{^{40}\mathrm{K}} = 39.96\times10^{-3}$ kg/mol is the isotope mass of ^{40}K . Of interest as it pertains to the 2 – 4 keV region of the DAMA event spectrum is the activity from the K–capture decay mode:

$$R_{^{40}\mathrm{K}} = \lambda_{^{40}\mathrm{K}} \cdot N_{^{40}\mathrm{K}} \cdot f_{EC(1461)} \cdot P_K \sim 1000 \text{ dpd}, \tag{4.7}$$

where dpd $\equiv$ disintegrations per day, $\lambda_{^{40}\mathrm{K}} = \log 2/T_{1/2} = 1.52\times10^{-12}$ d^{-1}, $f_{EC(1461)} = 10.66\%$ is the EC branching fraction to the excited state of ^{40}Ar, and $P_K \sim 0.76$ is the fraction of EC decays involving a K shell electron. In principle the contribution from this activity to the single-hit spectrum is $\varepsilon \cdot R_{^{40}\mathrm{K}}$, where ε is the detection efficiency (which depends on the acceptance of events in the 2 – 4 keV energy window and the single-hit acceptance efficiency). Although many of these decay events are associated with 1461 keV photons, a significant fraction of them contribute the single-hit distribution—as evident from the peak in the cumulative distribution for single-hit events, see Fig. 4.3(a), as well as by the simulations carried out by [67]. This is expected since the collection efficiency is < 1 for the higher energy 1461 keV photons.

Furthermore, the events which correspond to the decay of ^{40}K to the ground state of ^{40}Ar represent an *irreducible background* in the DAMA 2 – 4 keV energy region. Since they are not associated with de-excitation photon emissions, they contribute solely to the single-hit event spectrum. This subset's activity is ~ 20 cpd which can be obtained in a similar fashion to Eq. (4.7) by replacing $f_{EC(1461)}$ with $f_{EC(gs)} = 0.20\%$ and setting $P_K = 0.88$. It is interesting to note that the contribution from this irreducible background may be large enough to completely account for the DAMA modulation (10 cpd) provided it has an event rate which exhibits an appropriate annual modulation.

4.4 Implications for DAMA and Other DM Detection Experiments

Although the mechanism responsible for the variation in decay rates associated with the isotopes reported in Table 1.1 is presently unknown, the implication for DM direct detection experiments is immediate. With the case of DAMA, the calculations

in Sec. 4.3.3 demonstrate that a sufficiently large portion of the DAMA single-hit event spectrum is attributable to ^{40}K contamination, so that if ^{40}K were to exhibit an annual modulation, it could account for the periodic effect reported (a yearly modulation with an amplitude of $\sim$ 10 cpd). The main argument given by DAMA to dismiss ^{40}K as the origin of their signal is the apparent lack of modulation in the 1461 keV photon event rate [72]. However, DAMA obtains this result by fixing a phase a priori to the best-fit regression curve, significantly reducing the confidence in the resulting best-fit modulation amplitude. Irrespective of this, it is worth noting that modulation in the low-energy events associated with ^{40}K decay is *not* necessarily correlated with a modulation in the 1461 keV event rate. Two examples readily emerge from the discussion in Sec. 4.3.3 and 4.2:

(1) The events associated with the EC decay directly to the ground state of ^{40}Ar ($\sim$ 20 cpd) are not associated with the emission higher energy photons—and therefore represent an *irreducible background* in the energy region in which DAMA claims a signal. Furthermore, the activity from this decay may be large enough, in principle, to account for the observed modulation.

(2) It may be that external factors (which are yearly periodic) bias the fractional capture probabilities (P_K, P_L, etc.) in the EC decay process. Such an effect may have no influence on the 1461 keV photon emission rate. However, this would affect the 2 – 4 keV event rate since only K–capture events ($E_K = 3.2$ keV) are represented within this energy range ($E_L = 0.3$ keV which is actually below the DAMA/LIBRA threshold).

In addition to the results from DAMA, the CoGeNT collaboration in recent publications has claimed the possible presence of an annual varying signal in their data which "may" be consistent with the annual modulation signature [46]. The strength of the annual modulation signature rests on the predictability of the phase for an observed annual signal. It has been demonstrated, however, that the phase itself is susceptible to astrophysical uncertainties and is dependent on the form of DM halo

adopted [77]. Unfortunately, this larger uncertainty in the phase allows many annual signals to appear consistent with a possible DM signal.

Moreover, the motion of the Earth through the big bang relic neutrinos (CνB) produces an annual variation in relic neutrino flux with a min(max) occurring on $\sim$Jun 12(Dec 10). This result is obtained presuming that the motion of the Earth through the CνB is identical to the motion through the cosmic microwave background (CMB). From the WMAP experiment, the velocity of the sun with respect to the CMB is determined to be

$$\vec{V}_{\odot} = 370 \cdot \langle -0.071337, -0.662049, 0.746057 \rangle \, \frac{\text{km}}{\text{s}}. \tag{4.8}$$

From the development in Appendix A, we see that the Earth's speed with respect to the CνB is given to a good approximation by

$$V_{\oplus}[t] = 371 + 29.2 \cos\left[\frac{360^{\circ}}{365.25}(t + 20)\right] \, \frac{\text{km}}{\text{s}}. \tag{4.9}$$

Given that the flux of relic neutrinos incident on the Earth is actually greater than the solar flux [38], it appears possible, albeit rather speculative, that the DAMA collaboration may be detecting relic neutrinos via a novel interaction with the ^{40}K contamination within their detector.

5. Summary

It is clear that the program presented in this work is not complete. We have tried to demonstrate that searching for anomalous beta decay through self-induced decay processes is somewhat more challenging than initially perceived. In one particular aspect, the relationship between SID event rates and detector bias presents a challenge for experimental detection efforts. However, there exists a large set of predictions that are, in principle, experimentally testable. For the experiments conducted at NIST, it was demonstrated that interpreting the disparity between pulser and decay data as arising from a SID process implies an effective cross section of $\sigma_\nu \sim 10^{-25}$ m^2.

For the case of DM experiments, it appears commonplace to take as a given the long-term stability of detection systems. This issue exists, in addition, for many of the experiments presented in Table 1.1. The possibility that the annual signal seen by the DAMA collaboration is in fact due to the radioactive contaminant ^{40}K, is not excluded by the treatment presented here.

APPENDIX

A. Celestial Coordinate Systems & Transformations

Many of the topics discussed in this work rely on knowledge of the relative motion of the Earth with respect to either the sun or larger structures, such as the galactic rest frame. For reference, we provide a brief description of celestial coordinate systems and develop the transformations necessary to jump among the various coordinates.

A.1 Coordinate Systems

In this section we will summarize the standard coordinate systems used in astronomy, which include equatorial, ecliptic, and galactic coordinate systems. Unless stated otherwise, we will express the quantities of interest in galactic coordinates.

A.1.1 The Equatorial Coordinate System

The *equatorial coordinate system* is defined by the projection of the Earth's geographic poles and equator onto the celestial sphere. The *celestial equator* is the projection of the Earth's equator onto this sphere. An object on the celestial sphere is referenced by its longitudinal angle α (referred to as the *right ascension*) and latitudinal angle δ (called the *declination*). The right ascension measures the angle of an object east from the apparent location of the sun at the time of the vernal equinox ($0^\circ \leq \alpha < 360^\circ$). The declination measures the angle of an object above or below the celestial equator ($-90^\circ \leq \delta \leq 90^\circ$). Hence by definition, the vernal equinox Υ is located at $\langle \alpha_\Upsilon, \delta_\Upsilon \rangle = \langle 0, 0 \rangle$ in equatorial coordinates (refer to Fig. A.1 for a diagram of the celestial sphere with an equatorial coordinate system).

The plane within which the Earth orbits the sun is called the *ecliptic plane*. This plane is inclined by $\varepsilon = 23.44^\circ$ from the plane of the celestial equator due to the

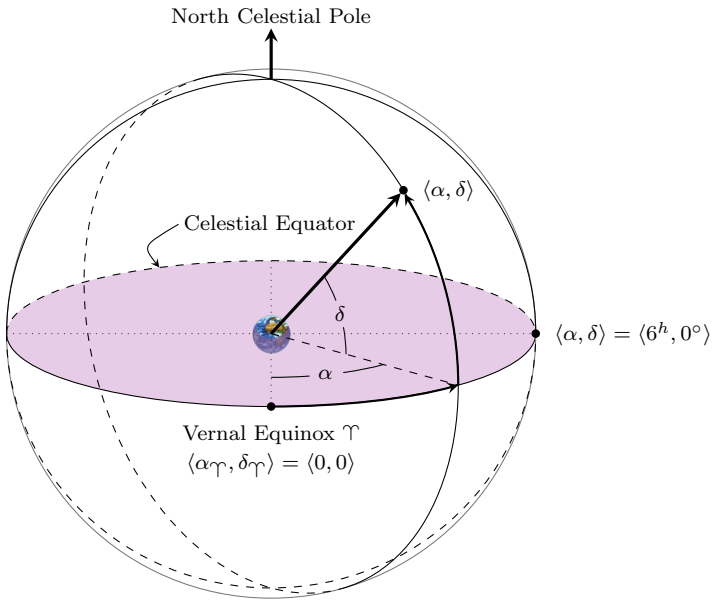

Figure A.1.: The Celestial Sphere illustrating the equatorial coordinate system. The right ascension α measures the angle of an object east from the apparent location of the Sun at the moment of the Spring Equinox Υ. The declination δ measures the angle of an object above or below the celestial equator.

obliquity of the earth's axis of rotation. The equinoxes (Spring equinox Υ, Autumn equinox $\simeq$) are the nodes where the ecliptic intersects the celestial equator - the spring equinox occurs when the apparent motion of the sun is in the direction from south to north. Figure A.4 depicts the apparent motion of sun on the celestial sphere as seen from the Earth.

The choice of basis for an orthogonal right-handed coordinate system is somewhat arbitrary. It is convention to assign the x-axis in the direction of $\langle \alpha_x, \delta_x \rangle = \langle 0, 0 \rangle$ and the y-axis in the direction of $\langle \alpha_y, \delta_y \rangle = \langle 6h, 0 \rangle$. The z-axis is therefore in the direction of the north celestial pole, $\delta = 90°$. We will denote this basis as

$$\begin{aligned} \hat{x} &= \text{unit vector in direction of } \langle 0, 0 \rangle \\ \hat{y} &= \text{unit vector in direction of } \langle 6h, 0 \rangle \\ \hat{z} = \hat{x} \times \hat{y} &= \text{unit vector in direction of } \delta = 90°. \end{aligned} \tag{A.1}$$

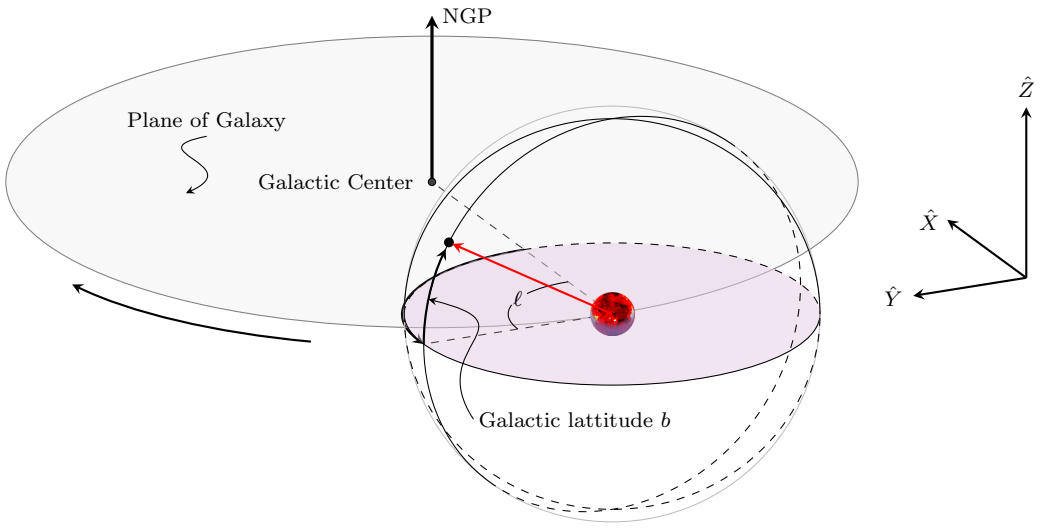

Figure A.2.: The galactic coordinate system centered on the sun. An object on the celestial sphere has galactic coordinates $\langle \ell, b \rangle$. The galactic Cartesian coordinate system is shown with $\hat{X}$ in the direction of the galactic center, $\hat{Y}$ in the direction of the sun's orbital motion, and $\hat{Z}$ in the direction of the NGP.

A.1.2 The Galactic Coordinate System

The galactic coordinate system (GCS) is a heliocentric celestial coordinate system with the plane of the Milky Way galaxy as its fundamental plane. The direction of an object on the celestial sphere is measured by its galactic longitude and latitude $\langle \ell, b \rangle$. The galactic latitude b measures the angle an object makes with the plane of the galaxy using the sun as vertex. The galactic longitude ℓ measures the angle to an object spanned in the galactic plane from the line connecting the sun to the apparent center of the galaxy (see Fig. A.2 for an illustration of the galactic coordinate system).

Similar to the case of equatorial coordinates, we designate the x-axis to be oriented along $\ell = b = 0$ in the direction of the center of the galaxy, and the z-axis to be along $b = 90^\circ$ in the direction of the north galactic pole (NGP).[1] The y-axis, defined by

[1]We note that although it is typical to assign "rotational North" to the pole from where a system rotates counter-clockwise, the assignment of the NGP is to point into the northern celestial hemisphere. Perhaps unfortunate, the galaxy has a clockwise rotation when viewed from the NGP, and hence there is ambiguity between "rotational north" and the "north galactic pole".

$\hat{Z} \times \hat{X}$, is in the direction of galactic rotation, $\ell = 90°, b = 0$. A visualization of this coordinate system can be found in Fig. A.2. Clearly, with this choice of axes, an arbitrary unit vector in the direction of galactic coordinates $\langle \ell, b \rangle$ will have galactic Cartesian coordinates $\langle X, Y, Z \rangle$ given by,

$$\begin{aligned} X &= \cos b \cos \ell \\ Y &= \cos b \sin \ell \\ Z &= \sin b. \end{aligned} \tag{A.2}$$

We note that for the equatorial coordinate axes defined in Eq. (A.1), the equatorial coordinates $\langle x, y, z \rangle$ are also given by Eq. (A.2) with the substitution of galactic longitude and latitude for right ascension and declination (i.e. $\ell \mapsto \alpha$ and $b \mapsto \delta$).

A.1.3 The Ecliptic (Solar) Coordinate System

The ecliptic coordinate system is constructed by choosing the ecliptic as the fundamental plane for the celestial sphere, and additionally, with the sun designated as the origin. The ecliptic latitude β measures the angle above or below the ecliptic plane with the sun as vertex. The solar longitude ϑ measures the angle spanned in the ecliptic plane east from the direction of the vernal equinox. As an orthogonal right-handed basis for this system, we take the x-axis to be in the direction of the apparent location of the sun at the moment of the vernal equinox.[2] The y-axis is chosen to be in the direction of the apparent location of the sun during the Summer solstice, occurring 1/4 of a year later. Thus, the positive z-axis points in the direction of the earth's orbital axis, which we will refer to as the north ecliptic pole (refer to Fig. A.3). We will denote this basis as

$$\begin{aligned} \hat{e}_{\Upsilon} &= \text{unit vector in direction of } \langle 0, 0 \rangle \\ \hat{e}_{\text{ss}} &= \text{unit vector in direction of } \langle 6h, 0 \rangle \\ \hat{e}_{\text{nep}} \equiv \hat{e}_{\Upsilon} \times \hat{e}_{\text{ss}} &= \text{unit vector in direction of } \beta = 90°, \end{aligned} \tag{A.3}$$

[2]Consequently, this is the same choice as $\hat{x}$ in equatorial coordinates, see Eq. (A.1).

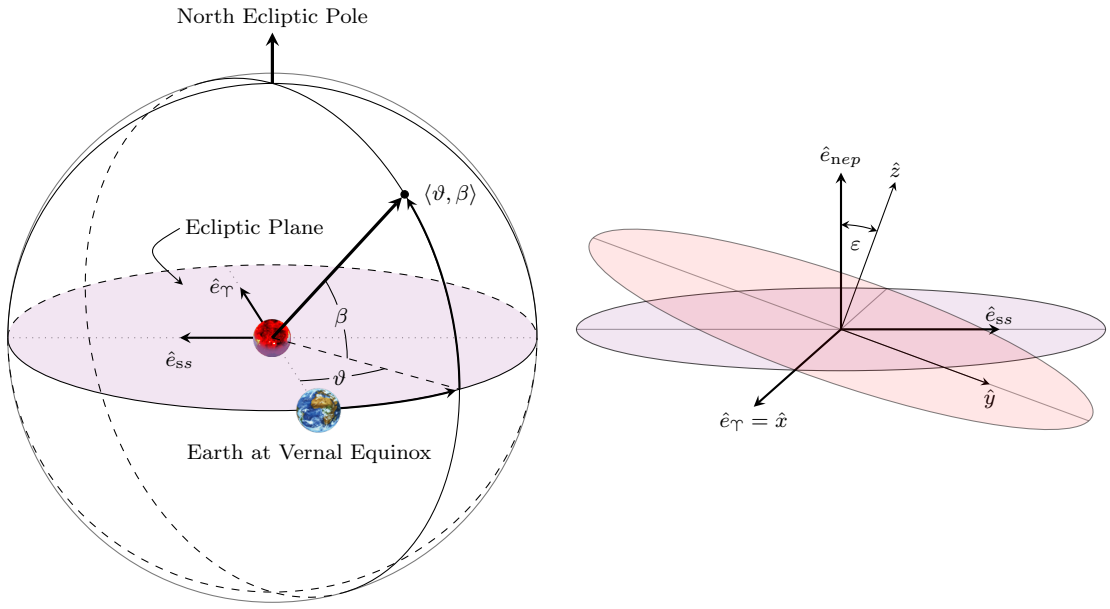

Figure A.3.: (a) The heliocentric ecliptic coordinate system with $\hat{e}_\Upsilon$ and $\hat{e}_{ss}$ forming a basis for the Earth's orbit about the sun. (b) The ecliptic and equatorial planes superimposed with orthonormal bases as described in the text.

where we stress that the pair of angles $\langle \cdot, \cdot \rangle$ on the right-hand side of Eq. (A.3) are the ecliptic longitude and latitude, as opposed to the right ascension and declination.

Because $\hat{e}_\Upsilon$ and $\hat{e}_{ss}$ span the plane of the Earth's orbit, they become a natural basis in which to express the Earth's position and velocity—which is the primary objective of the current discussion. Before doing this however, we provide a brief discussion of the transformations between different celestial coordinates so that we may express this desired basis in a more useful manner, galactic Cartesian coordinates.

A.2 Coordinate Transformations

There are, although not independent of one another, two sets of transformations to consider: one being how the longitudinal and latitudinal angles transform and the other being how the coordinate axes transform. The former of these two has taken

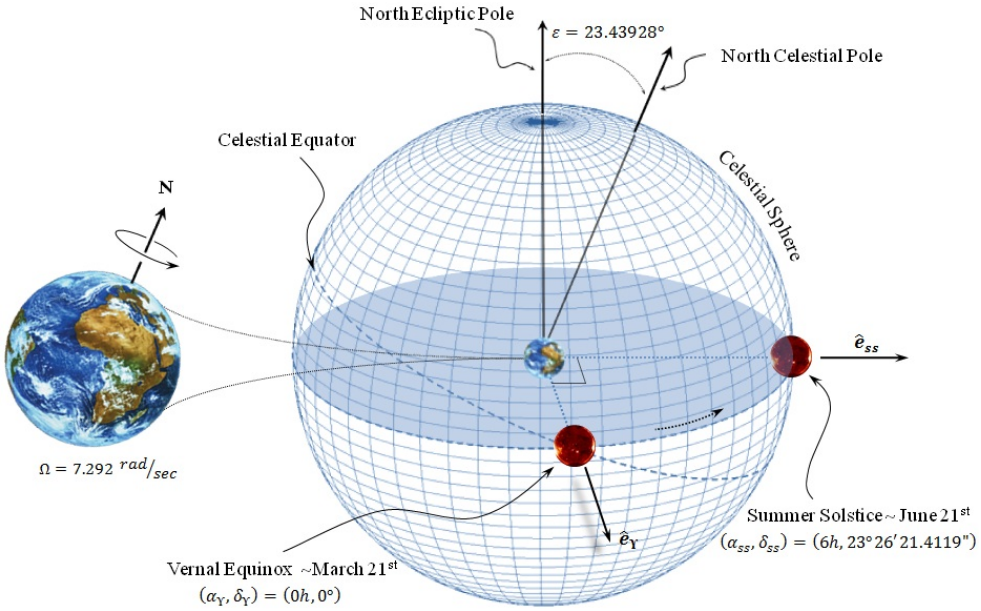

Figure A.4.: The Celestial Sphere showing the right ascension α and declination δ of the sun at the vernal equinox (Υ) and summer solstice (ss). The apparent path traced by the Sun lies within the Ecliptic Plane - which is inclined by an angle of ε from the plane of the Celestial Equator. The node where the sun crosses the celestial equator (from south to north) represents the vernal equinox. The summer solstice is the most northerly point of the ecliptic (with respect to the celestial equator) and occurs 1/4 year after the vernal equinox. The vectors $\hat{e}_{\Upsilon}$ and $\hat{e}_{\rm ss}$ are unit vectors in the directions of $\langle 0h, 0° \rangle$ and $\langle 6h, 23°26'21''.4119 \rangle$, respectively. Together with $\hat{e}_{\Upsilon} \times \hat{e}_{\rm ss}$ (a unit vector in the direction of the north ecliptic pole), these vectors form a convenient basis for describing the motion of the earth about the Sun.

a "canonical" form that can be found readily within the literature. This is not true, however, for designation of orthogonal right-handed coordinate systems to these celestial frames. As such, it has become commonplace for authors to prescribe their own choice for orthogonal bases. This leads to unavoidable discrepancies and occasional minus signs in coordinate transformations, and challenges the reader to jump between treatments. Unfortunately we are no exception, but we briefly outline the derivation

of these types of transformations—consistent with our choice of coordinates presented in Sec. A.1.

A.2.1 Equatorial ↔ Ecliptic

It should be evident that the x-axes for both the equatorial and ecliptic coordinate systems point in the direction of the apparent location of the sun at the moment of the vernal equinox and hence coincide. The direction of the ecliptic positive y-axis $\hat{e}_{ss}$ has equatorial coordinates $\langle \alpha_{ss}, \delta_{ss} \rangle = \langle 6h, \varepsilon \rangle$, where $\varepsilon = 23^{\circ}26'21''.4119$ is the obliquity of the ecliptic. In fact, the ecliptic system is simply the equatorial system under a counter-clockwise rotation by ε about their common x-axis, as seen in Fig. A.3b:

$$\begin{pmatrix} \hat{e}_{\Upsilon} \\ \hat{e}_{\rm ss} \\ \hat{e}_{\rm nep} \end{pmatrix} = \begin{pmatrix} 1 & 0 & 0 \\ 0 & \cos\varepsilon & \sin\varepsilon \\ 0 & -\sin\varepsilon & \cos\varepsilon \end{pmatrix} \begin{pmatrix} \hat{x} \\ \hat{y} \\ \hat{z} \end{pmatrix} \tag{A.4}$$

The inverse transformation matrix is readily obtained by assigning $\varepsilon \mapsto -\varepsilon$, or by transposing. To obtain a relationship between the longitudinal and latitudinal coordinates of these two frames, we consider an arbitrary unit vector $\hat{r} = \langle x, y, z \rangle$ pointing in the direction $\langle \alpha, \delta \rangle$ in equatorial coordinates. By inspection, it is evident that

$$\begin{aligned} \hat{r} \cdot \hat{e}_{\rm nep} &= z' = \sin\beta \\ \hat{r} \cdot \hat{e}_{\Upsilon} &= x' = \cos\beta\cos\vartheta \\ \hat{r} \cdot \hat{e}_{\rm ss} &= y' = \cos\beta\sin\vartheta \end{aligned} \tag{A.5}$$

where $\langle \vartheta, \beta \rangle$ are the ecliptic longitude and latitude representing the direction of $\hat{r} = \langle x', y', z' \rangle$ in ecliptic coordinates. Using Eq. (A.4), we write the basis vectors of the ecliptic system in terms of those for the equatorial system and the relations in Eq. (A.5) become,

$$\begin{aligned} \sin\beta &= \cos\varepsilon\sin\delta - \sin\varepsilon\cos\delta\sin\alpha \\ \cos\beta\cos\vartheta &= \cos\delta\cos\alpha \\ \cos\beta\sin\vartheta &= \cos\varepsilon\cos\delta\sin\alpha + \sin\varepsilon\sin\delta. \end{aligned} \tag{A.6}$$

The inverse transformation can be obtained by projecting $\hat{r}$ onto the equatorial basis vectors in Eq. (A.5), expressed in the basis for ecliptic coordinates.

A.2.2 Equatorial $\leftrightarrow$ Galactic

The relationship between equatorial and galactic coordinates follows from knowing the right ascension and declination of the NGP and galactic center (GC). In other words, we need knowledge of the directions of two of the three galactic basis vectors $(\hat{X}, \hat{Y}, \hat{Z})$ in equatorial coordinates. In J2000 coordinates, these values are:

$$\begin{aligned} \alpha_{\mathrm{NGP}} &= 12^{\mathrm{h}}51^{\mathrm{m}}26.282^{\mathrm{s}} \quad , \quad \delta_{\mathrm{NGP}} = 27^{\circ}07'42.01'' \\ \alpha_{\mathrm{GC}} &= 17^{\mathrm{h}}45^{\mathrm{m}}37.224^{\mathrm{s}} \quad , \quad \delta_{\mathrm{GC}} = -28^{\circ}56'10.23''. \end{aligned} \tag{A.7}$$

Using a relation identical to Eq. (A.2) with $b \mapsto \delta, \ell \mapsto \alpha$, we obtain equatorial coordinates for the NGP and GC to be

$$\begin{aligned} \hat{X} &= (\cos\alpha_{\mathrm{GC}} \cos\delta_{\mathrm{GC}})\,\hat{x} + (\cos\delta_{\mathrm{GC}} \sin\alpha_{\mathrm{GC}})\,\hat{y} + \sin\delta_{\mathrm{GC}}\hat{z} \\ \hat{Z} &= (\cos\alpha_{\mathrm{NGP}} \cos\delta_{\mathrm{NGP}})\,\hat{x} + (\cos\delta_{\mathrm{NGP}} \sin\alpha_{\mathrm{NGP}})\,\hat{y} + \sin\delta_{\mathrm{NGP}}\hat{z}, \end{aligned} \tag{A.8}$$

where $\hat{Y} = \hat{Z} \times \hat{X}$ is readily obtained. Combining these relations with the coordinates given in Eq. (A.7), we can write the transformation matrix for the basis vectors as,

$$\begin{pmatrix} \hat{X} \\ \hat{Y} \\ \hat{Z} \end{pmatrix} = \begin{pmatrix} -0.05487 & -0.87344 & -0.48384 \\ 0.49411 & -0.44483 & 0.74698 \\ -0.86767 & -0.19808 & 0.45599 \end{pmatrix} \begin{pmatrix} \hat{x} \\ \hat{y} \\ \hat{z} \end{pmatrix}. \tag{A.9}$$

Again, the inverse transformation can be obtained by inverting the rotation matrix given in Eq. (A.9). To obtain a relationship between the longitudinal and latitudinal coordinates of these two frames, we follow a procedure very similar to the one presented in Sec. A.2.1. We consider an arbitrary unit vector $\hat{r} = \langle x, y, z \rangle$ point-

ing in the direction $\langle \alpha, \delta \rangle$ in equatorial coordinates, which has galactic coordinates $\hat{r} = \langle X, Y, Z \rangle$ pointing in the direction $\langle \ell, b \rangle$ Then we have,

$$\begin{aligned} \sin b &= Z = \hat{r} \cdot \hat{Z} \\ &= x \cos \alpha_{\mathrm{NGP}} \cos \delta_{\mathrm{NGP}} + y \cos \delta_{\mathrm{NGP}} \sin \alpha_{NGP} + z \sin \delta_{\mathrm{NGP}} \\ &= \cos \delta_{\mathrm{NGP}} \cos \delta \left(\cos \alpha_{\mathrm{NGP}} \cos \alpha + \sin \alpha_{\mathrm{NGP}} \sin \alpha \right) + \sin \delta \sin \delta_{\mathrm{NGP}} \\ &= \cos \delta_{\mathrm{NGP}} \cos \delta \cos \left(\alpha - \alpha_{\mathrm{NGP}} \right) + \sin \delta \sin \delta_{\mathrm{NGP}}, \end{aligned} \tag{A.10}$$

where we have used the expression for $\hat{Z}$ given in Eq. (A.8). To finish out this set of transformations, we project $\hat{r}$ onto $\hat{X}$ and $\hat{Y}$. It simplifies matters to express the final result in terms of the galactic longitude of the celestial north pole, denoted as ℓ_C. We can determine this angle by noting that

$$\begin{aligned} \tan \ell_C &= \frac{\hat{z} \cdot \hat{Y}}{\hat{z} \cdot \hat{X}} \\ &= -1.54386 \\ \Rightarrow \ell_C &= 122^\circ 55' 55.2'', \end{aligned} \tag{A.11}$$

where we reference the fact that $\hat{z} \cdot \hat{Y} = 0.74698$ and $\hat{z} \cdot \hat{X} = -0.48384$ as given in Eq. (A.9). Thus, the full set of transformations can be presented as

$$\begin{aligned} \sin b &= \cos \delta_{\mathrm{NGP}} \cos \delta \cos \left(\alpha - \alpha_{\mathrm{NGP}} \right) + \sin \delta \sin \delta_{\mathrm{NGP}} \\ \cos b \sin \left(\ell_C - \ell \right) &= \cos \delta \sin \left(\alpha - \alpha_{\mathrm{NGP}} \right) \\ \cos b \cos \left(\ell_C - \ell \right) &= \cos \delta_{\mathrm{NGP}} \sin \delta - \sin \delta_{\mathrm{NGP}} \cos \delta \cos \left(\alpha - \alpha_{\mathrm{NGP}} \right). \end{aligned} \tag{A.12}$$

A.2.3 Galactic $\leftrightarrow$ Ecliptic

Obtaining the transformation between galactic and ecliptic coordinates is trivial now that we have the transformations presented in Eq. (A.4) and Eq. (A.9). We can rewrite the transformation from equatorial to ecliptic coordinates as

$$\hat{e}_i = R_{ij} \hat{x}_j, \tag{A.13}$$

where R_{ij} denotes the transformation matrix presented in Eq. (A.4). Similarly, the transformation from equatorial to galactic coordinates can be expressed as

$$\hat{X}_i = A_{ij}\hat{x}_j, \tag{A.14}$$

with A_{ij} denoting the transformation matrix presented in Eq. (A.9). Therefore, we can write the transformation from ecliptic to galactic coordinates as

$$\begin{aligned} \hat{X}_i = A_{ij}R^T_{jk}\hat{x}_k &= A_{ij}R_{kj}\hat{x}_k \\ &= S_{ik}\hat{x}_k, \end{aligned} \tag{A.15}$$

where the elements of S_{ik} are explicitly given by

$$S = \begin{pmatrix} -0.05487 & -0.99382 & -0.09646 \\ 0.49411 & -0.11098 & 0.86229 \\ -0.86767 & -0.00035 & 0.49715 \end{pmatrix}. \tag{A.16}$$

As stated in the introduction, the primary objective of the current discussion has been to express the Earth's position and velocity relative to larger structures beyond our solar system. Because $\hat{e}_\Upsilon$ and $\hat{e}_{\rm ss}$ span the plane of the Earth's orbit, they are a natural basis in which to express the Earth's position and velocity. The transformation presented in Eq. (A.16) enables us to meet our objective and express this basis in galactic Cartesian coordinates as

$$\begin{aligned} \hat{e}_\Upsilon &= \langle -0.05487, 0.4941, -0.8676 \rangle \\ \hat{e}_{ss} &= \langle -0.9938, -0.1110, -0.0003452 \rangle . \end{aligned} \tag{A.17}$$

We conclude this section with two comments: (1) it is useful to know the angle of inclination between the ecliptic and galactic planes, $\gamma_{\text{♄}}$. Since $\gamma_{\text{♄}}$ is the angle spanned between the NGP and NEP, we have $\hat{Z} \cdot \hat{e}_{nep} = \cos\gamma_{\text{♄}}$, which is given by element S_{33} in Eq. (A.16). From this, we find that $\gamma_{\text{♄}} = 60.1885°$. (2) As a final remark, all transformation matrices developed throughout this section are clearly unitary, and consequently their inverses are simply their transposes.

A.3 Motion of the Earth

We are motivated on several fronts to obtain an accurate understanding of Earth's motion, in particular with respect to structures such as the rest frame of our local dark matter halo or the cosmic microwave background. We will begin by calculating the velocity of the Earth with respect to the sun, denoted throughout this work as $\vec{v}_{\earth}$, and then address the motion of the sun with respect to these larger structures.

A.3.1 Orbit about the Sun

In principle, an accurate description of the Earth's motion can only be attained by accounting for such things as the ellipticity of the Earth's orbit and the aberration in the ecliptic longitude. However, insofar as the Earth's orbit is approximately circular (eccentricity $\varepsilon_{\earth} = 0.01671$), it is reasonable to neglect the perturbation in velocity from that of a circular orbit. In fact, all relevant quantities pertaining to the Earth's motion (such as the Earth–sun distance $r_{\earth}$, orbital angular momentum, etc.) have perturbations which scale with $\varepsilon_{\earth}$ or higher powers of $\varepsilon_{\earth}$.

A key feature of circular orbits is that their velocity at any point is perpendicular to their position vector ($\vec{r} \cdot \vec{v} = 0$), or equivalently, the velocity at any point is parallel to the position vector 1/4 of a cycle later. For an elliptical orbit with eccentricity ε, it is easily shown that to first order in ε

$$\vec{r} \cdot \vec{v} = \varepsilon r v \sin 2\pi\tau, \tag{A.18}$$

where $\tau \in [0, 1]$ parametrizes the orbit such that $\tau = 0$ corresponds to the orbit's aphelion. Thus, the angle spanned by the velocity and position vectors is given by

$$\begin{aligned} \cos\delta &= \frac{\vec{r} \cdot \vec{v}}{vr} = \varepsilon \sin\tau \\ &\Rightarrow \quad \delta = \frac{\pi}{2} - \varepsilon \sin 2\pi\tau, \end{aligned} \tag{A.19}$$

where, explicitly, $|\delta - \pi/2| \leq \varepsilon$ denotes the largest departure from perpendicularity. For Earth's orbit, it is evident that $\vec{r}_{\earth}$ and $\vec{v}_{\earth}$ are always "almost perpendicular" with a maximal discrepancy of $\sim 1°$.

Proceeding from the discussion in Sec. A.2.3, $\hat{e}_{\Upsilon}$ and $\hat{e}_{\rm ss}$ form a natural basis in which to express the Earth's position and velocity. At the vernal equinox, occurring at time t_{Υ}, the Earth's velocity is anti-parallel to $\hat{e}_{\rm ss}$, while the Earth's ecliptic longitude ϑ is zero (see Fig. A.3a). Similary, a quarter of a year later when the Earth's ecliptic longitude is $\vartheta = 90°$, the velocity of the Earth is parallel to $\hat{e}_{\Upsilon}$. More generally, at a time t after t_{Υ}, the Earth's velocity vector has rotated through an angle

$$\vartheta\left[t\right] = \frac{360°}{365.25}\left(t - t_{\Upsilon}\right), \tag{A.20}$$

where time t is in units of days with $t = 0$ corresponding to Jan. 1st. The spring equinox usually occurs around March 21st, corresponding to $t_{\Upsilon} = 80$ days.[3] Furthermore, we can represent the Earth's velocity at time t by

$$\vec{v}_{\earth}\left[t\right] = v_{\earth} \cdot \Big(\sin\vartheta\left[t\right] \cdot \hat{e}_{\Upsilon} - \cos\vartheta\left[t\right] \cdot \hat{e}_{ss} \Big), \tag{A.21}$$

where $v_{\earth} = 2\pi \cdot \mathrm{AU}/1 \text{ year} = 29.8$ km/s.

A.3.2 Motion of the Sun through (Extra)–Galactic Structures

To find the motion of the Earth with respect to the local DM halo, for example, we need the velocity of the Sun with respect to the DM halo. Since we will be interested in Earth's motion with respect to several different systems, we will first finish our calculation (as far as we can take it) for the Earth's velocity more generally. We will denote the velocity of the sun (with respect to whatever frame) as $\vec{V}_{\odot}$, where the sun's velocity in this frame is understood to be represented in galactic Cartesian coordinates. Therefore by adding this to Eq. (A.21), we find that the velocity of Earth (with respect to whatever) is given by

$$\vec{V}_{\earth}\left[t\right] = \vec{V}_{\odot} + \vec{v}_{\earth}\left[t\right]. \tag{A.22}$$

We note that the "lack" of time dependence in $\vec{V}_{\odot}$ is simply a consequence of the very long time scales for this very large structure through which the sun is moving.

[3]Strictly speaking, ones needs to measure time from the beginning of the epoch (i.e. from noon of 31 Dec 1999) to be accurate, however this can be accommodated by resetting t_{Υ} year by year.

Perhaps the more relevant quantity (as is the case for DM direct detection event rates) is the Earth's speed through this larger medium. Since it is reasonable to expect $v_{\earth}/V_{\odot} \ll 1$, we determine the Earth's speed is given to a good approximation by

$$\begin{aligned} V_{\earth}[t] &= \left|\vec{V}_{\odot} + \vec{v}_{\earth}[t]\right| \\ &= \sqrt{V_{\odot}^2 + v_{\earth}[t]^2 + 2\vec{V}_{\odot}\cdot\vec{v}_{\earth}[t]} \\ &\approx V_{\odot} + \frac{v_{\earth}^2}{2V_{\odot}} + v_{\earth}\left(\hat{V}_{\odot}\cdot\hat{e}_{\Upsilon}\right)\sin\vartheta[t] - v_{\earth}\left(\hat{V}_{\odot}\cdot\hat{e}_{\rm ss}\right)\cos\vartheta[t] \\ &= V_{\odot} + \frac{v_{\earth}^2}{2V_{\odot}} + v_{\earth}A\cos\Big(\vartheta[t] + \vartheta_0\Big), \end{aligned} \tag{A.23}$$

where $\hat{V}_{\odot} \equiv \vec{V}_{\odot}/V_{\odot}$,

$$A \equiv \sqrt{\left(\hat{V}_{\odot}\cdot\hat{e}_{\Upsilon}\right)^2 + \left(\hat{V}_{\odot}\cdot\hat{e}_{\rm ss}\right)^2}, \tag{A.24}$$

and

$$\vartheta_0 \equiv \tan^{-1}\left[\frac{\hat{V}_{\odot}\cdot\hat{e}_{\Upsilon}}{\hat{V}_{\odot}\cdot\hat{e}_{\rm ss}}\right], \tag{A.25}$$

with the arc-tangent taken in the appropriate quadrant. It is worth noting that A as defined in Eq. (A.24) is simply the cosine of the angle spanned between the ecliptic plane and the sun's velocity $\vec{V}_{\odot}$. In other words, we can write A as

$$A = \cos\beta_{V_{\odot}} = \frac{V_{\odot,\parallel}}{V_{\odot}}, \tag{A.26}$$

where $\beta_{V_{\odot}}$ denotes the ecliptic latitude of the sun's velocity,[4] and $V_{\odot,\parallel}$ represents the component of $\vec{V}_{\odot}$ projected onto the ecliptic plane. As one would expect, we see that maximal modulation in the Earth's speed occurs in frames within which the sun's motion is almost entirely confined to the ecliptic plane. Furthermore, Earth's maximum (minimum) speed in this frame occurs when its velocity is parallel (anti-parallel) to $\vec{V_{\odot,\parallel}}$.

[4]Incidentally, $\hat{V}_{\odot}\cdot\hat{e}_{\rm nep}$ is clearly seen to be given by $\cos\left(90^\circ - \beta_{V_{\odot}}\right) = \sin\beta_{V_{\odot}}$.

Motion through the DM Halo

The standard choice for the DM halo enveloping our galaxy is a non-rotating, isothermal sphere. As such, the bulk component of this halo is presumed at rest with respect to the galaxy, and the motion of the sun through this halo is simply the sun's motion through the galactic rest frame.

We can divide $\vec{V}_\odot$ into two components: the motion of our local standard of rest (LSR) and the sun's peculiar motion with respect to the LSR. The motion of the LSR (in galactic Cartesian coordinates) is, by definition, $\langle 0, v_c\left[R\right], 0\rangle$, where $v_c\left[R\right]$ denotes the rotational speed at at a distance R from the center of the galaxy. We will use the determination of $v_c\left[R_\odot\right]$ given by Kerr and Lynden-Bell [78] to be

$$v_c\left[R_\odot\right] = 222.2 \pm 20 \ \frac{\mathrm{km}}{\mathrm{s}}. \tag{A.27}$$

The peculiar motion of the sun $V_{\odot,\mathrm{pec}}$ determined recently using data from the Hipparcos satellite [79] is

$$\vec{V}_{\odot,\mathrm{pec}} = \langle 10.0,\ 5.2,\ 7.2\rangle \ \frac{\mathrm{km}}{\mathrm{s}}. \tag{A.28}$$

Therefore, the motion of the sun through the rest frame of the galaxy is given by

$$\begin{aligned} \vec{V}_\odot &= \vec{V}_{\odot,\mathrm{pec}} + \langle 0, v_c\left[R_\odot\right], 0\rangle \\ &= \langle 10.0, 227.4, 7.2\rangle \ \frac{\mathrm{km}}{\mathrm{s}} \\ &= 227.7 \cdot \langle 0.04391, 0.9985, 0.03162\rangle \ \frac{\mathrm{km}}{\mathrm{s}}. \end{aligned} \tag{A.29}$$

Thus, from Eq. (A.23) we determine the speed of the Earth through the galactic rest frame (and hence the standard DM halo) to be

$$V_{\oplus}\left[t\right] = 230 + 14.5 \cos\left[\frac{360^\circ}{365.25}\left(t - 152\right)\right] \ \frac{\mathrm{km}}{\mathrm{s}}, \tag{A.30}$$

where again t is in units days from Jan. 1st. Hence, in the galactic rest frame, $V_{\oplus}\left[t\right]$ varies about its mean with an amplitude of $14.5/230 = 6.3\%$ with maximum speed at $t = 152$ days (corresponding to June 2nd) and minimum speed 1/2 of a year later.

LIST OF REFERENCES

LIST OF REFERENCES

[1] E. Rutherford, J. Chadwick, and C.D. Ellis. *Radiations from Radioactive Substances*, Cambridge University Press, Cambridge, 1930.

[2] E. D. Falkenberg. Radioactive Decay Caused by Neutrinos? *Apeiron*, 8: 32–45, 2001.

[3] S. E. Shnoll, V. A. Kolombet, E. V. Pozharskii, T. A. Zenchenko, J. M. Zvereva, A. A. Konradov. Realization of discrete states during fluctuations in macroscopic processes. *Physics-Uspekhi*, 41:1025–35, 1998.

[4] D. P. Veprev, V. I. Muromtsev. Evidence of solar influence on the tritium decay rate. *Astropart. Phys.*, 36:26–30, 2012.

[5] V. M. Lobashev et al. Direct search for mass of neutrino and anomaly in the tritium beta-spectrum *Phys. Lett. B*, 460:227–235, 1999.

[6] D. O'Keefe, B. Morreale, E. Fischbach, D. Javorsek II, J. H. Jenkins, R. H. Lee, F. Morris, P. A. Sturrock. Spectral content of 22Na/44Ti decay data: implications for a solar influence. *Astrophysics and Space Science*, 344(2):297–303, 2012.

[7] J. H. Jenkins, E. Fischbach, J. B. Buncher, J. T. Gruenwald, D. E. Krause, J. J. Mattes. Evidence of correlations between nuclear decay rates and Earth–Sun distance. *Astropart. Phys.*, 32:42–46, 2009.

[8] P. A. Sturrock, J. B. Buncher, E. Fischbach, J. T. Gruenwald, D. Javorsek II, J. H. Jenkins, R. H. Lee, J. J. Mattes, J. R. Newport. Power spectrum analysis of BNL decay rate data. *Astropart. Phys.*, 34:121–127, 2010.

[9] P. A. Sturrock, E. Fischbach, and J. H. Jenkins. Further Evidence Suggestive of a Solar Influence on Nuclear Decay Rates. *Sol. Phys.*, 272:1–10, 2011.

[10] J. H. Jenkins, K. R. Herminghuysen, T. E. Blue, E. Fischbach, D. Javorsek II, A. C. Kauffman, D. W. Mundy, P. A. Sturrock, and J. W. Talnagi. Additional Experimental Evidence for a Solar Influence on Nuclear Decay Rates. *Astropart. Phys.*, 37:81–88, 2012.

[11] J. H. Jenkins, E. Fischbach. Perturbation of nuclear decay rates during the solar flare of 2006 December 13. *Astropart. Phys.*, 31(6):407–411, 2009.

[12] J. H. Jenkins, E. Fischbach, P. A. Sturrock, and D. W. Mundy. Analysis of Experiments Exhibiting Time-Varying Nuclear Decay Rates: Systematic Effects or New Physics?. *XLVIIth Rencontres de Moriond and GPhyS Colloquium, Gravitational Waves and Experimental Gravity*. Gioi Publishers, La Thuile, Aosta Valley, Italy, 2011.

[13] K. J. Ellis. The effective half-life of a broad beam ^{238}Pu/Be total body neutron irradiator. *Phys. Med. Biol.*, 35:1079–1087, 1990.

[14] A. G. Parkhomov. Researches of alpha and beta radioactivity at long-term observations. *arXiv:1004.1761v1* [physics.gen-ph], 2010.

[15] A. G. Parkhomov. Periods Detected During Analysis of Radioactivity Measurements Data. *arXiv:1012.4174v1* [physics.gen-ph], 2010.

[16] Y. A. Baurov, Yu. G. Sobolev, Yu. V. Ryabov, and V. F. Kushniruk. Experimental investigations of changes in the rate of beta decay of radioactive elements. *Phys. Atom. Nucl.*, 70:1825–35, 2007.

[17] H. Schrader. Half-life measurements of long-lived radionuclides—New data analysis and systematic effects. *Appl. Radiat. Isotopes*, 68:1583–1590, 2010.

[18] P. A. Sturrock, A. G. Parkhomov, E. Fischbach, and J. H. Jenkins. Power spectrum analysis of LMSU (Lomonosov Moscow State University) nuclear decay-rate data: Further indication of r-mode oscillations in an inner solar tachocline. *Astropart. Phys.*, 35:755–758, 2012.

[19] J. H. Jenkins, E. Fischbach, D. Javorsek II, R. H. Lee, and P. A. Sturrock. Concerning the time dependence of the decay rate of ^{137}Cs. *Appl. Radiat. and Isotopes*, 74:50–55, 2013.

[20] H. Siegert, H. Schrader, U. Schötzig. Half-life measurements of Europium radionuclides and the long-term stability of detectors. *Appl. Radiat. Isotopes*, 49:1397–1401, 1998.

[21] G. Steinitz, O. Piatibratova, and P. Kotlarsky. Possible effect of solar tides on radon signals. *J. Environ. Radioactiv.*, 102(8):749–765, 2011.

[22] P. A. Sturrock, G. Steinitz, E. Fischbach, D. Javorsek II, and J. H. Jenkins. Analysis of gamma radiation from a radon source: Indications of a solar influence. *Astropart. Phys.*, 36:18–25, 2012.

[23] P. A. Sturrock, J. B. Buncher, E. Fischbach, J. T. Gruenwald, D. Javorsek II, J. H. Jenkins, R. Lee, J. J. Mattes, and J. Newport. Power Spectrum Analysis of Physikalisch-Technische Bundesanstalt Decay-Rate Data: Evidence for Solar Rotational Modulation. *Solar Physics*, 267:251–265, 2010.

[24] J. H. Jenkins, E. Fischbach, J. B. Buncher, J. T. Gruenwald, D. E. Krause, and J. J. Mattes. Evidence of correlations between nuclear decay rates and Earth–Sun distance. *Astropart. Phys.*, 32(1):42–46, 2009.

[25] P. A. Sturrock, J. B. Buncher, E. Fischbach, J. T. Gruenwald, D. Javorsek II, J. H. Jenkins, R. H. Lee, J. J. Mattes, and J. R. Newport. Power Spectrum Analysis of BNL Decay-rate Data. *Astropart. Phys.*, 34:121–127, 2010.

[26] G. J. Stephenson Jr. and T. Goldman. Observable consequences of a scalar boson coupled only to neutrinos. *arXiv:hep-ph/9309308*, 1993.

[27] G. J. Stephenson and T. Goldman. A possible solution to the tritium endpoint problem. *Phys. Lett. B*, 440:89–93, 1998.

[28] G. J. Stephenson, T. Goldman, and B. McKellar. Neutrino Clouds. *Int. J. Mod. Phys. A*, 13:2765–2790, 1998.

[29] R. Horvat. Recent results of the neutrino mass squared measurements and the coherent neutrino cold-dark-matter interaction. *Phys. Rev. D*, 57:5236–5238, 1998.

[30] E. Bellotti, C. Broggini, G. Di Carlo, M. Laubenstein, R. Menegazzo, and M. Pietroni. Search for time modulations in the decay rate of ^{40}K and ^{232}Th. *Astropart. Phys.*, 61:82–87, 2015.

[31] J. C. Hardy, J. R. Goodwin and V. E. Iacob. Do radioactive half-lives vary with Earth-to-Sun distance? *Appl. Radiat. Isot.*, 70:1931–1933, 2012.

[32] P. S. Cooper. Searching for modifications to the exponential radioactive decay law with the Cassini spacecraft. *Astropart. Phys.*, 31(4):267–269, 2009.

[33] E. B. Norman, E. Browne, H. A. Shugart, T. H. Joshi and R. B. Firestone. Evidence against correlations between nuclear decay rates and Earth-Sun distance. *Astropart. Phys.*, 31(2):135-137, 2009.

[34] H. Schrader. Half-life measurements of long-lived radionuclides—New data analysis and systematic effects. *Appl. Rad. and Isotopes*, 68:1583–1590, 2010.

[35] K. Bikit, J. Nikolov, I. Bikit, D. Mrda, N. Todorovic, S. Forkapic, J. Slivka and M. Veskovic. Reinvestigation of the irregularities in the ^{3}H decay. *Astropart. Phys.*, 47:38–44, 2013.

[36] R. J. de Meijer, M. Blaauw and F. D. Smit. No evidence for antineutrinos significantly influencing exponential β^+ decay. *Appl. Rad. and Isotopes*, 69(2):320–326, 2011.

[37] D. Griffiths. *Introduction to Elementary Particles*. Wiley-VCG, Weinhein, 2008.

[38] J. Mattes. *Detecting Relic Neutrinos through Coherent Processes*. Ph.D. thesis, Purdue University, 2013.

[39] E. Fischbach, J. B. Buncher, J. T. Gruenwald, J. H. Jenkins, D. E. Krause, J. J. Mattes, and J. R. Newport. Time–Dependent Nuclear Decay Parameters: New Evidence for New Forces? *Space Sci. Rev.*, 145(3):285–335, 2009.

[40] R. M. Lindstrom, E. Fischbach, J. B. Buncher, G. L. Greene, J. H. Jenkins, D. E. Krause, J. J. Mattes, and A. Yue. Study of the dependence of ^{198}Au half-life on source geometry. *Nucl. Instrum. Methods Phys. Res. A*, 622(1):93–96, 2010.

[41] R. M. Lindstrom, E. Fischbach, J. B. Buncher, J. H. Jenkins, and A. Yue. *Nucl. Instrum. Methods Phys. Res. A*, 659(1):269–271, 2011.

[42] R. M. Lindstrom, R. Zeisler, E. Mackey, P. Liposky, R. Popelka-Filcoff, and R. Williams. Neutron irradiation in activation analysis: A new rabbit for the NBSR. *J. Radioanal. Nucl. Chem.*, 278(3):665–669, 2008.

[43] R. M. Lindstrom and R. Fleming. Dead Time, Pileup, and Accurate Gamma-Ray Spectrometry. *Radioactivity & Radiochemistry*, 6(2):20–27, 1995.

[44] R. Bernabei, P. Belli, F. Cappella, R. Cerulli, C. J. Dai, A. d'Angelo, H. L. He, A. Incicchitti, H. H. Kuang, X. H. Ma, F. Montecchia, F. Nozzoli, D. Prosperi, X. D. Sheng, R. G. Wang, and Z. P. Ye. New results from DAMA/LIBRA. *Eur. Phys. J. C*, 67(1):39–49, 2010.

[45] R. Bernabei, P. Belli, F. Cappella, R. Cerulli, C. J. Dai, A. d'Angelo, H. L. He, A. Incicchitti, H. H. Kuang, X. H. Ma, F. Montecchia, F. Nozzoli, D. Prosperi, X. D. Sheng, R. G. Wang, and Z. P. Ye. First results from DAMA/LIBRA and the combined results with DAMA/NaI. *Eur. Phys. J. C*, 56(3):333–355, 2008.

[46] C. E. Aalseth, P. S. Barbeau, J. Colaresi, J. I. Collar, J. Diaz Leon, J. E. Fast, N. Fields, T. W. Hossbach, M. E. Keillor, J. D. Kephart, A. Knecht, M. G. Marino, H. S. Miley, M. L. Miller, J. L. Orrell, D. C. Radford, J. F. Wilkerson, and K. M. Yocum [CoGeNT Collaboration]. Search for an Annual Modulation in a p-Type Point Contact Germanium Dark Matter Detector. *Phys. Rev. Lett.*, 107:141301, 2011.

[47] P. Belli, R. Bernabei, A. Bottino, F. Cappella, R. Cerulli, N. Fornengo, and S. Scopel. Observations of annual modulation in direct detection of relic particles and light neutralinos. *Phys. Rev. D*, 84(5):055014, 2011.

[48] D. S. Akerib *et al.* [CDMS Collaboration]. New results from the Cryogenic Dark Matter Search experiment. *Phys. Rev. D*, 68(8):082002, 2003.

[49] D. S. Akerib *et al.* [CDMS Collaboration]. Limits of spin-independent WIMP-nucleon interactions from the two-tower run of the Cryogenic Dark Matter Search. *Phys. Rev. Lett.*, 96(1):011302, 2006.

[50] Z. Ahmed *et al.* [CDMS Collaboration]. Search for Weakly Interacting Massive Particles with the First Five-Tower Data from the Cryogenic Dark Matter Search at the Soudan Underground Laboratory. *Phys. Rev. Lett.*, 102:011301, 2009.

[51] J. Angle *et al.* [XENON Collaboration]. First Results from the XENON10 Dark Matter Experiment at the Gran Sasso National Laboratory. *Phys. Rev. Lett.*, 100(2):021303, 2008.

[52] E. Aprile *et al.* [XENON100 Collaboration]. Dark Matter Results from 100 Live Days of XENON100 Data. *Phys. Rev. Lett.*, 107(13):131302, 2011.

[53] E. Armengaud *et al.* [EDELWEISS Collaboration]. A search for low-mass WIMPs with EDELWEISS-II heat-and-ionization detectors. *Phys. Rev. D*, 86(5):051701, 2012.

[54] D. Tucker-Smith and N. Weiner. Inelastic dark matter. *Phys. Rev. D*, 64:043502, 2001.

[55] S. Chang, G. D. Kribs, D. Tucker-Smith, and N. Weiner. Inelastic Dark Matter in Light of DAMA/LIBRA. *Phys. Rev. D*, 79:043513, 2009.

[56] J. L. Feng, J. Kumar, and L. E. Strigari. Explaining the DAMA Signal with WIMPless Dark Matter. *Phys. Lett. B*, 670:37–40, 2008.

[57] R. Foot. Mirror dark matter and the new DAMA/LIBRA results: A simple explanation for a beautiful experiment. *Phys. Rev. D*, 78:043529, 2008.

[58] S. Andreas, T. Hambye, and M. H. G. Tytgat. WIMP dark matter, Higgs exchange and DAMA. *Journal of Cosmology and Astroparticle Physics*, 2008:034, 2008.

[59] P. Ullio, M. Kamionkowski, and P. Vogel. Spin-Dependent WIMPs in DAMA? *JHEP*, 2001(07):44, 2001.

[60] C. Savage, P. Gondolo, and K. Freese. Can WIMP Spin Dependent Couplings explain DAMA data, in light of Null Results from Other Experiments? *Phys. Rev. D*, 70:123513, 2004.

[61] A. Bottino, F. Donato, N. Fornengo, and S. Scopel. Light Neutralinos and WIMP direct searches. *Phys. Rev. D*, 69:037302, 2004.

[62] P. Gondolo and G. Gelmini. Compatibility of DAMA Dark Matter Detection with Other Searches. *Phys. Rev. D*, 71:123520, 2005.

[63] R. Bernabei, P. Belli, F. Cappella, R. Cerulli, C. J. Dai, H. L. He, A. Incicchitti, H. H. Kuang, X. H. Ma, F. Montecchia, F. Nozzoli, D. Prosperi, and Z. P. Ye. Investigating pseudoscalar and scalar dark matter. *International Journal of Modern Physics A*, 21(7):1445–1469, 2006.

[64] K. Blum. DAMA vs. the annually modulated muon background. *arXiv:1110.0857v1* [astro-ph.HE], 2011.

[65] D. Nygren. A testable conventional hypothesis for the DAMA-LIBRA annual modulation. *arXiv:1102.0815v1* [astro-ph.IM], 2011.

[66] J. P. Ralston. One Model Explains DAMA/LIBRA, CoGENT, CDMS, and XENON. *arXiv:1006.5255v1* [hep-ph], 2010.

[67] V. A. Kudryavtsev, M. Robinson, and N. J. C. Spooner. The expected background spectrum in NaI dark matter detectors and the DAMA result. *J. Phys. Conf. Ser.*, 203:012039, 2010.

[68] C. Galbiati. *Future Direct Dark Matter Searches: An Outlook*. Talk at the WIN workshop, Perugia, Italy, 2009.

[69] B. Sadoulet. *WIMP Direct Detection: An Outlook*. Talk at the TeV Particle Astrophysics, SLAC, USA, 2009. [http://www-conf.slac.stanford.edu/tevpa09].

[70] R. W. Schnee. Introduction to Dark Matter Experiments. *Physics of the Large and Small: Proceedings of the 2009 Theoretical Advanced Study Institute in Elementary Particle Physics*, World Scientific, Singapore, 629–681, 2010. arXiv:1101.5205v1 [astro-ph.CO].

[71] J. Pradler, B. Singh, and I. Yavin. On an unverified nuclear decay and its role in the DAMA experiment. *Physics Letters B*, 720(4-5):399–404, 2013.

[72] R. Bernabei, P. Belli, F. Cappella, R. Cerulli, C. J. Dai, A. d'Angelo, H. L. He, A. Incicchitti, X. H. Ma, F. Montecchia, F. Nozzoli, D. Prosperi, X. D. Sheng, R. G. Wang, and Z. P. Ye. Particle Dark Matter and DAMA/LIBRA. *AIP Conf. Proc.*, 1223:50, 2009.

[73] R. Bernabei, P. Belli, F. Cappella, R. Cerulli, C. J. Dai, A. d'Angelo, H. L. He, A. Incicchitti, X. H. Ma, F. Montecchia, F. Nozzoli, D. Prosperi, X. D. Sheng, R. G. Wang, and Z. P. Ye. Particle Dark Matter in DAMA/LIBRA. *arXiv:1007.0595v1*, 2010.

[74] R. Bernabei, P. Belli, A. Bussolotti, F. Cappella, R. Cerulli, C. J. Dai, A. d'Angelo, H. L. He, A. Incicchitti, H. H. Kuang, X. H. Ma, A. Mattei, F. Montecchia, F. Nozzoli, D. Prosperi, X. D. Sheng, and Z. P. Ye. The DAMA/LIBRA apparatus. *Nucl. Instr. & Meth. A*, 592:297–315, 2008.

[75] D. W. Engelkemeir, K. F. Flynn, and L. E. Glendenin. Positron Emission in the Decay of ^{40}K. *Physical Review*, 126:1818, 1962.

[76] K. Freese, J. A. Frieman, and A. Gould. Signal modulation in cold dark matter detection. *Phys. Rev. D*, 37:3388, 1988.

[77] A. M. Green. Effect of realistic astrophysical inputs on the phase and shape of the weakly interacting massive particles annual modulation signal. *Phys. Rev. D*, 68:023004, 2003.

[78] F. J. Kerr and D. Lynden-Bell. Review of galactic constants. *Mon. Not. R. Astron. Soc.*, 221:1023–1038, 1986.

[79] J. J. Binney and M. Merrifield. *Galactic Astronomy*. Princeton University Press, Princeton, NJ, 1998.

VITA

VITA

Jonathan Michael Nistor was born at 26.2164° N, 98.2363° W.

He fell in love at 40.4287° N, 86.9138° W .

He hopes his final resting place will be 48.3738° N, 91.5943° W.